STRUCTURAL BASIS OF VERTEBRATE VISION, A G PROTEIN-COUPLED RECEPTOR SIGNALING CASCADE

A Dissertation

Presented to the Faculty of the Graduate School

of Cornell University

in Partial Fulfillment of the Requirements for the Degree of

Doctor of Philosophy

by

Yang Gao

August 2018

STRUCTURAL BASIS OF VERTEBRATE VISION,

A G PROTEIN-COUPLED RECEPTOR SIGNALING CASCADE

Yang Gao

Cornell University, 2018

The visual photo-transduction cascade is a prototypical G protein-coupled receptor (GPCR) signaling system, in which light-activated rhodopsin, the GPCR, catalyzes the exchange of GDP for GTP on the heterotrimeric G protein transducin. This results in the dissociation of transducin into its component GTP-bound α subunit and the βγ subunit complex. Structural information for the rhodopsin-transducin complex will be essential for understanding the molecular mechanism of visual photo-transduction. Moreover, it will shed light on how GPCRs selectively couple to and activate their G protein signaling partners. I have purified a stable detergent-solubilized complex between rhodopsin and transducin. The complex was formed on native rod outer segment membranes upon light activation, solubilized in lauryl maltose neopentyl glycol (LMNG) detergent, and purified with a combination of affinity and size exclusion chromatography. The complex is fully functional, with the stoichiometry of rhodopsin to transducin being 1:1. The molecular weight of the complex was calculated from small angle X-ray scattering (SAXS) data and is in good agreement with a model consisting of one rhodopsin molecule and one transducin molecule. The complex was visualized by negative-stain electron microscopy (EM), which revealed an overall architecture similar to that of the β2 adrenergic receptor-G_S complex including a flexible helical domain in the transducin α subunit. The monodispersity, stability, and high yield of the purified

complex allowed for further efforts toward obtaining a high-resolution structure of this important signaling complex.

Recent X-ray and cryo-electron microscopy (cryo-EM) structures of complexes between different GPCRs and the stimulatory G_S protein have revealed how these receptors converge structurally at the cytoplasmic end and engage the same G_S protein, whereas, the cryo-EM structures of two GPCR-G_i protein complexes show how the inhibitory G_i protein binds receptors in a different manner than the G_S protein. In order to further our understanding of the mechanisms that underlie the specificity of GPCR-G protein interactions, and how they result in the G protein activation event, we determined a high-resolution cryo-EM structure of the light-activated, native bovine rhodopsin complexed with its cognate G protein partner transducin, which belongs to the inhibitory G_i family. The outward movement of transmembrane helix (TM) 6 and the rearrangement of TM5 at the intracellular side of Rho open up a binding cleft for the transducin α subunit, which engages rhodopsin in a different orientation than previously observed in other GPCR-G_S protein complexes. The orientation of G_T is also different from that of the G_i protein in the recently reported GPCR-G_i complexes, revealing the unexpected diversity regarding how GPCRs engage their G protein partners, even within the same G protein family. Moreover, the helical domain of the $G\alpha_T$ subunit is less flexible than those resolved in previous GPCR-G protein complex structures and adopts an open conformation contacting the transducin β subunit, thus shedding new light on its involvement in the G protein activation event.

BIOGRAPHICAL SKETCH

The author, Yang Gao (高洋), was born in 1990 in Xi'an, a city located in northwestern China. His hometown, being the oldest capital of China, is steeped in history and is home to the terracotta warriors and numerous other ancient Chinese relics. One of Yang's favorite things to do whenever he goes back home is to walk on top the historic city walls that encircle the old city and marvel at the striking contrast between the ancient and the modern on opposite sides of the walls. Both his parents are university professors in the field of telecommunications engineering and they have inspired and fostered Yang's fascination with science ever since his childhood. During his middle school and high school days, Yang thoroughly enjoyed studying the natural sciences and chemistry and biology gradually became his favorite subjects. He participated in science Olympiads while in high school and obtained first-place prize in biology and second-place prizes in math, physics and chemistry at the provincial level. As a result of his academic achievements in high school, Yang was matriculated into the chemistry department of Peking University, one of the best universities in China, without having to take the national college entrance exams. Yang majored in both chemistry and biology while studying at Peking University and in his sophomore year joined Dr. Luhua Lai's lab where he took part in designing and screening bivalent drugs targeting key enzymes involved in the arachidonic acid inflammation pathway, such as 5-lipoxygenase and cyclooxygenase-2. This research experience inspired him to appreciate the importance of high-resolution protein structures in drug development and when he started his graduate studies across the Pacific at the chemistry department of Cornell University, he decided to step into the field of protein structural biology. While at Cornell, Yang joined the lab

of Dr. Richard Cerione and spent most of his PhD years in the dark room working on a light-sensitive G protein-coupled receptor-G protein complex, the rhodopsin-transducin complex, which is a key signaling complex in vertebrate vision. After years of toiling in the dark, both literally and figuratively, Yang finally emerged out of the dark room victorious with possible supernatural night vision and a high-resolution structure of the rhodopsin-transducin complex. In the near future, Yang will continue his research on the vertebrate visual phototransduction system, and attempt to obtain more structures of the signaling proteins involved in vision.

To my parents, Xiangyu Cao and Jun Gao

ACKNOWLEDGEMENT

I would like to thank my advisor Dr. Richard Cerione, who has entrusted me with such a challenging, yet, rewarding project of studying a G protein-coupled receptor-G protein complex and has done his utmost best to provide me with all the resources needed. During my PhD studies, he has given me nothing but encouragement and support and his contagious passion for science has always been an inspiration.

I am really grateful for the mentorship I've received from Dr. Sekar Ramachandran, who has pioneered the research project that I undertook and has taught me everything I know in the lab, from molecular biology to protein purification and crystallization. I would also like to thank Dr. Jon Erickson who is always interested in discussing my research and sharing his insights, and Dr. Shawn Milano who is always willing to lend a helping hand both in lab and in daily life. And to all my other lab mates, I really appreciate their friendship and the attention and suggestions they've provided during numerous student meetings and group meetings.

I am also thankful for the support and advice I've received from my committee members Dr. Brian Crane and Dr. Toshi Kawate during my PhD studies. Dr. Brian Crane's lab, being our next-door neighbor, has always been willing to help whenever we're in need. Dr. Toshi Kawate has generously opened up his lab to us for growing insect cell cultures and using the crystallization robot.

I am really thankful for the fruitful collaboration we've had with Dr. Georgios Skiniotis and his lab member Dr. Hongli Hu at Stanford University in determining complex structures using cryo-EM.

Finally, I would like to thank my parents for their boundless love and support. They have always expressed earnest interest in listening to me talking about my research progress, even though they don’t quite understand protein structural biology.

TABLE OF CONTENTS

LIST OF FIGURES

LIST OF ABBREVIATIONS

GPCR	G protein-coupled receptor
TM	transmembrane helix
ICL	intracellular loop
Rho	rhodopsin
G_T	transducin
α_T	transducin α subunit
GDP	guanosine-5'-diphosphate
GTP	guanosine-5'-triphosphate
GTPγS	guanosine-5'-O-(3-thiotriphosphate)
cGMP	cyclic guanosine monophosphate
PDE	cGMP phosphodiesterase
EM	electron microscopy
cryo-EM	cryo electron microscopy
SAXS	small-angle X-ray scattering

Chapter 1

Introduction

1.1 Vertebrate visual phototransduction

Cells, the minimal functional unit of all living organisms, are separated from their outside environment by the membrane boundary. The ability to sense and respond to extracellular signals and the capability of inter-cellular communications are essential for the survival and prosperity of all living beings. This is typically achieved through the so-called signal transduction triad (receptor-transducer-effector) involving transmembrane receptor proteins that convey outside stimuli across the plasma membrane and the resulting signals are relayed and amplified in the cytoplasm by transducer and effector molecules leading to appropriate cellular responses[1]. The visual phototransduction machinery in vertebrates is a classic example of such a process. Retinal rod cells are highly differentiated neurons that are responsible for the detection of light (Fig. 1a). They are so exquisitely sensitive that the signal from just a single photon can be detected[2,3]. The rod cells are separated into two compartments, the inner and outer segments, by a cilium structure. The rod outer segment (ROS) contains stacks of tightly packed lipid bilayer discs that are enclosed by the rod cell plasma membrane and the disc membranes are highly enriched with proteins that are involved in phototransduction (Fig. 1b), namely the receptor rhodopsin, the transducer tranducin and the effector cGMP phosphodiesterase (PDE6). The receptor rhodopsin is composed of its protein moiety opsin and a covalently bound chromophore *11-cis* retinal. Absorption of a single photon

triggers the *cis-trans* isomerization of retinal, which causes a series of structural changes in opsin, ultimately converting the receptor from an inactive state to an activated signaling state, termed Metarhodopsin II (Meta II), within one millisecond. Transducin is a guanine nucleotide binding protein (G protein) that is GDP-bound in its inactive state. Metarhodopsin II activates transducin by catalyzing the exchange of its nucleotide GDP for GTP. The effector molecule PDE6 contains two non-identical catalytic subunits α_{PDE} and β_{PDE}, which are kept inactive by two inhibitor γ_{PDE} subunits. The GTP-bound transducin can bind to γ_{PDE} subunits and displace them from the catalytic subunits, thus alleviating the inhibition and turning on the cGMP hydrolysis activity of PDE6. The activation of PDE6 lowers cGMP levels in the cytosol. On the rod cell plasma membrane, there are non-gated potassium channels maintaining an ongoing outward K^+ current, which tends to hyperpolarize the photoreceptor cell. There are also cGMP-gated sodium channels on the ROS plasma membrane, which are kept open by the high cGMP concentration in the dark, allowing an inward flux of Na^+ that maintains the rod photoreceptor cells in a partially depolarized state. Depletion of cGMP by PDE6 leads to closure of these cGMP-gated channels, resulting in the hyperpolarization of the rod cell membrane. This hyperpolarization slows down the release of the neurotransmitter glutamate from the synaptic terminal and leads to visual neural responses.[4,5]

The signal from light is amplified in every step of the phototransduction cascade. One photon is sufficient to convert one rhodopsin molecule to its Meta II state, which can activate hundreds of transducin molecules per second[6]. Activated transducin then binds and stimulates PDE6 in a 1:1 or 2:1 stoichiometry[7] and each activated PDE6 can hydrolyze thousands of cGMP second messenger molecules per second[8].

Figure 1.1 Vertebrate visual phototransduction. a, Diagram of a rod photoreceptor cell. **b,** Schematic representation of the receptor-transducer-effector triad in visual phototranduction signaling cascade.

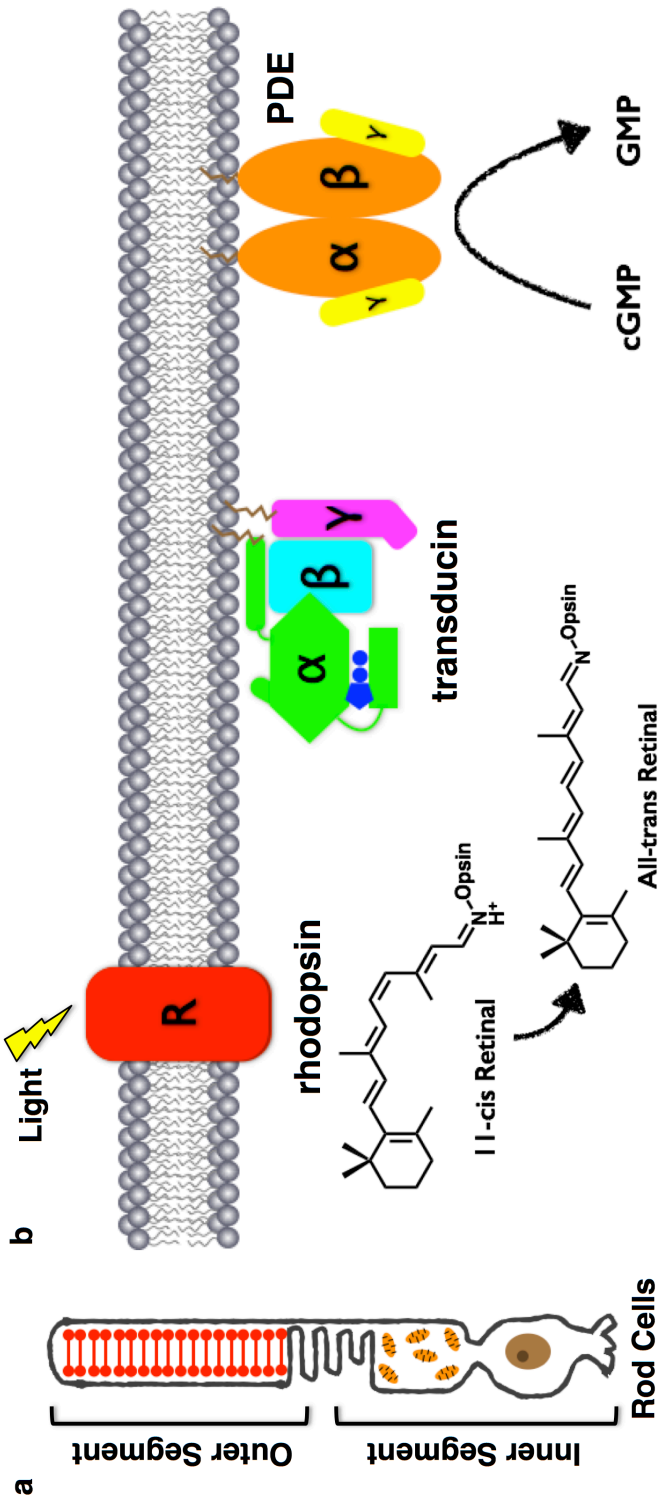
a
Outer Segment
Inner Segment
Rod Cells
b
Light
R
rhodopsin
11-cis Retinal
Opsin
All-trans Retinal
transducin
α
β
γ
PDE
cGMP
GMP

The final stage of amplification is achieved on the cGMP-gated channels. The binding of cGMP on these channels is positively cooperative with a Hill coefficient of about 3 for channel opening[9]. Thus the decrease of cGMP concentration is amplified about 3-fold in the decrease of the inward Na^+ current.

1.2 The G protein-coupled receptor superfamily

The vertebrate visual phototransduction pathway is a classic G protein-coupled receptor (GPCR) signaling cascade, in which the photoreceptor rhodopsin is a prototypical member of the GPCR family of transmembrane proteins. GPCRs constitute the largest group of membrane receptors in humans with over 800 members[10]. They are involved in detecting and transducing signals from an extremely diverse range of extracellular stimuli, including photons, odorants, hormones and neurotransmitters[11]. GPCRs share a signature structural motif of seven transmembrane α helices (TM) with an extracellular N-terminal domain and an intracellular C terminus. The 7TM bundle conveys signals of ligand binding (ligand photoisomerization in the case of rhodopsin) on the extracellular side to conformational changes on its cytoplasm surface, allowing for binding and activation of heterotrimeric G proteins. Based on similarities in sequence and structural features, GPCRs can be classified into five main families, namely rhodopsin, secretin, glutamate, adhesion and frizzled/taste2[12]. The rhodopsin-like GPCRs represent the largest and most studied group with about 700 members. They differ from other GPCR family members in having a much smaller N terminus and most of the rhodopsin-like GPCRs contain an NPxxY motif on TM7 and a DRY motif on the cytoplasm end of TM3, which are important for receptor stabilization and G protein activation[13]. The

secretin-like receptors have a large N terminus containing multiple conserved cysteine bridges that are important for ligand binding and they respond to relatively large peptide hormones, such as glucagon and parathyroid hormone[12]. The glutamate-family receptors form obligate dimers and have large extracellular ligand-binding domains that form a 'Venus flytrap' structure[14]. This family includes the metabotropic receptors for gamma-aminobutyric acid (GABA) and glutamate. Members of the adhesion family contain adhesion-like motifs in the N terminus, such as epidermal growth factor (EGF)-like repeats and mucin-like regions, which are likely to mediate cell-cell adhesion[15]. In addition, they also have GPCR autoproteolysis-inducing (GAIN) domains on the extracellular side that have been shown to modulate receptor activity[16]. The frizzled receptors play crucial roles in developmental biology by transmitting signals from the Wnt family of secreted glycoproteins, which bind to the Cys-rich N-terminal domain of these receptors[17]. As a result of the wide-ranging roles played by GPCRs in human physiology, GPCRs are very effective drug targets with over one third of small-molecule pharmaceuticals today targeting this receptor superfamily[18].

1.3 Heterotrimeric G proteins

G proteins act as binary signaling switches by alternating between two states: the inactive GDP-bound "off" state and the active GTP-bound "on" state[19]. There are two major classes of G proteins: the Ras-related monomeric small G proteins[20] and the large heterotrimeric G proteins[21]. The heterotrimeric G proteins are composed of three subunits: the guanine nucleotide binding α subunit and the constitutively associated β and γ subunits. The α subunit of heterotrimeric G proteins shares a homologous GTPase

domain with small G proteins. However, they differ from Ras-like small G proteins in that the α subunit contains an additional helical domain that forms a clamshell structure over the nucleotide-binding pocket and the GDP-bound α subunit exists in a heterotrimer with the βγ subunits. Activated GPCRs act as guanine nucleotide exchange factors for heterotrimeric G proteins and promote the dissociation of GDP from the nucleotide-binding pocket. The resulting high-affinity ligand-GPCR-nucleotide-free G protein ternary complex forms the active state of GPCR signaling. As the concentration of GTP is much higher than GDP in physiological conditions, GTP can enter the pocket and its binding causes structural changes in the α subunit, lowering its affinity for both βγ subunits and the receptor and resulting in the dissociation of the active-state complex. The GTP-bound α subunit and sometimes the free βγ subunits can engage their downstream effectors to turn on signaling. As the α subunits has an intrinsic GTP hydrolysis activity, which can be further promoted through binding to the regulator of G protein signaling (RGS) proteins, the G protein signaling is terminated with the conversion of GTP to GDP. The GDP-bound α subunit reassociates with βγ subunits to form the inactive-state heterotrimer, thus completing the G protein cycle (Fig. 1.2).

In contrast to the striking diversity of the GPCR superfamily there is only a relatively small number of heterotrimeric G proteins to relay the signals to downstream effectors. In humans, there are 21 α subunits encoded by 16 genes, 6 β subunits encoded by 5 genes, and 12 γ subunits[22]. Several different βγ subunits can interact with the same α subunit isoform, suggesting that subcellular localization and expression levels can be important in modulating G protein signaling[23]. Based on amino acid sequence similarity

in the α subunit, heterotrimeric G proteins can be classified into four main families: G_S, G_i, G_q and G_{12}[24].

One of the best-characterized G proteins is the retinal rod transducin, which belongs to the inhibitory G_i family. X-ray crystal structures have been solved for the transducin α subunit in both the GDP-bound[25] and the GTP-bound[26] states, as well as in its GTP hydrolysis transition state[27]. In addition, structures of the transducin heterotrimer[28] and the transducin α subunit in complex with both its GTPase-activating protein (GAP) RGS9 and a peptide fragment of the effector PDE6[29] have been determined. These structures have provided mechanistic details of how the transducin α subunit is associated with βγ subunits in the inactive state, how it engages the downstream effector and how the signaling is turned off through GTP hydrolysis. The GTPase domain of the α subunit is structurally very similar to the overall architecture of Ras-like small G proteins and contains five α helices (α1-α5) surrounding a six-stranded β sheet (β1-β6) (Fig. 1.3a). It forms the nucleotide-binding pocket by providing the consensus nucleotide-binding sequences found in all G proteins, such as the NKxD motif and the TCAT motif for guanine ring binding and the DxxG Mg^{2+} binding motif. The helical domain is connected to the GTPase domain through two flexible linkers and has a rigid α-helical structure with a long central helix (αA) surrounded by five shorter helices (αB-αF). It forms a lid over the nucleotide-binding pocket burying nucleotides in the core of the α subunit and helps to reduce any spontaneous nucleotide exchange in the absence of an activated receptor. In addition, the helical domain also acts as a built-in GAP domain that provides a key Arg residue, termed the arginine finger, which stabilizes the transition state for GTP hydrolysis and facilitates the release of GTP γ phosphate.

Figure 1.2 The G protein cycle. An activated GPCR engages a heterotrimeric G protein and promotes GDP dissociation from the α subunit, forming the active-state ternary complex. GTP binding to the α subunit causes dissociation of the complex and the GTP-bound α subunit and the free βγ subunits then engage downstream effectors to turn on signaling. Due to the intrinsic GTPase activity of the the α subunit, GTP is converted back to GDP over time and the GDP-bound α re-associates with βγ to reform the heterotrimer.

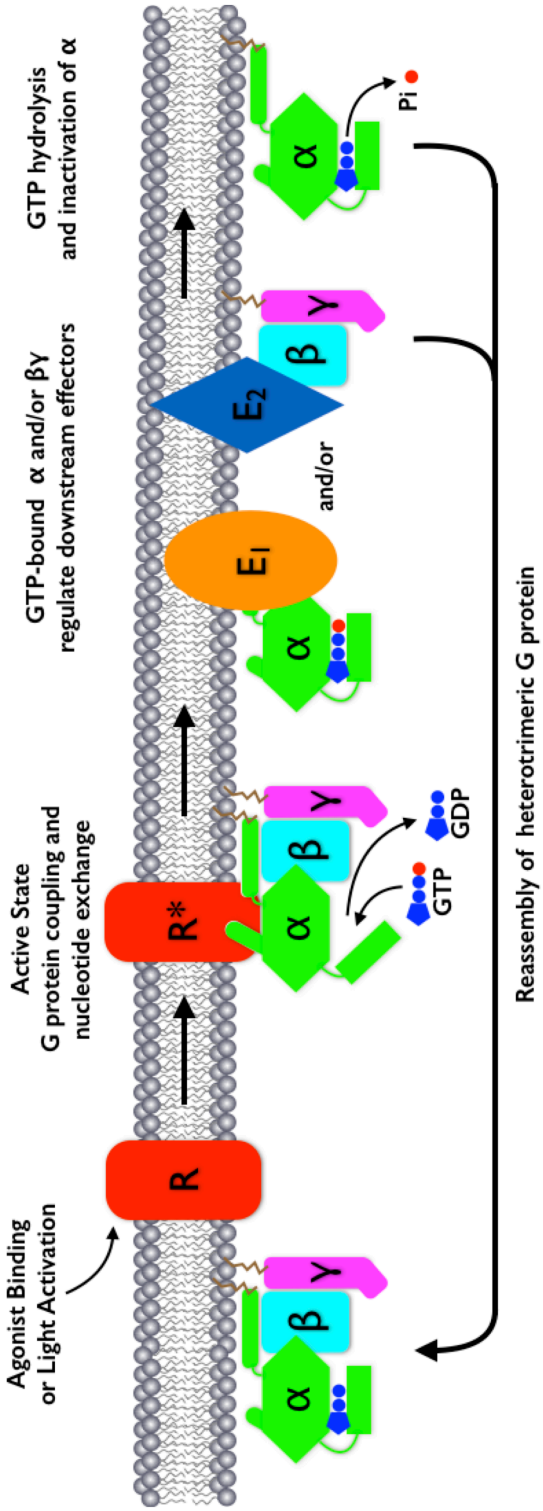
Agonist Binding
or Light Activation
R
Active State
G protein coupling and
nucleotide exchange
R*
GTP
GDP
GTP-bound α and/or βγ
regulate downstream effectors
E1
and/or
E2
GTP hydrolysis
and inactivation of α
Pi
Reassembly of heterotrimeric G protein

Comparisons between the inactive and active state structures of the α subunit have revealed that there are three flexible loops, designated switches I, II and III, in the GTPase domain that undergo significant structural changes upon nucleotide exchange (Fig. 1.3b). These conformational changes are initiated by the direct contact of conserved residues in Switch I and II with the terminal γ phosphate of GTP. These changes are then propagated through a series of conformational transitions to Switch III, which is a unique feature in heterotrimeric G proteins and is involved in effector activation. The β subunit is composed of seven WD40 sequence repeats that form a seven-bladed β-propeller structure in the core of the protein (Fig. 1.3a). The N terminus of the β subunit forms an α helix that is involved in a coiled-coil interaction with the N terminus of the γ subunit, with the C terminus of γ further contributing to the interaction by binding to the β-propeller core of the β subunit. In the GDP-bound inactive state, the α subunit interacts with the βγ subunits through its N-terminal helix and a hydrophobic pocket formed by switches I and II. Both the α and γ subunits are lipid-modified. All α subunits, with the exception of transducin, are palmitoylated at the N terminus and members of the G_i family also have N-terminal myristoylation[30]. All γ subunits undergo post-translational isoprenylation at the C terminus with either a farnesyl ($G\gamma_1$, $G\gamma_8$ and $G\gamma_{11}$) or geranylgeranyl (all others) moiety[31]. The N terminus of the α subunit and the C terminus of the γ subunit are in close proximity with each other and the lipid modifications help to increase the affinity between the α and the βγ subunits and facilitate the localization of the heterotrimer to the membrane[32].

Figure 1.3 G protein structures. a, Structure of the transducin heterotrimer (PDE 1GOT). The α GTPase domain is colored green, the α helical domain is yellow, the β subunit is cyan, the γ subunit is magenta and the switches I, II and III are red. **b,** Comparison between structures of transducin α subunit in GDP-bound (grey) and GTP-bound (green) states. The switches I, II and III are colored red.

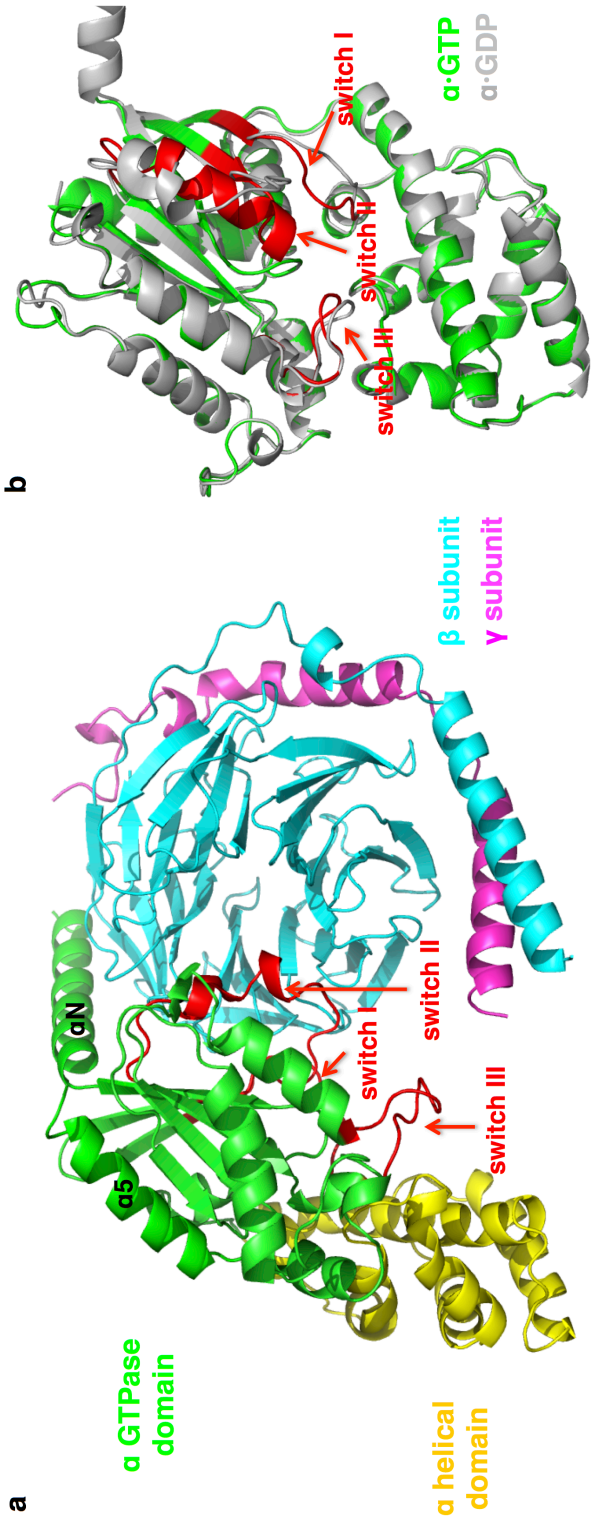
a
α GTPase domain
αN
α5
switch I
switch II
switch III
β subunit
γ subunit
α helical domain
b
switch I
switch II
switch III
α-GTP
α-GDP

1.4 GPCR desensitization

Cells have devised a specialized desensitization mechanism to terminate GPCR signaling. Activated receptors can recruit GPCR kinases (GRK), which phosphorylate the receptor at its C terminal tail. Phosphorylations on the receptor allows for the high-affinity recruitment of arrestin[33], which engages the receptor first at its the C-tail and subsequently binds to the transmembrane core. The latter interaction occludes G protein binding on the receptor and therefore sterically prevents further G protein activation[34,35]. Binding of arrestin also initiates receptor internalization through interactions with the endocytic machinery[36]. Furthermore, arrestins also serve as an alternative signaling system by acting as adaptors and scaffolds for interactions with numerous other signaling molecules, such as Src family nonreceptor tyrosine kinases[37] and ERK1/2 MAP kinase cascades[38]. In this distinctive model of GPCR signaling, arrestin binding mediates distinct downstream signaling events from the receptor at the same time that it uncouples the receptor from activating its cognate G proteins. The finding that arrestin-bound M2 muscarinic receptors exhibit increased affinity for agonists, but not antagonists, has led to the notion that the agonist-receptor-arrestin complex represents an "alterative ternary complex"[39]. Interestingly studies on the secretin-family GPCRs have shown that they are able to promote sustained G protein signaling despite their tight interaction with arrestin[40,41]. More recently, negative-stain electron microscopy studies have provided direct evidence that these receptors are capable of simultaneously interacting with both arrestin and G protein, forming a "megacomplex"[42]. Taken together, GPCR signaling has proven to be far more complex than the canonical receptor-G protein pathway.

1.4 GPCR X-ray crystallography

As GPCRs are capable of sensing diverse ligands and regulating multiple signaling pathways, GPCRs have evolved to be structurally dynamic and adopt various flexible conformations. As a result, they are biochemically unstable once extracted from their native lipid bilayer environment and are very challenging targets for structural studies. The first structural image of a GPCR was obtained in the 1990s with dark-state bovine rhodopsin by using electron diffraction with two-dimensional crystals[43]. This 9Å structure revealed the relative orientation of the seven transmembrane helices in rhodopsin and also proved the existence of a folded extracellular domain. However, due to the low resolution of the structure, amino acid side chains were not resolvable. The first high-resolution GPCR structure was solved by X-ray crystallography for dark-state rhodopsin in the year 2000[44]. In addition to revealing the previously observed 7TM fold, the rhodopsin crystal structure shows that the covalently bound ligand *11-cis* retinal is buried within the top half of the transmembrane bundle and is further occluded from the extracellular side by the N-terminal β-sheet lid, and on the cytoplasm side there is an eighth amphipathic helix parallel to the membrane plane. Subsequently, structures of rhodopsin in the apo state[45], the active *all-trans* retinal-bound state[46] and in complex with a G protein α subunit C-terminal peptide[46] were also determined. The successes of rhodopsin crystallization is largely due to the use of $Zn(OAc)_2$ that precipitates non-ligand-bound receptors during purification and the addition of the small molecule additive heptanetriol that reduces detergent micelle size allowing for exposure of larger polar surfaces on the receptor[47]. However, the methods used for crystallizing rhodopsin cannot be easily applied to the structural determination of other GPCRs. Unlike

rhodopsin, which can be extracted from native bovine retinae in milligram quantities, other GPCRs are not abundant from native sources. Moreover, most GPCRs have long flexible loops connecting the transmembrane helices that would hinder crystallization efforts and they are also significantly less stable than rhodopsin.

The determination of the first human GPCR structure, the β_2 adrenergic receptor[48], in 2007 showcased the first generalizable approach for GPCR crystallization and ushered in a new era of GPCR structural biology with the number of GPCR structures growing rapidly in the following years. As of today, there are over 250 GPCR structures for 52 different GPCRs. Two key technological advances have propelled this recent explosion of new GPCR structures: novel receptor engineering and lipidic cubic phase crystallization.

The first key technique involves engineering the receptor to allow it to become more tractable towards crystallization. There have been two main approaches for GPCR engineering, namely T4 lysozyme fusion[49] and alanine-scanning thermostabilization[50]. As most GPCRs have large flexible loops, especially the 3rd intracellular loop (ICL3), that confers structural heterogeneity to the receptor, which would be problematic in crystallization, the T4 lysozyme fusion method involves replacing ICL3 with a stable soluble protein such as T4 lysozyme. The distance between the N and C termini of T4 lysozyme matches the predicted spanning range of ICL3 and improves the rigidity of this otherwise flexible region. Moreover, the introduction of the soluble protein significantly increases the polar surface on the receptor, which would facilitate crystallographic lattice contacts. Although introduction of the bulky T4 lysozyme often blocks receptor-G protein interactions, the ligand-binding affinity of the engineered receptor typically

remains unaffected, suggesting that the structural features observed in the ligand-binding pocket should be unperturbed. Following the initial successes of T4 lysozyme, many other fusion partners have been developed and have significantly increased the success rate of obtaining high-resolution GPCR structures[51]. The other approach for GPCR engineering involves the use of alanine-scanning mutagenesis coupled with thermostability assays so as to identify mutations that increase the thermostability of the receptor. The rationale behind this approach is that the melting temperature (T_m) of membrane proteins often correlates strongly with their stability in harsh short-chain detergents. The introduction of mutations that increase the T_m of the receptor would allow it to remain stable for the duration of the crystallization process in short-chain detergents, which have small micelles that would expose more hydrophilic surfaces on the receptor, allowing it to be crystallized with conventional *in surfo* vapor diffusion methods. This method was first demonstrated in the determination of the turkey β_1 adrenergic receptor structure[52] and has subsequently been applied to the crystallization of many other GPCRs. And in some challenging cases, both receptor thermostabilization and the introduction of a fusion partner in ICL3 have been utilized and have proven that the two engineering approaches are compatible with each other[53]. The engineered GPCRs need to be expressed in eukaryotic expression systems, such as *Sf9* insect cells, as prokaryotes exhibit very low level of functional receptor expression. Recently, a directed evolutionary method has been developed to allow for simultaneous screening for mutations that allow for both high levels of functional GPCR expression in *E. coli* and increased receptor thermostability, leading to the determination of a GPCR structure in a conformation that is distinct from that obtained from previous engineering methods[54].

The second key technique is lipidic cubic phase crystallography[55]. It involves reconstituting purified detergent-solubilized receptor into a lipid crystalline phase, termed the mesophase, of monoacyl glycerol lipids, such as monoolein. During crystallization trials, the added precipitant reagents permeate the cubic phase through its bicontinuous aqueous channels and induce the formation of local lamella phase patches that act as nucleation centers for crystal formation. The surrounding cubic phase serves as a reservoir of proteins that feed growing crystals that form through ordered stacking of lipid bilayer sheets. This technique was first utilized in the crystallization of bateriorhodopsin in the 1990s[56], but was not widely adopted at the time, as the lipidic cubic phase is difficult to handle due to its high viscosity and there was no efficient high-throughput method for crystallization screening. The development of the coupled-syringe mixing method and crystallization robots capable of dispensing the viscous cubic phase has enabled the application of this method to low-yielding precious samples such as purified GPCRs[57]. The typical crystals grown from the cubic phase are very small and are often invisible after cryo-cooling. The development of bright mini synchrotron X-ray beams and raster-scanning software has been instrumental in enabling structure determination with cubic phase crystals[58].

1.5 Active-state GPCR structures

Most of the GPCR structures determined to date are of the inactive antagonist-bound state. The difficulties in capturing the active-state structure result from the increased conformational plasticity of GPCRs upon activation. Early attempts at the crystallization of the β_2 adrenergic receptor bound to a covalent agonist resulted in a

structure that resembled the inactive conformation[59], suggesting that the active state does not represent the energy minima in such preparations. This has been further supported by molecular dynamics simulations, which revealed spontaneous relaxation of the agonist-bound, activated receptor to the inactive state[59]. Subsequent biophysical characterizations utilizing nuclear magnetic resonance (NMR)[60] and electron paramagnetic resonance (EPR)[61] have shown that high-affinity full agonists alone do not suffice to stabilize the β_2 adrenergic receptor in the active conformation.

In order to stabilize GPCRs in the active state, nanobodies have been developed as a G protein mimetic binding partner for the receptor. Nanobodies are isolated V_{HH} domain fragments derived from single-chain camelid antibodies[62]. Radioligand-binding assays have confirmed that nanobodies are capable of increasing the binding affinity of agonists to receptors in a similar manner as G proteins. The structural rigidity and small size of nanobodies make them ideal crystallization chaperones and the use of a nanobody raised against agonist-bound β_2 adrenergic receptor, termed Nb80, has allowed for the first successful determination of an active-state non-rhodopsin GPCR structure[63]. In addition to being used as a substitute for G proteins in capturing active-state receptors, the development of a different nanobody, Nb35, has proven to be instrumental in obtaining the first high-resolution GPCR-G protein complex structure, the β_2 adrenergic receptor-G_S protein complex[64] (Fig 1.4a). Nb35 was obtained through injecting llamas with liposomes embedded with cross-linked β_2 adrenergic receptor-G_S protein complex. Negative-stain electron microscopy (EM) studies have shown that Nb35 binds at the interface between α and β subunits of the G protein[65]. Nb35 significantly improved the diffraction quality of the complex crystals and contributed to key crystal lattice contacts.

Figure 1.4 Structure of the β_2 adrenergic receptor-G_S protein complex. a, Comparison of the complex structure (PDB 3SN6) with that of the inactive receptor (PDB 2RH1, colored grey). T4 lysozyme is colored orange, the activated receptor is red, the G protein α subunit is green, the β subunit is cyan, the γ subunit is magenta, and Nb35 is yellow. **b,** Comparison between structures of the nucleotide-free complex and the G_i heterotrimer (PDB 1GP2, colored grey).

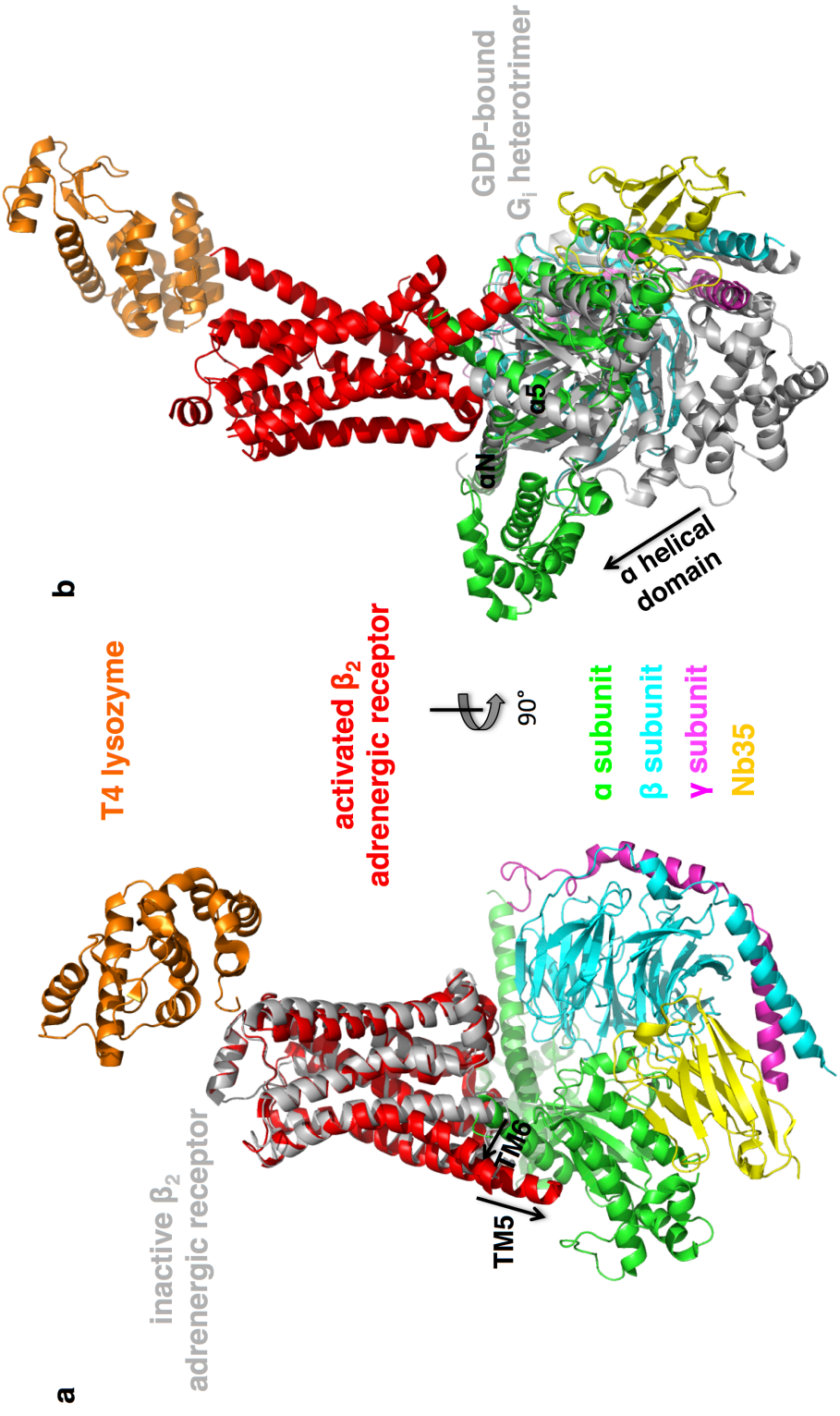
a
b
T4 lysozyme
inactive β_2 adrenergic receptor
activated β_2 adrenergic receptor
90°
GDP-bound G_i heterotrimer
α subunit
β subunit
γ subunit
Nb35
TM5
TM6
αN
α5
α helical domain

Negative-stain EM has also revealed that the helical domain of the G protein α subunit is flexible in the receptor-G protein complex and the addition of a pyrophosphate-mimetic small molecule foscarnet improved the rigidity of the helical domain[65]. As T4 lysozyme fusion at ICL3 would occlude G protein binding, it was fused directly to the N terminal end of TM1 instead replacing the flexible extracellular domain[64]. The addition of T4 lysozyme at the extracellular side significantly increased the polar surface on this end of the complex and contributed to forming crystallographic contacts.

The β_2 adrenergic receptor-G_S protein complex structure reveals that the receptor engages with the G protein only through the α subunit. When compared to the inactive state structure, the most significant changes in the β_2 adrenergic receptor involve a 14Å outward movement of the cytoplasmic end of TM6 accompanied by a downward extension of TM5 (Fig. 1.4a). These conformational changes open up a binding surface for the G protein on the cytoplasmic side of the receptor. The most striking changes in the G protein involve the 127° rotation of the helical domain relative to the GTPase domain of the α subunit (Fig. 1.4b). Similar domain separation in the active-state complex has also been observed in double electron-electron resonance (DEER) spectroscopy studies on the rhodopsin-G_i protein complex[66]. In the nucleotide-free complex, the C terminal α5 helix of the α subunit extends upward to insert into the cleft opened up by the conformational changes in receptor TM5 and TM6 of the receptor (Fig. 1.4b). The α5 helix connects receptor interaction to the nucleotide-binding pocket through its connection to the β6-α5 loop, which contains the conserved TCAT motif for binding the guanine base. In addition, the activated β_2 adrenergic receptor also interacts with the αN-β1 loop, which is linked to the GDP β-phosphate binding P-loop through the β1 strand.

Hydrogen-deuterium exchange mass spectrometry (HXMS) studies of the β_2 adrenergic receptor-G_S protein complex have revealed that there is elevated deuterium exchange in both the N terminal part of the α5 helix and the β1 strand[67], supporting the notion that the receptor promotes GDP dissociation by perturbing both the β6-α5 loop and the P-loop.

1.6 Overview of thesis research

My thesis research started on the heels of the *tour de force* structure of the β_2 adrenergic receptor-G_S protein complex. The ultimate goal is to obtain a high-resolution structure of the rhodopsin-transducin complex, which is the GPCR-G protein complex involved in vertebrate scotoptic vision. The determination of such a structure would shed light on key questions that still surround the mechanisms underlying GPRC-G protein interactions.

The first key question concerns the role of the G protein βγ subunits in the G protein activation process. Comparison of the structure of the nucleotide-free G_S protein to that of the GDP-bound G protein heterotrimer shows that there is little change in the conformation of the βγ subunits. The activated β_2 adrenergic receptor does not interact with the βγ subunits of the G_S protein. Therefore, based on the complex structure, it seems likely that the function of the βγ subunits is merely to stabilize the N terminus of the α subunit and help present the α subunit for engagement with the activated receptor. However, a significant amount of earlier biophysical evidence has suggested that the βγ subunits may play an active role in G protein activation. Alanine-scanning mutagenesis performed on the transducin β subunit has identified several β subunit mutants that behave normally in G protein heterotrimer assembly, but are functionally impaired in

supporting rhodopsin-catalyzed nucleotide exchange[68]. Also a farnesylated C-terminal peptide of transducin γ subunit has been shown to stabilize the active MetaII state of rhodopsin[69] and this Gγ peptide forms an amphipathic helix upon interaction with activated rhodopsin based on NMR studies[70]. Therefore, additional GPCR-G protein complex structures may reveal features in the βγ subunits that would shed further light on their role in GPCR-dependent G protein activation.

The second key question is how different GPCRs selectively engage their cognate G proteins. The β_2 adrenergic receptor-G_S protein complex still remains the only GPCR-G protein crystal structure solved to date. In the past few years, with the development of direct-electron detectors[71] and motion-correction software[72], cryo electron microscopy (cryo-EM) has emerged as a powerful tool for high-resolution protein structure determination. Cryo-EM has been utilized to determine the structures of two secretin-family GPCRs, the calcitonin receptor[73] and the glucagon-like peptide 1 (GLP1) receptor[74,75], bound to G_S proteins. In the past few months, structures of four additional complexes between different GPCRs and the inhibitory G_i family proteins, namely the μ-opioid receptor[76], rhodopsin[77], and adenosine A1 receptor[78] complexed with the G_i protein and the serotonin 5-HT_{1B} receptor-G_O complex[79], have been solved by cryo-EM. These recent structures reveal that the G_S protein engages different receptors in virtually the same conformation and the G_i family proteins interact with activated GPCRs in a slightly different orientation than the G_S protein. However, the G protein-interacting residues on these different receptors are not conserved and there does not seem to be a correlation between the existence of specific residues on the receptor and the G protein-coupling preference. Therefore, the G protein specificity is likely to be determined by

more complex three-dimensional topology on the cytoplasmic end of the receptor. Additional GPCR-G protein complex structures would be needed to allow for predictions of the G protein-coupling preference based on receptor primary sequence. The G protein transducin is a member of the inhibitory G_i family and the structure of the rhodopsin-transducin complex would help to provide further insights into the structural determinants of receptor-G protein interaction.

As described in chapter 2, we have been able to extract a light-activated rhodopsin-transducin complex from the native retinal membrane using detergents and then purify this complex by using affinity and size exclusion chromatography. The resulting rhodopsin-transducin complex is active, as it readily dissociates upon the addition of GTP. Negative-stain electron microscopy and small-angle X-ray scattering have been utilized to biophysically characterize the purified complex and have revealed that the particles are monodisperse and that the helical domain of the transducin α subunit adopts flexible open conformations, similar to what has been observed for the β_2 adrenergic receptor-G_S complex.

We have been able to obtain a 4.5Å-resolution structure of the rhodopsin-transducin complex using cryo-EM, as described in chapter 3. Surprisingly this structure reveals that the G protein transducin engages the receptor in an orientation significantly different from those in both the G_S complex structures and other G_i complex structures. Furthermore, our structure points to a possible interaction between the G protein α helical domain and the β subunit, which may play an active role in G protein activation.

REFERENCES

1. Rodbell, M. The role of hormone receptors and GTP-regulatory proteins in membrane transduction. *Nature* **284,** 17–22 (1980).
2. Baylor, D. A., Lamb, T. D. & Yau, K. W. Responses of retinal rods to single photons. *J. Physiol.* **288,** 613–634 (1979).
3. Sampath, A. P. & Rieke, F. Selective transmission of single photon responses by saturation at the rod-to-rod bipolar synapse. *Neuron* **41,** 431–443 (2004).
4. Burns, M. E. & Baylor, D. A. Activation, deactivation, and adaptation in vertebrate photoreceptor cells. *Annu. Rev. Neurosci.* **24,** 779–805 (2001).
5. Arshavsky, V. Y., Lamb, T. D. & Pugh, E. N. G proteins and phototransduction. *Annu. Rev. Physiol.* **64,** 153–187 (2002).
6. Vuong, T. M., Chabre, M. & Stryer, L. Millisecond activation of transducin in the cyclic nucleotide cascade of vision. *Nature* **311,** 659–661 (1984).
7. Min, K. C., Gravina, S. A. & Sakmar, T. P. Reconstitution of the vertebrate visual cascade using recombinant heterotrimeric transducin purified from Sf9 cells. *Protein Expr. Purif.* **20,** 514–526 (2000).
8. Wensel, T. G. & Stryer, L. Reciprocal control of retinal rod cyclic GMP phosphodiesterase by its γ subunit and transducin. *Proteins Struct. Funct. Bioinforma.* **1,** 90–99
9. Burns, M. E. & Arshavsky, V. Y. Beyond Counting Photons: Trials and Trends in Vertebrate Visual Transduction. *Neuron* **48,** 387–401 (2005).

10. Bjarnadóttir, T. K. *et al.* Comprehensive repertoire and phylogenetic analysis of the G protein-coupled receptors in human and mouse. *Genomics* **88,** 263–273 (2006).

11. Kristiansen, K. Molecular mechanisms of ligand binding, signaling, and regulation within the superfamily of G-protein-coupled receptors: molecular modeling and mutagenesis approaches to receptor structure and function. *Pharmacol. Ther.* **103,** 21–80 (2004).

12. Fredriksson, R., Lagerström, M. C., Lundin, L.-G. & Schiöth, H. B. The G-Protein-Coupled Receptors in the Human Genome Form Five Main Families. Phylogenetic Analysis, Paralogon Groups, and Fingerprints. *Mol. Pharmacol.* **63,** 1256–1272 (2003).

13. Ballesteros, J. A., Shi, L. & Javitch, J. A. Structural mimicry in G protein-coupled receptors: implications of the high-resolution structure of rhodopsin for structure-function analysis of rhodopsin-like receptors. *Mol. Pharmacol.* **60,** 1–19 (2001).

14. Kunishima, N. *et al.* Structural basis of glutamate recognition by a dimeric metabotropic glutamate receptor. *Nature* **407,** 971–977 (2000).

15. Stacey, M., Lin, H. H., Gordon, S. & McKnight, A. J. LNB-TM7, a group of seven-transmembrane proteins related to family-B G-protein-coupled receptors. *Trends Biochem. Sci.* **25,** 284–289 (2000).

16. Paavola, K. J., Stephenson, J. R., Ritter, S. L., Alter, S. P. & Hall, R. A. The N Terminus of the Adhesion G Protein-coupled Receptor GPR56 Controls Receptor Signaling Activity. *J. Biol. Chem.* **286,** 28914–28921 (2011).

17. Dann, C. E. *et al.* Insights into Wnt binding and signalling from the structures of two Frizzled cysteine-rich domains. *Nature* **412,** 86–90 (2001).

18. Santos, R. *et al.* A comprehensive map of molecular drug targets. *Nat. Rev. Drug Discov.* **16,** 19–34 (2017).

19. Vetter, I. R. & Wittinghofer, A. The guanine nucleotide-binding switch in three dimensions. *Science* **294,** 1299–1304 (2001).

20. Rojas, A. M., Fuentes, G., Rausell, A. & Valencia, A. The Ras protein superfamily: evolutionary tree and role of conserved amino acids. *J. Cell Biol.* **196,** 189–201 (2012).

21. Anantharaman, V., Abhiman, S., de Souza, R. F. & Aravind, L. Comparative genomics uncovers novel structural and functional features of the heterotrimeric GTPase signaling system. *Gene* **475,** 63–78 (2011).

22. Downes, G. B. & Gautam, N. The G protein subunit gene families. *Genomics* **62,** 544–552 (1999).

23. Graf, R. *et al.* Studies on the interaction of α subunits of GTP-binding proteins with βγ dimers. *Eur. J. Biochem.* **210,** 609–619

24. Simon, M. I., Strathmann, M. P. & Gautam, N. Diversity of G proteins in signal transduction. *Science* **252,** 802–808 (1991).

25. Lambright, D. G., Noel, J. P., Hamm, H. E. & Sigler, P. B. Structural determinants for activation of the α-subunit of a heterotrimeric G protein. *Nature* **369,** 621–628 (1994).

26. Noel, J. P., Hamm, H. E. & Sigler, P. B. The 2.2 Å crystal structure of transducin-α complexed with GTPγS. *Nature* **366,** 654–663 (1993).

27. Sondek, J., Lambright, D. G., Noel, J. P., Hamm, H. E. & Sigler, P. B. GTPase mechanism of Gproteins from the 1.7-Å crystal structure of transducin α - GDP AIF−4. *Nature* **372,** 276–279 (1994).

28. Lambright, D. G. *et al.* The 2.0 Å crystal structure of a heterotrimeric G protein. *Nature* **379,** 311–319 (1996).

29. Slep, K. C. *et al.* Structural determinants for regulation of phosphodiesterase by a G protein at 2.0 Å. *Nature* **409,** 1071–1077 (2001).

30. Chen, C. A. & Manning, D. R. Regulation of G proteins by covalent modification. *Oncogene* **20,** 1643–1652 (2001).

31. Zhang, F. L. & Casey, P. J. Protein prenylation: molecular mechanisms and functional consequences. *Annu. Rev. Biochem.* **65,** 241–269 (1996).

32. Harald R. Seitz, ‡ *et al.* Molecular Determinants of the Reversible Membrane Anchorage of the G-Protein Transducin†. (1999). doi:10.1021/bi990298+

33. Moore, C. A. C., Milano, S. K. & Benovic, J. L. Regulation of receptor trafficking by GRKs and arrestins. *Annu. Rev. Physiol.* **69,** 451–482 (2007).

34. Shukla, A. K. *et al.* Visualization of arrestin recruitment by a G-protein-coupled receptor. *Nature* **512,** 218–222 (2014).

35. Kang, Y. *et al.* Crystal structure of rhodopsin bound to arrestin by femtosecond X-ray laser. *Nature* **523,** 561–567 (2015).

36. Ferguson, S. S. Evolving concepts in G protein-coupled receptor endocytosis: the role in receptor desensitization and signaling. *Pharmacol. Rev.* **53,** 1–24 (2001).

37. Luttrell, L. M. *et al.* Beta-arrestin-dependent formation of beta2 adrenergic receptor-Src protein kinase complexes. *Science* **283,** 655–661 (1999).

38. McDonald, P. H. *et al.* Beta-arrestin 2: a receptor-regulated MAPK scaffold for the activation of JNK3. *Science* **290,** 1574–1577 (2000).

39. Gurevich, V. V., Pals-Rylaarsdam, R., Benovic, J. L., Hosey, M. M. & Onorato, J. J. Agonist-receptor-arrestin, an alternative ternary complex with high agonist affinity. *J. Biol. Chem.* **272,** 28849–28852 (1997).

40. Calebiro, D. *et al.* Persistent cAMP-signals triggered by internalized G-protein-coupled receptors. *PLoS Biol.* **7,** e1000172 (2009).

41. Feinstein, T. N. *et al.* Noncanonical control of vasopressin receptor type 2 signaling by retromer and arrestin. *J. Biol. Chem.* **288,** 27849–27860 (2013).

42. Thomsen, A. R. B. *et al.* GPCR-G Protein-β-Arrestin Super-Complex Mediates Sustained G Protein Signaling. *Cell* **166,** 907–919 (2016).

43. Schertler, G. F. X., Villa, C. & Henderson, R. Projection structure of rhodopsin. *Nature* **362,** 770–772 (1993).

44. Palczewski, K. *et al.* Crystal Structure of Rhodopsin: A G Protein-Coupled Receptor. *Science* **289,** 739–745 (2000).

45. Park, J. H., Scheerer, P., Hofmann, K. P., Choe, H.-W. & Ernst, O. P. Crystal structure of the ligand-free G-protein-coupled receptor opsin. *Nature* **454,** 183–187 (2008).

46. Choe, H.-W. *et al.* Crystal structure of metarhodopsin II. *Nature* **471,** 651–655 (2011).

47. Okada, T. *et al.* X-Ray diffraction analysis of three-dimensional crystals of bovine rhodopsin obtained from mixed micelles. *J. Struct. Biol.* **130,** 73–80 (2000).

48. Cherezov, V. *et al.* High-Resolution Crystal Structure of an Engineered Human β2-Adrenergic G Protein–Coupled Receptor. *Science* **318,** 1258–1265 (2007).

49. Rosenbaum, D. M. *et al.* GPCR Engineering Yields High-Resolution Structural Insights into β2-Adrenergic Receptor Function. *Science* **318,** 1266–1273 (2007).

50. Serrano-Vega, M. J., Magnani, F., Shibata, Y. & Tate, C. G. Conformational thermostabilization of the β1-adrenergic receptor in a detergent-resistant form. *Proc. Natl. Acad. Sci.* **105,** 877–882 (2008).

51. Chun, E. *et al.* Fusion Partner Toolchest for the Stabilization and Crystallization of G Protein-Coupled Receptors. *Struct. England1993* **20,** 967–976 (2012).

52. Warne, T. *et al.* Structure of a β_1-adrenergic G-protein-coupled receptor. *Nature* **454,** 486–491 (2008).

53. White, J. F. *et al.* Structure of the agonist-bound neurotensin receptor. *Nature* **490,** 508–513 (2012).

54. Egloff, P. *et al.* Structure of signaling-competent neurotensin receptor 1 obtained by directed evolution in Escherichia coli. *Proc. Natl. Acad. Sci.* **111,** E655–E662 (2014).

55. Caffrey, M. & Cherezov, V. Crystallizing Membrane Proteins Using Lipidic Mesophases. *Nat. Protoc.* **4,** 706–731 (2009).

56. Pebay-Peyroula, E., Rummel, G., Rosenbusch, J. P. & Landau, E. M. X-ray structure of bacteriorhodopsin at 2.5 angstroms from microcrystals grown in lipidic cubic phases. *Science* **277,** 1676–1681 (1997).

57. Caffrey, M. A comprehensive review of the lipid cubic phase or in meso method for crystallizing membrane and soluble proteins and complexes. *Acta Crystallogr. Sect. F Struct. Biol. Commun.* **71,** 3–18 (2015).

58. Smith, J. L., Fischetti, R. F. & Yamamoto, M. Micro-crystallography comes of age. *Curr. Opin. Struct. Biol.* **22,** 602–612 (2012).

59. Rosenbaum, D. M. *et al.* Structure and Function of an Irreversible Agonist-β2 Adrenoceptor complex. *Nature* **469,** 236–240 (2011).

60. Nygaard, R. *et al.* The Dynamic Process of β2-Adrenergic Receptor Activation. *Cell* **152,** 532–542 (2013).

61. Manglik, A. *et al.* Structural Insights into the Dynamic Process of β 2 - Adrenergic Receptor Signaling. *Cell* **161,** 1101–1111 (2015).

62. Steyaert, J. & K Kobilka, B. Nanobody stabilization of G protein coupled receptor conformational states. *Curr. Opin. Struct. Biol.* **21,** 567–572 (2011).

63. Rasmussen, S. G. F. *et al.* Structure of a nanobody-stabilized active state of the β_2 adrenoceptor. *Nature* **469,** 175–180 (2011).

64. Rasmussen, S. G. F. *et al.* Crystal structure of the β2 adrenergic receptor–Gs protein complex. *Nature* **477,** 549–555 (2011).

65. Westfield, G. H. *et al.* Structural flexibility of the Gαs α-helical domain in the β2-adrenoceptor Gs complex. *Proc. Natl. Acad. Sci.* **108,** 16086–16091 (2011).

66. Van Eps, N. *et al.* Interaction of a G protein with an activated receptor opens the interdomain interface in the alpha subunit. *Proc. Natl. Acad. Sci. U. S. A.* **108,** 9420–9424 (2011).

67. Chung, K. Y. *et al.* β2 adrenergic receptor-induced conformational changes in the heterotrimeric G protein Gs. *Nature* **477,** 611–615 (2011).

68. Ford, C. E. *et al.* Molecular Basis for Interactions of G Protein βγ Subunits with Effectors. *Science* **280,** 1271–1274 (1998).

69. Kisselev, O., Pronin, A., Ermolaeva, M. & Gautam, N. Receptor-G Protein Coupling is Established by a Potential Conformational Switch in the βγ Complex. *Proc. Natl. Acad. Sci. U. S. A.* **92,** 9102–9106 (1995).

70. Kisselev, O. G. & Downs, M. A. Rhodopsin controls a conformational switch on the transducin gamma subunit. *Struct. Lond. Engl. 1993* **11,** 367–373 (2003).

71. Li, X. *et al.* Electron counting and beam-induced motion correction enable near-atomic-resolution single-particle cryo-EM. *Nat. Methods* **10,** 584–590 (2013).

72. Zheng, S. Q. *et al.* MotionCor2: anisotropic correction of beam-induced motion for improved cryo-electron microscopy. *Nat. Methods* **14,** 331–332 (2017).

73. Liang, Y.-L. *et al.* Phase-plate cryo-EM structure of a class B GPCR–G-protein complex. *Nature* **546,** 118–123 (2017).

74. Zhang, Y. *et al.* Cryo-EM structure of the activated GLP-1 receptor in complex with a G protein. *Nature* **546,** 248–253 (2017).

75. Liang, Y.-L. *et al.* Phase-plate cryo-EM structure of a biased agonist-bound human GLP-1 receptor–Gs complex. *Nature* **555,** 121–125 (2018).

76. Koehl, A. *et al.* Structure of the μ-opioid receptor–G i protein complex. *Nature* 1 (2018). doi:10.1038/s41586-018-0219-7

77. Kang, Y. *et al.* Cryo-EM structure of human rhodopsin bound to an inhibitory G protein. *Nature* 1 (2018). doi:10.1038/s41586-018-0215-y

78. Draper-Joyce, C. J. *et al.* Structure of the adenosine-bound human adenosine A 1 receptor–G i complex. *Nature* 1 (2018). doi:10.1038/s41586-018-0236-6

79. García-Nafría, J., Nehmé, R., Edwards, P. C. & Tate, C. G. Cryo-EM structure of the serotonin 5-HT 1B receptor coupled to heterotrimeric G o. *Nature* 1 (2018). doi:10.1038/s41586-018-0241-9

Chapter 2

Isolation and Structure-function Characterization of the Rhodopsin-Transducin Complex

INTRODUCTION

G protein-coupled receptors (GPCRs), the largest family of transmembrane proteins, are the targets for nearly 50% of all pharmaceutical drugs (1). These receptors modulate cellular responses to a vast array of extracellular signals through the activation of heterotrimeric G proteins, with the active state being defined as the complex that forms between the agonist-bound (or light-stimulated) GPCR and nucleotide-free G protein (2). Attempts to obtain structural information for GPCRs, and especially for signaling-active GPCR-G protein complexes, have garnered a great deal of interest, both as a means to better understand the underlying mechanisms by which this important family of receptors mediates a wide range of biological outcomes, and as a critical step in the design of more selective and effective drug treatments. Recent technological advancements, including novel protein engineering (3), *in meso* crystallization (4) and micro-focus beamlines at synchrotron facilities (5), have ushered in significant progress in the determination of high-resolution GPCR structures. However, only a few of those structures are of activated GPCRs, and thus far, only two GPCR-G protein complex structures have been solved, namely that of the β_2-adrenergic receptor-G_S protein complex (6), and the calcitonin receptor-G_S protein complex (7). Furthermore, virtually all of these structures, with the

This chapter is adapted from an article originally published in the Journal of Biological Chemistry.
Gao, Y. *et al.* Isolation and structure–function characterization of a signaling-active rhodopsin–G protein complex. *J. Biol. Chem.* **292,** 14280–14289 (2017).

exception of rhodopsin, have been obtained with GPCRs which were heavily modified so as to facillitate crystallization. Therefore, to help fully understand the mechanisms of GPCR-mediated G protein activation, it will be important to obtain structural information of active complexes formed between native receptors and their different G protein partners.

Rhodopsin, the photoreceptor responsible for dim light vision, is a prototypical member of the GPCR superfamily. Absorption of a single photon by rhodopsin activates many transducin (G_T) molecules (the subunits designated as α_T, β_1, and γ_1) in less than a second, generating GTP-bound α_T subunits that activate the effector enzyme, cGMP phosphodiesterase (PDE) (8). The photo-transduction system offers certain advantages for obtaining structural insights into GPCR-signaling, as its principle components can be purified from native tissue in large quantities. As a result, rhodopsin represents the first and only GPCR for which X-ray crystal structures (9-13) have been solved in the native form.

The determination of an X-ray crystal structure of an activated rhodopsin-transducin complex not only is essential to providing a comprehensive picture of photo-transduction, but also for obtaining a better understanding of how the specificity between GPCRs and G proteins is achieved, as well as establishing the stoichiometry of the GPCR-G protein complex in the signaling-active state. In order to facilitate future crystallographic studies, here we describe a milligram-scale purification of an active rhodopsin-G protein complex formed with native light-activated rhodopsin (Rho) and a $G\alpha_T/G\alpha_{i1}$ chimera (α_T) together with the retinal β_1 and γ_1 subunits (G_T). The resulting complex is stable and homogeneous, and the stoichiometry between Rho and G_T is 1:1, as determined by both

UV/Vis spectroscopy and radiolabeled nucleotide binding. Small angle X-ray scattering (SAXS) studies conducted with the purified Rho-G_T complex further confirm that the complex is monodisperse, and molecular weight values calculated based on SAXS data suggest that the complex is composed of a monomeric Rho bound to one G_T molecule. Negative-stain electron microscopy (EM) analyses of the complex confirm its homogeneity and reveal an overall architecture that is reminiscent of both EM (14) and crystallographic (6) results of the β_2-adrenergic receptor-G_S protein complex.

RESULTS

Detergent selection for Rho-G_T complex purification

In order to purify the Rho-G_T complex, a suitable detergent is needed not only to extract the complex from its native rod outer segment membrane, but also to maintain its stability. The first crystal structures of rhodopsin were solved using receptor solubilized in short-chain detergents, such as nonylglucoside (9), C_8E_4 (10), and octylglucoside (11-13). Although these detergents can maintain the stability of dark inactivated rhodopsin for several days, the complex formed with light-activated rhodopsin and transducin cannot survive the extraction process and dissociates quickly upon solubilization. Therefore, we set out to select a detergent in which the Rho-G_T complex would remain stably associated.

A fluorescence assay, monitoring the change in the intrinsic tryptophan fluorescence of α_T upon nucleotide exchange (15), was utilized to examine the rhodopsin-catalyzed nucleotide exchange activity in various detergents. When α_T exchanges GDP for GTPγS, a non-hydrolyzable GTP analog, there is an increase in the intrinsic tryptophan

fluorescence due to a conformational change in the Switch II region, one of three regions of α_T that change conformation upon GTP binding. Therefore, the rate of Rho-catalyzed nucleotide exchange can be used to assay the activity of Rho under various detergent conditions. Commercially available detergents from the maltoside and maltose neopentyl glycol (MNG) (16) families were tested. Most of these detergents were able to maintain the Rho-catalyzed nucleotide exchange activity at higher concentrations than their corresponding critical micelle concentration (i.e. 2 × CMC), with a rate constant of ~3 min^{-1} (Figs. 2.1A and 2.1B). There is a clear dependence of Rho activity on the length of the detergent hydrophobic chain. However, when using detergent concentrations above or below 2 × CMC, the Rho-stimulated nucleotide exchange activity in most of the tested detergents decreased significantly (Fig. 2.1C, see dodecyl maltoside), suggesting that these detergents are not well-suited for extracting the complex from rod outer segment (ROS) membranes, for which an initial high detergent concentration (typically around 1% w/v) would be required. Of the various detergents tested, only LMNG (lauryl maltose neopentyl glycol) was able to maintain high Rho-stimulated nucleotide exchange activity at various concentrations (Fig. 2.1D) and was therefore selected to be used for Rho-G_T complex purification.

Purification of the Rho-G_T complex

The purification scheme for the Rho-G_T complex is illustrated in Fig. 2.2A. The Coomassie blue-stained SDS-PAGE profiles for the proteins at each step of the purification scheme are shown in Fig. 2.2B.

Figure 2.1 Rho-catalyzed nucleotide exchange activity of α_T in various detergents. A. Tryptophan fluorescence emission profiles of Rho-catalyzed nucleotide exchange in maltoside detergents at a concentration of 2xcmc (HM: Hexyl Maltoside, NM: Nonyl Maltoside, DM: Decyl Maltoside, UM: Undecyl Maltoside, DDM: Dodecyl Maltoside), *Inset*: rate constants obtained from single exponential fits of the data (n=3). B. Tryptophan fluorescence emission profiles of Rho-catalyzed nucleotide exchange in maltose neopentyl glycol detergents at a concentration of 2xcmc (OMNG: Octyl Maltose Neopentyl Glycol, DMNG: Decyl Maltose Neopentyl Glycol, LMNG: Lauryl Maltose Neopentyl Glycol), *Inset*: rate constants obtained from single exponential fits of the data (n=3). C. Tryptophan fluorescence emission profiles of Rho-catalyzed nucleotide exchange in DDM at various detergent concentrations (cmc=0.0087% w/v). D. Tryptophan fluorescence emission profiles of Rho-catalyzed nucleotide exchange in LMNG at various detergent concentrations (cmc=0.001% w/v).

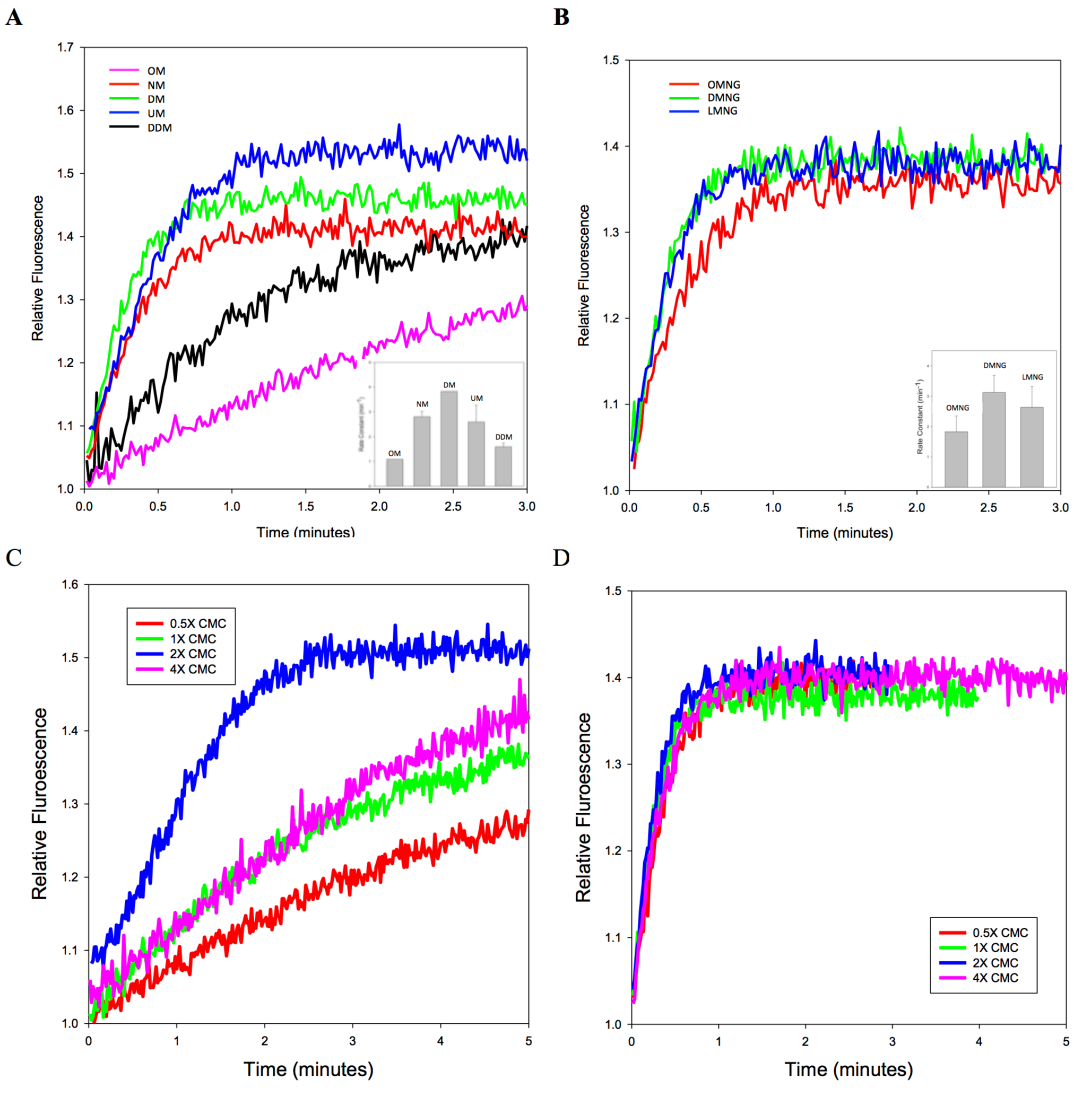
A
OM
NM
DM
UM
DDM
Relative Fluorescence
Time (minutes)
B
OMNG
DMNG
LMNG
Relative Fluorescence
Time (minutes)
C
0.5X CMC
1X CMC
2X CMC
4X CMC
Relative Fluroescence
Time (minutes)
D
0.5X CMC
1X CMC
2X CMC
4X CMC
Relative Fluroescence
Time (minutes)

Figure 2.2 Purification of the Rho-G_T complex. A, Purification scheme. B, SDS-PAGE gel of the purification process (This is a representative of more than 20 repetitions of the purification process).

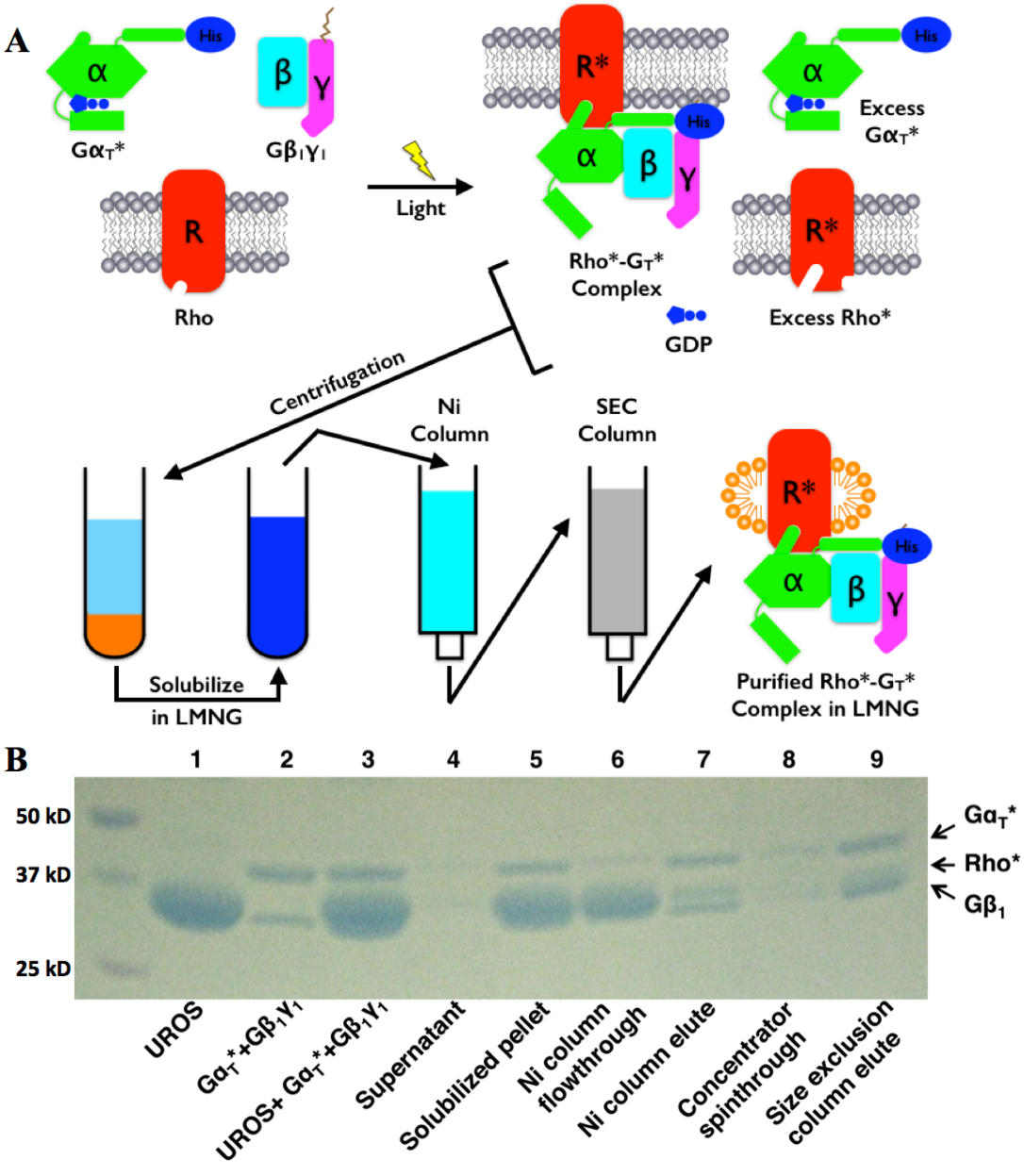
A
His
α
β
γ
Gαt*
Gβ1γ1
R
Rho
Light
R*
Rho*-Gt*
Complex
GDP
Excess
Gαt*
Excess Rho*
Centrifugation
Ni
Column
SEC
Column
Solubilize
in LMNG
Purified Rho*-Gt*
Complex in LMNG
B
1
2
3
4
5
6
7
8
9
50 kD
37 kD
25 kD
Gαt*
Rho*
Gβ1
UROS
Gαt*+Gβ1γ1
UROS+ Gαt*+Gβ1γ1
Supernatant
Solubilized pellet
Ni column
flowthrough
Ni column elute
Concentrator
spinthrough
Size exclusion
column elute

The complex was formed by first mixing α_T, a chimeric protein comprised of an α_T backbone with a stretch of residues from α_{i1}, with $\beta_1\gamma_1$ in a 1:1:1 molar ratio.

The α_T subunit was expressed in *E. coli* with an N-terminal His_6-tag and purified by Ni-NTA chromatography followed by ion exchange and size exclusion chromatography. The $\beta_1\gamma_1$ complex was purifed from bovine retina. The resulting G_T heterotrimer was then mixed with urea-washed bovine ROS membranes containing native Rho in its dark state. Because of the high-density of Rho in ROS, a significant amount of Rho may not be accessible to G_T upon light-activation. Therefore, a substantial excess of Rho was used to assemble the Rho-G_T complex (typically 7 Rho per G_T). The mixture was subjected to illumination at 4ºC, resulting in the light-activation of Rho (Rho) and the induction of complex formation on the native ROS membranes. The mixture was then centrifuged and, as a result, the Rho-G_T complex and excess Rho were in the pellet, whereas the GDP released during G_T activation, together with the unbound α_T subunit, remained in the supernatant. The pellet was solubilized with buffer containing the detergent LMNG and applied to a Ni-sepharose column. Due to the His_6-tag present at the N-terminus of α_T, the Rho-G_T complex remained bound to the column and was thus separated from free Rho. The Rho-G_T complex was eluted from the column with imidazole and further purified by size exclusion chromatography. The Rho-G_T complex eluted as a single symmetrical peak (Fig. 2.3C). The yield of a typical purification process was about 80% based on the amount of $\beta_1\gamma_1$ complex used.

Figure 2.3 Stoichiometry determination and SEC profiles of the purified Rho-G_T complex A, UV-Vis spectrum of purified complex. (This is a representative of more than 20 similar specta of the purified complex) B, Rho:G_T ratio determined by [^{35}S]GTPγS binding assay and rhodopsin A_{380nm}. (This experiment was repeated 3 times) C, SEC profiles of purified complex (red) and complex dissociation with the addition of GTPγS (green). (This is a representative of more than 10 similar sets of SEC profiles) D, SEC profiles of Day 1 (blue) and Day 7 (orange) complexes. (This is a representative of more than 20 similar sets of SEC profiles)

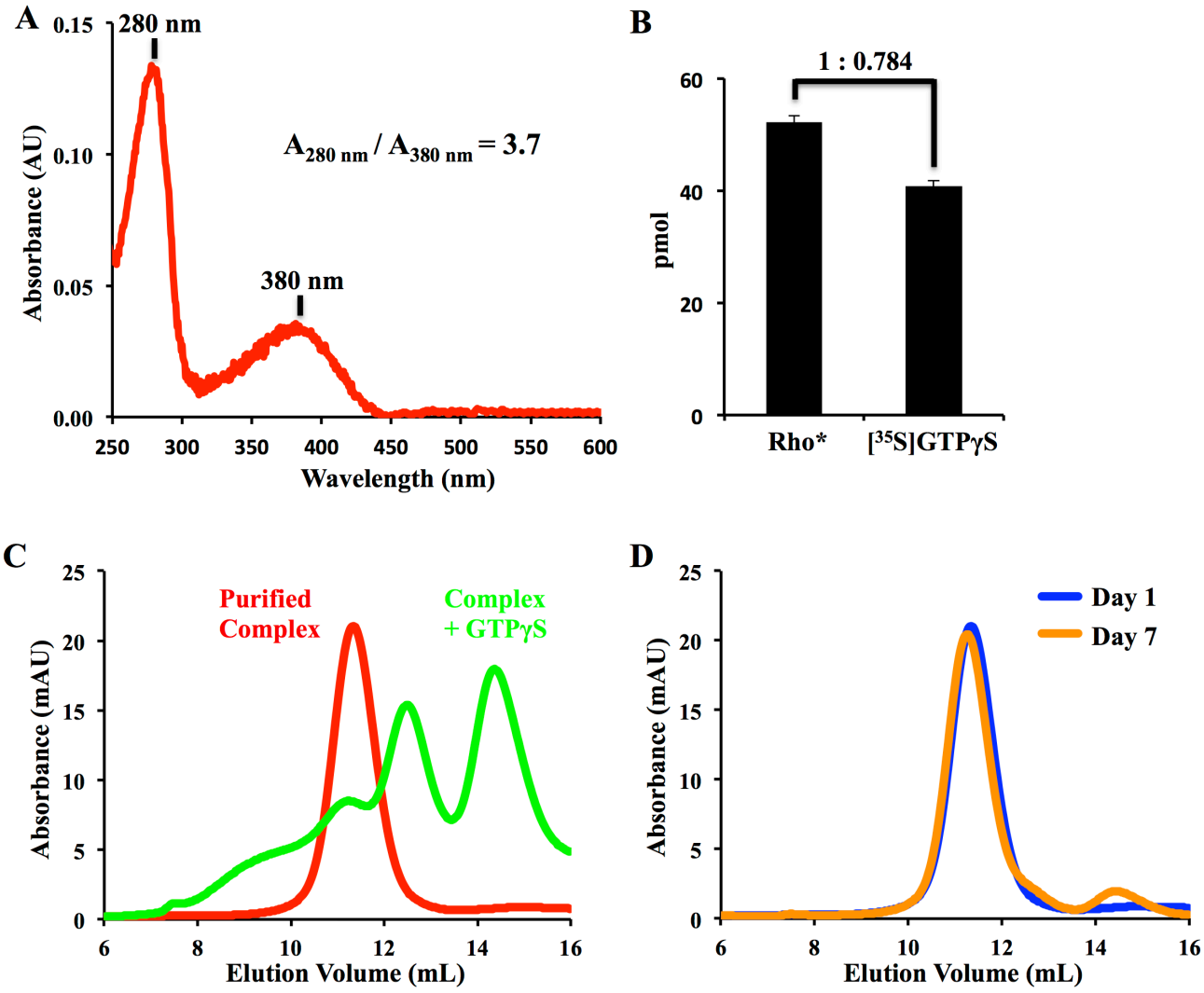
A
280 nm
380 nm
$A_{280\ nm} / A_{380\ nm} = 3.7$
Absorbance (AU)
Wavelength (nm)
B
1 : 0.784
pmol
Rho*
[35S]GTPγS
C
Purified Complex
Complex + GTPγS
Absorbance (mAU)
Elution Volume (mL)
D
Day 1
Day 7
Absorbance (mAU)
Elution Volume (mL)

Stoichiometry, activity and stability of the Rho-G_T complex

Bovine Rho has been shown to form arrays of dimers in ROS membranes (17) and there have been questions raised regarding whether the stoichiometry between Rho and G_T in the signaling complex is 1:1 or 2:1.

The UV/Vis spectrum of the purified complex reveals two peaks at 280 nm and 380 nm (Fig. 2.3A), corresponding to the absorbance of the protein moiety, and that of the unprotonated all-trans retinal in the meta-II Rho state, respectively. The A_{280nm}/A_{380nm} ratio is 3.7, which agrees with a 1:1 stoichiometry based on the reported extinction coefficients for the protein components (18-20) (a 2:1 stoichiometry would result in a A_{280nm}/A_{380nm} ratio of 2.58).

Additionally, the stoichiometry between Rho and G_T was determined with a radio-nucleotide filter binding assay, in which the purified Rho-G_T complex was incubated with [^{35}S]GTPγS and then applied to a nitrocellulose filter. The amount of G_T present in the complex was estimated based on its nucleotide binding capacity, i.e. the amount of bound [^{35}S]GTPγS, and was compared with the amount of Rho calculated from the 380 nm absorbance. The result showed that for one mole of Rho, there was 0.784 ± 0.003 mole GTPγS present, supporting the idea of a 1:1 Rho-G_T complex (Fig. 2.3B).

The purified Rho-G_T complex was fully active as it dissociated upon the addition of GTPγS, a non-hydrolysable analogue of GTP (Fig. 2.3C). The complex was stable at 4ºC in the dark for at least 7 days, as it remained nearly completely intact with less than 5% dissociation (Fig. 2.3D).

Figure 2.4 SAXS data and analyses of the Rho-G_T complex. A, SAXS data, curves from top to bottom are from 1, 0.5, 0.25 mg/mL respectively. (Each curve was the average of 10 scattering curves) B, Guinier plots for $q*R_g<1.3$ region of the scattering curve. C, Pair distribution function calculated from 1 mg/mL scattering profile. D, SAXS parameters and calculation results.

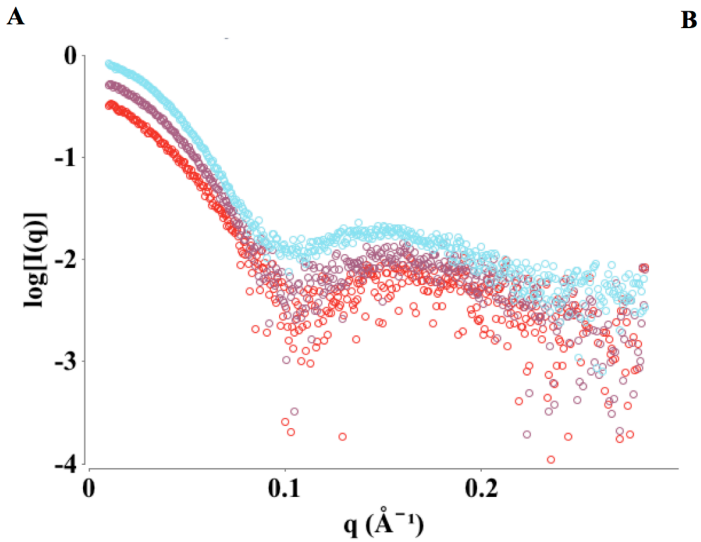

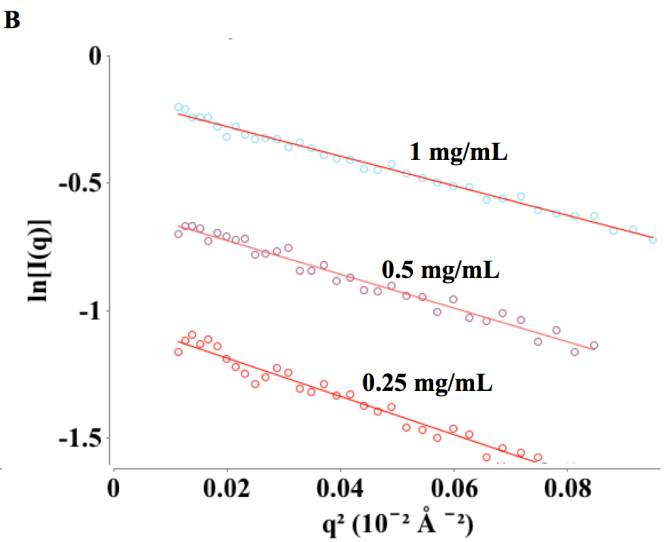

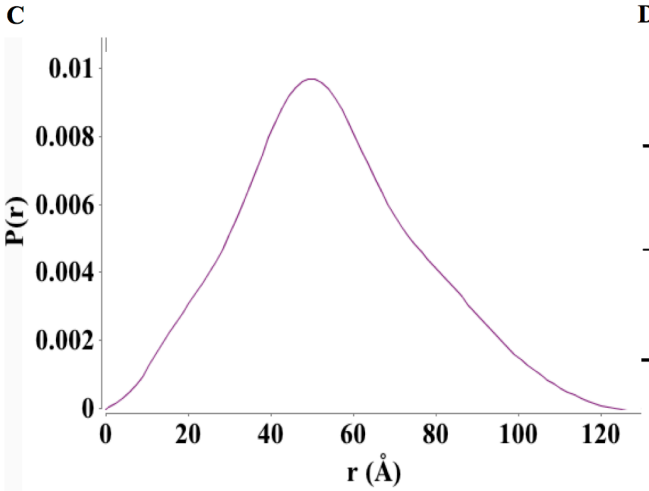

D

Conc. (mg/mL)	I(0)	R_g (Å)		R_c (Å)	Molecular Mass (kD)	
		Guinier	P(r)		ScÅtter	SAXS MoW
1.00	0.812	41.7	41.9	34.9	143.8	128.9
0.50	0.549	42.7	43.9	34.3	134.5	126.7
0.25	0.354	43.9	42.0	32.5	129.6	127.4

Small Angle X-ray Scattering (SAXS) analysis of Rho-G_T complex

To further study the overall conformation of the active state of the Rho-G_T complex, SAXS data were collected over a concentration range of the purified complex, with corrections for the background scattering being obtained by subtracting the scattering due to the SEC buffer from the scattering profiles of the Rho-G_T samples (Fig. 2.4A). The Guinier regions ($qR_g<1.3$) of these curves are linear (Fig. 2.4B), confirming that the Rho-G_T complex is monodisperse. All the parameters calculated from the SAXS scattering profiles are summarized in Fig. 2.4C. The radius of gyration (R_g) values for the Rho-G_T complex calculated from the Guinier plots range from 41.7 to 43.9 Å, which agree well with those calculated from pair distribution functions (P(r)) using GNOM (21) (41.9 to 43.9 Å). These results demonstrate that the value for R_g is concentration-independent. The molecular mass of the Rho-G_T complex was calculated using both the particle mass determination method with ScÅtter software developed by Rambo *et al.* (22) and SAXS M_r developed by Fischer *et al*. (23). The results from ScÅtter (129.6 to 143.8 kD) and SAXS M_r (127.4 to 128.9 kD) agree well with each other and confirm that the complex is composed of 1 Rho and 1 G_T, which gives a molecular mass value of 125 kD. The P(r) curve (Fig. 2.4D) calculated from GNOM is skewed to the right, indicating an elongated overall particle shape. The cross-sectional R_g (R_c) values calculated using ScÅtter software range from 32.5 to 34.9 Å, which are about 9 Å smaller than the R_g values, confirming the existence of an elongated shape for the Rho-G_T complex.

FIGURE 2.5 *Ab initio* envelopes and model of the Rho-G_T complex. A. DAMMIN envelopes (averaged and filtered envelopes are colored in grey and blue respectively). B. GASBOR envelope. C. Superimposition of complex model with GASBOR envelope. Rho is in red, $G\alpha_T$ GTPase domain is in green, $G\alpha_T$ helical domain is in yellow, $G\beta_1$ is in cyan, $G\gamma_1$ is in grey, detergents are shown as orange beads. D. Theoretical scattering profile of the model (red line) overlain with experimental data (grey dots) E. Position of $G\alpha_T$ helical domain (gold) in the model compared with open (purple) and close (blue) positions from crystal structures.

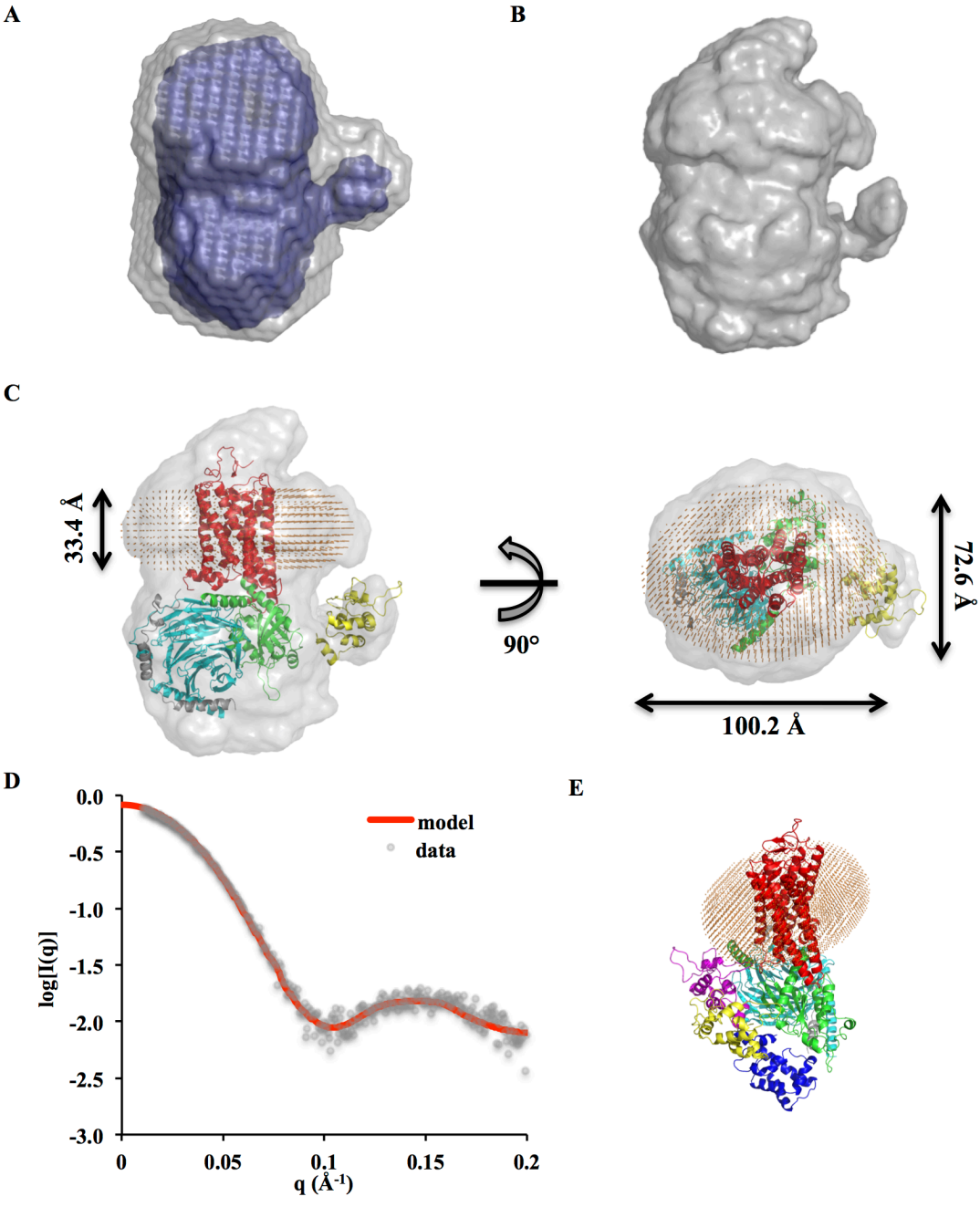
A
B
C
33.4 Å
90°
72.6 Å
100.2 Å
D
model
data
log[I(q)]
0.0
-0.5
-1.0
-1.5
-2.0
-2.5
-3.0
0
0.05
0.1
0.15
0.2
q (Å-1)
E

SAXS-based modeling of Rho-G_T complex

The P(r) curve (D_{max}=128 Å) calculated from the scattering profile for the 1 mg/mL Rho-G_T sample was used for generating *ab initio* models of the complex. Two different algorithms, DAMMIN (24) and GASBOR (25), were used. The resulting envelopes obtained using each method agree well with each other. Both revealed a small bulge protruding out from the bottom half of the envelopes, indicating the position of the helical domain of α_T (Figs. 5A and 5B). A structural model of the Rho-G_T complex, using the crystal structure of the β_2AR-G_S complex (PDB 3SN6) as a template, was generated to fit the envelopes. There is significant discrepancy between the structural model and *ab initio* envelopes at the Rho region, which can be attributed to the existence of a detergent micelle around the receptor in solution and, as a result, the model fits poorly to the experimental data with χ^2=24.2. In order to improve the quality of the structural model, a detergent corona shaped as an elliptical torus was built around Rho using the Memprot program developed by Pérez *et al*. (26). The resulting micelle model is composed of 78 LMNG detergent tails and 74 detergent heads, and its dimensions are shown in Fig. 2.5C. After incorporating the detergent corona into the complex model, the χ^2 value decreased to 3.27, indicating a significant improvement of fitness to the experimental data. In addition, the position of the helical domain was further optimized with the program CORAL (26) and the χ^2 value of the model improved to 1.83 (Fig. 2.5D and E). The helical domain position in the resulting model resides between the close and open positions as indicated from X-ray crystal structures (PDB 1GOT and 3SN6 respectively) (Fig. 2.5E).

Figure 2.6 2D projection analysis of the Rho-G_T complex. A, Raw EM image of detergent solubilized Rho-G_T complex embedded in negative stain. B, Representative EM class averages of the Rho-G_T complex (positions of α_T helical domain indicated by arrow). The cartoon model represents the conformations reflected by the EM averages, depicting the variable positioning of the helical domain (the position of the detergent micelle is indicated by gray shaded arcs and labeled with "m").

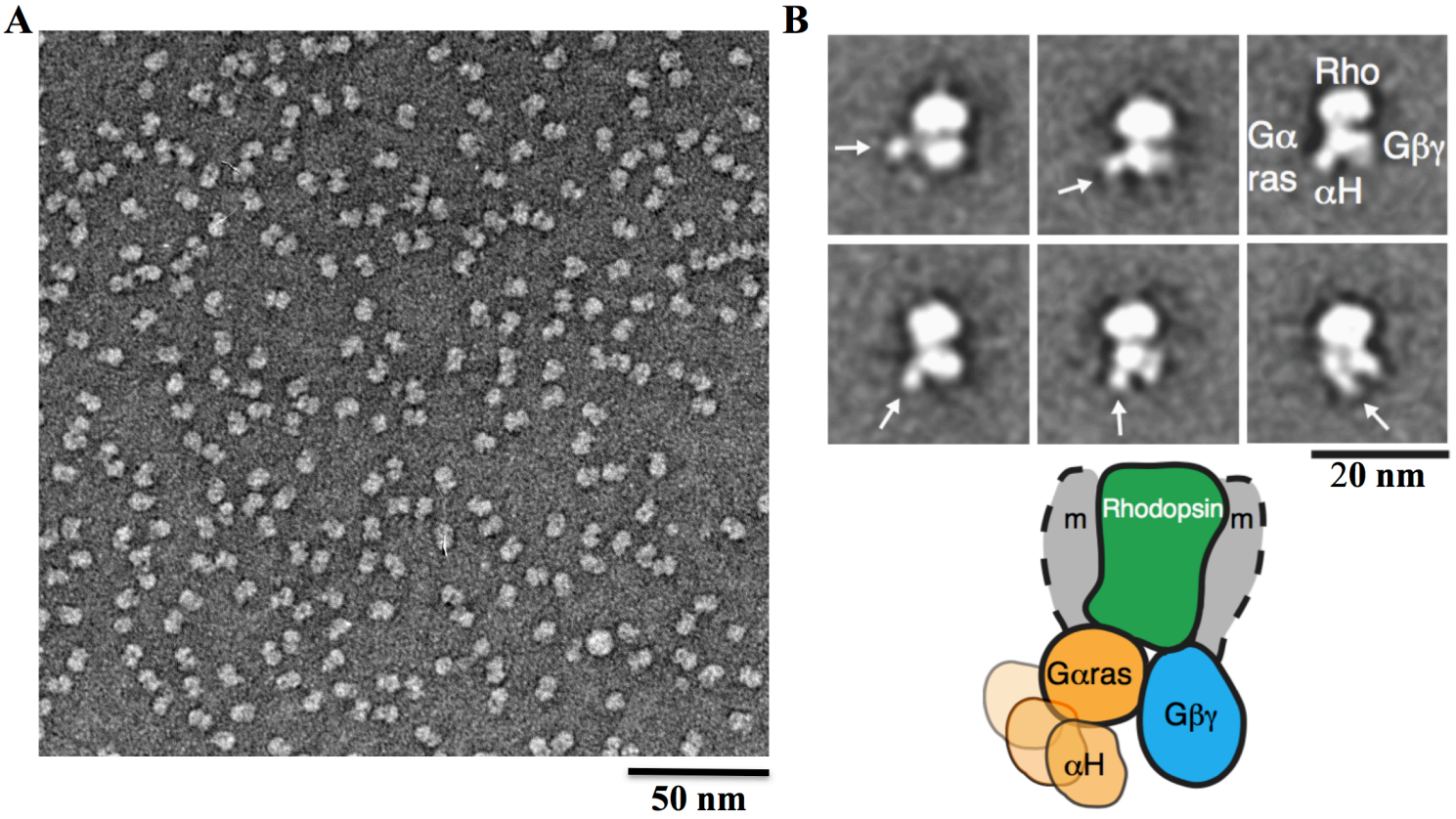
A
50 nm
B
Rho
Gα
ras
αH
Gβγ
20 nm
m
Rhodopsin
m
Gαras
Gβγ
αH

Electron microscopy characterization of negatively stained Rho-$G_T$complex

EM visualization of the negatively stained complex samples showed a monodisperse particle population (Fig. 2.6A). Reference-free alignment and classification of particle projections revealed class averages with an overall density similar to that of the β_2 adrenergic receptor-G_S protein complex (β_2AR-G_S) (14) (Fig. 2.6B). A central oval density represents Rho in a detergent micelle with a small protruding density often observed on top corresponding to the N-terminus of Rho. At the bottom of Rho, two major densities representing the G_T heterotrimer are clearly visible. One of the two densities has extensive contact with the receptor density and shows an additional small globular density in various orientations in several class average images. This is similar to what was observed for the β_2AR-G_S complex (14) and represents the Ras-like domain of the α_T subunit, with a flexible helical domain in the Rho-G_T complex. The other density therefore corresponds to $\beta_1\gamma_1$.

DISCUSSION

Structural information obtained from a variety of approaches will be invaluable in shedding light on how the photoreceptor Rho engages and activates its signaling partner, the G protein G_T. Such analyses will also provide insights with broad relevance toward understanding the underlying mechanisms by which GPCRs demonstrate remarkable specifity for their G protein targets, as well as whether different GPCRs use common or distinct mechanisms in catalyzing the G protein activation event. Recently, there have been several reports of the purification of detergent-solubilized Rho-G_T complexes, in which either native (28,29) or recombinant Rho (30,31) was utilized. Our approach

toward obtaining an active Rho-G protein complex differs from these previous efforts in two major aspects. First, rather than detergent-solubilizing and purifying Rho prior to allowing it to associate with a purified G protein, the Rho-G protein complex was obtained by directly light-activating the urea-washed ROS membranes in the presence of the heterotrimeric, chimeric G protein G_T. This allowed the formation of a Rho-G_T complex within a native membrane environment. The subsequent pelleting step readily removed the released GDP, which may otherwise destabilize the complex. Secondly, instead of using either the glycan linkages or C-terminus of Rho as purification handles, we utilized the N-terminal His-tag on the recombinant α_T subunit to achieve a simple and efficient one-step purification of the detergent-solubilized Rho-G_T complex. The resulting complex dissociated with the addition of GTPγS, demonstrating that the complex isolated in this manner is fully active.

Near-infrared light scattering studies of ROS membranes in the early 1980's by Kuhn and colleagues suggested a 1:1 stoichiometric association of G_T with Rho (32). However, atomic force microscopy images of ROS membranes revealed that Rho exists in the form of dimeric arrays in its native environment (17). Recent studies using native rhodopsin solubilized from ROS with detergent for complex formation (28,29) argued for the existence of a pentameric complex consisting of two Rho molecules and one G_T heterotrimer as the minimal functioning unit. While in these settings, it may appear that Rho can form dimers, the important question is what stoichiometry of Rho and G_T is required to achieve full activation. Based on our studies of a signaling active Rho-G_T complex, as analyzed by UV/Vis spectroscopy and radioactive nucleotide binding, as well as by SAXS and EM, we conclude that the minimal unit necessary for full activation

is 1 Rho and 1 G protein. This conclusion is supported by recent studies using rhodopsin embeded nanodiscs which have shown that one Rho is sufficient for coupling to and activating G_T (33-34). Moreover, based on nanodisc reconstitution, monomeric rhodopsin has been shown to be sufficient for phosphorylation by G protein-coupled receptor kinase (GRK) and interaction with arrestin (35-36). And the recent X-ray crystallography structure of a rhodopsin-arrestin complex (37), have futher illustrated that rhodopsin binds arrestin in a 1:1 stoichiometry. Similarly, β2- adrenergic receptor has been demonstrated to interact with Gs in a monomeric manner (6, 14, 38). Therefore several lines of evidence now point to class A GPCR monomers being sufficient for promoting their downstream signals.

In addition to the limit stoichiometry necessary to achieve a signaling-active complex, another question of interest is the positioning of the helical domain of the Gα subunit in the receptor-G protein complex. The first high-resolution structure of a G protein α subunit, that for GTPγS-bound α_T (39), revealed that the nucleotide is buried inside a cleft formed by the Ras-like domain and helical domain, and it was postulated that an activated receptor must induce an opening of the cleft in order to allow for nucleotide exchange. The first direct evidence of this inter-domain opening was provided by double electron-electron resonance (DEER) experiments (40), in which distance increases as large as 20 Å between the Ras-like and helical domains of the $G_i\alpha$ subunit were observed upon binding to light-activated ROS. The crystal structure of the β_2AR-G_S complex (6) shows a very dramatic 127° rotation of the $G_S\alpha$ helical domain, which results in the opening of the nucleotide-binding pocket. Our SAXS model of the Rho-G_T complex shows that the helical domain of α_T adopts a similar open position in solution. However,

the opening is not as dramatic as displayed in the β_2AR-G_S complex crystal structure. Negative stain electron microscopy (EM) studies of the β_2AR-G_S complex (14) reveal the flexible positioning of the $G_S\alpha$ helical domain and suggest an ensemble of open helical domain positions which exist under physiological conditions. Since a similarly flexible helical domain is also observed in the negative-stain EM images of the Rho-G_T complex, it is most likely that a displacement of the helical domain is a universal mechanism of receptor-mediated nucleotide exchange for different families of heterotrimeric G proteins.

In conclusion, here we describe procedures for isolating a Rho-G protein complex with very high yield that is amenable to a variety of types of biochemical and structural analyses. Given the availability of a number of interesting mutants of α_T, which mimic different stages in the activation event, we should soon be in position to address fundamentally important questions regarding how different members of the GPCR family engage their G protein signaling partners and induce the necessary structural changes to drive G protein-mediated signal propagation.

METHODS

Materials

Frozen dark-adapted bovine retinae were purchased from W.L. Lawson Co. (Lincoln, NE). Detergents were from Anatrace and all other chemicals were obtained from Sigma-Alrich.

Purification of retinal proteins

Urea-washed rod outer segment (UROS) membranes were isolated as described (41), flash-frozen and stored at −80°C in HMN buffer (20 mM HEPES, pH 7.5, 2 mM $MgCl_2$,

100 mM NaCl, 1 mM DTT) at a concentration of 300 μM. UROS membranes were used as the source for Rho in Rho-G_T complex formation. The $\beta_1\gamma_1$ subunit complex was purified essentially as described previously (42). Bovine retinae were exposed to light and subjected to sucrose gradient ultra-centrifugation to prepare purified rod outer segment (ROS) membranes. After a series of isotonic and hypotonic washes, 100 μM GTP was added to release G_T subunits from the membrane. $\beta_1\gamma_1$ was separated from α_T through a 5 mL HiTrap Blue HP (GE Healthcare) column and the resulting $\beta_1\gamma_1$ complex was further purified by anion exchange chromatography through a 5 mL HiTrap Q HP (GE Healthcare) column, using Buffer A (20 mM HEPES, pH 7.5, 2 mM $MgCl_2$, 1 mM DTT, 10% glycerol) and Buffer B (Buffer A + 1 M NaCl) to form the gradient. The $\beta_1\gamma_1$ complex typically elutes at 100 mM NaCl and was concentrated to 20 μM, flash-frozen and stored at –80°C.

Expression and purification of α_T

An α_T/α_{i1} chimeric construct designated as pHis$_6$Chi8 was obtained from Dr. Heidi Hamm (Vanderbilt University) (43), in which α_T residues 215 to 295 were replaced with the corresponding residues from α_{i1} and a His_6 tag was introduced at the N terminus. In addition, residues 244 and 247 were changed back to the original amino acids in α_T, resulting in the α_T construct. The α_T subunit can undergo Rho-catalyzed nucleotide exchange and activate the effector enzyme, PDE, in a similar manner as retinal α_T. α_T was expressed in BL21(DE3) competent cells and purified as described previously (18). The protein was concentrated to 20 μM in HMN buffer with the addition of 10% glycerol, flash-frozen and stored at −80°C.

Detergent selection for Rho-G_T complex purification

Fluorescence measurements were carried out with a Varian eclipse spectrofluorimeter. UROS was light activated (Rho) by incubation on ice under ambient light for 5 min. Rho-catalyzed nucleotide exchange on the α_T subunit in detergents was monitored by premixing 5 nM Rho and 300 nM $\beta_1\gamma_1$ in HMN buffer with 50 μM GTPγS and different detergents at various concentrations, monitoring tryptophan fluorescence (excitation: 300 nm; emission: 345 nm) in real-time upon the addition of 300 nM α_T. All kinetic traces were corrected for the fluorescence from Rho and $\beta_1\gamma_1$, and the data were fitted to a single exponential equation:

$$F = F_\infty - (F_\infty - F_0) \cdot e^{-k_{obs} \cdot t}$$

where F is the fluorescence signal at any time t, F_0 is the fluorescence signal at time $t = 0$, F_∞ is the fluorescence signal at time $t = \infty$, and k_{obs} is the observed rate constant.

Rhodopsin-G_T complex formation and purification

The G protein heterotrimer G_T was formed by mixing 22 nmol of α_T with 20 nmol $\beta_1\gamma_1$, and then incubated on ice for 5 minutes. The Rho-G_T complex was formed on ROS membranes by mixing G_T with UROS containing 140 nmol Rho and illuminating the mixture under a halogen lamp covered with a UV-absorbing glass and a 495 nm long-pass filter at 4°C for 30 min. The suspension was aliquoted into 1.5 mL eppendorf tubes and centrifuged at 14,000g for 30 min. From here on, all subsequent steps were carried out in the dark under dim red light. The supernatant was disgarded and the pellets containing the Rho-G_T complex and excess Rho were resuspended in 3 mL HMN buffer + 1% (w/v) LMNG. The mixture was incubated at 4°C with rocking for 30 min to allow

for complete solubilization. HMN buffer (12 mL) was then added to lower the LMNG concentration to 0.2% and the sample was further incubated at 4°C with rocking for 1 hour. Solubilized complex was loaded onto a 1 mL HisTrap FF column (GE Healthcare) pre-equilibrated with HMN buffer + 0.02% LMNG. The Rho-G_T complex was eluted from the column with an imidazole gradient in HMN buffer + 0.02% LMNG, as a single peak at ~100 mM imidazole. Peak fractions were pooled and concentrated with an Amicon Ultra-0.5 100 kD MWCO concentrator (EMD Millipore) to 500 μL and injected onto a Superdex 200 10/300 GL column (GE Healthcare), pre-equilibrated with HMN buffer + 0.02% LMNG. Peak fractions were pooled and concentrated with an Amicon Ultra-0.5 100 kD MWCO concentrator (EMD Millipore) to 50 μL, resulting in a complex concentration of ~40 mg/mL.

Determination of the stoichiometry of the Rho-G_T complex

The stoichiometry of Rho and G_T within the complex was determined using two methods, UV/Vis absorption spectroscopy and a [^{35}S]GTPγS binding assay. For stoichiometry determinations using UV/Vis spectroscopy, a 100 μL sample of the purified Rho-G_T complex was examined in a quartz cuvette with a 1 cm path length, using a Beckman DU600 UV/Vis spectrophotometer scanning from 240 nm to 700 nm at 240 nm/min. The ratio for Rho to G_T within the complex was determined from the A_{280nm}/A_{380nm} ratio, using the following extinction coefficients: Rho (ε_{280nm} = 61,800 $M^{-1}cm^{-1}$, ε_{380nm} = 42,000 $M^{-1}cm^{-1}$) (19, 20), α_T (ε_{280nm} = 35,870 $M^{-1}cm^{-1}$), and $\beta_1\gamma_1$ (ε_{280nm} = 57,400 $M^{-1}cm^{-1}$). The extinction coefficients for α_T and $\beta_1\gamma_1$ were calculated based on protein sequence using the ExPASy ProParam tool (44). Therefore, a 1:1 Rho:G_T

stoichiometry would result in an A_{280nm}/A_{380nm} value of 3.69, whereas a 2:1 Rho:G_T stoichiometry would yield a A_{280nm}/A_{380nm} value of 2.58.

For stoichiometry determinations using a [^{35}S]GTPγS binding assay, purified Rho-G_T complex was incubated with 50 μM [^{35}S]GTPγS for 10 minutes on ice in 20 μL HMN buffer + 0.003% LMNG. The solution was then applied to prewet nitrocellulose filters (Schleicher & Schuell, pore size 0.45 μm) on a suction manifold. The filters were washed twice with HMN buffer and added to scintillation liquid (30% LSC Scintisafe Mixture) and counted in a scintillation counter (LS6500 multipurpose scintillation counter). The calculated amount of bound [^{35}S]GTPγS was used as an estimate for the amount of G_T in the complex and was compared with the amount of Rho calculated from A_{380nm}, using the extinction coefficient of Meta II rhodopsin, ε_{380nm} = 42,000 $M^{-1}cm^{-1}$.

SAXS data collection and processing

SAXS data was collected at the G1 station of the Cornell High Energy Synchrotron Source (CHESS). G1 operated with an energy of 9.86 keV and provided a flux of 3×10^{11} photons/sec for a 250×250 μm beam. Purified Rho-G_T complex was eluted through a Superdex 200 5/150 GL column (GE Healthcare), pre-equilibrated with HMN buffer without detergent, immediately prior to the collection of SAXS data. The center peak fraction was collected and a concentration series, 0.25, 0.5 and 1 mg/mL, was prepared in HMN buffer and kept on ice. Samples were centrifuged at 14,000g for 10 minutes before being loaded into the SAXS sample exposure window. Samples were exposed for 30 seconds with oscillation. Ten datasets were collected for each sample for possible radiation damage detection and undamaged exposures were averaged. Buffer

measurements with HMN buffer were conducted in-between each sample measurement. Data reduction and background subtraction were done with RAW data reduction software (45). The program ScÅtter (22) was used to obtain the Guinier plot and calculate the radius of gyration (R_g) and I(0) values. Particle distance distribution P(r) was calculated using GNOM (20).

SAXS-based modeling of the Rho-G_T complex

Ab initio models were calculated using two different programs, DAMMIN (24) and GASBOR (25). In DAMMIN calculations, 17 envelopes were generated (average χ^2=0.90) and the results were averaged using DAMAVER (46) to produce the averaged and filtered envelopes. None of the 17 DAMMIN envelopes was rejected during the DAMAVER calculation and the mean normalized special discrepancy value (NSD) was 0.482 ± 0.053, indicating the model is of good quality. In addition to DAMMIN, GASBOR calculations were performed to fit the intensity in reciprocal space. The resulting envelope fits well to the experimental curve with χ^2=0.895. A structural model was built using the X-ray crystal structure of the β_2AR-G_S complex (3SN6) as a template. In this model, the X-ray crystal structures of meta-rhodopsin II (PDB 3PXO), and the $\beta_1\gamma_1$ complex from the G_T heterotrimer (PDB 1GOT), were used for Rho and $\beta_1\gamma_1$ respectively. A homology model of the α_T subunit was built based on the α_S subunit from the X-ray crystal structure of the β_2AR-G_S complex (PDB 3SN6) using the SWISS-MODEL server (44). The program Memprot (26) was used to model the LMNG detergent micelle around Rho, in which a coarse-grained fitting algorithm was used to add detergent molecules by assuming an elliptical model for the detergent corona. Electron density values of 0.28 and 0.52 $e \cdot Å^{-3}$ were used for the hydrophobic and

hydrophilic portions of the LMNG detergent molecule, respectively. The position of the helical domain (residues 57-176 in α_T) was optimized using the program CORAL (27), in which the linker regions (residues 51-56 and 177-181) connecting the helical domain to the GTPase domain were set to be random flexible loops. The resulting structural model was aligned with the envelopes using the SUPCOMB (47) program.

Specimen preparation and EM imaging of negative-stained samples

Purified Rho-G_T complex was prepared for electron microscopy using the conventional negative staining protocol (48), and imaged at room temperature with a Tecnai T12 electron microscope operated at 120 kV, using low-dose procedures. Images were recorded at a magnification of ×71,138 and a defocus value of ~1.5 μm on a Gatan US4000 CCD camera.

Two-dimensional classifications of the Rho-G_T complex

All images were binned (2 pixels × 2 pixels) to obtain a pixel size of 4.16 Å on the specimen level. Particles were manually excised using e2boxer (49) (part of the EMAN2 software suite). Two-dimensional reference-free alignment and classification of particle projections were performed using ISAC (50). A total of 9,303 projections of Rho-G_T were subjected to ISAC, producing 134 classes consistent over two-way matching and accounting for 6,774 particle projections.

REFERENCES

1. Ma, P., and Zemmel, R. (2002) Value of novelty? *Nat. Rev. Drug Discov.* **1**, 571-572
2. De Lean, A., Stadel, J.M., and Lefkowitz, R.J. (1980) A ternary complex model explains the agonist-specific binding properties of the adenylate cyclase-coupled beta-adrenergic receptor. *J. Biol. Chem*. **255**, 7108-7117
3. Rosenbaum, D.M., Cherezov, V., Hanson, M.A., Rasmussen, S.G., Thian, F.S., Kobilka, T.S., Choi, H.J., Yao, X.J., Weis, W.I., Stevens, R.C., and Kobilka, B.K. (2007) GPCR engineering yields high-resolution structural insights into β_2-adrenergic receptor function. *Science* **318**, 1266-1273
4. Caffrey, M., and Cherezov, V. (2009) Crystallizing membrane proteins using lipidic mesophases. *Nat. Protoc*. **4**, 706-731
5. Xu, S., and Fischetti R.F. (2007) Design and performance of a compact collimator on GM/CA-CAT at the advanced photon source *Proc. SPIE*. **6665**, 1-8
6. Rasmussen, S.G., DeVree, B.T., Zou, Y., Kruse, A.C., Chung, K.Y., Kobilka, T.S., Thian, F.S., Chae, P.S., Pardon, E., Calinski, D., Mathiesen, J.M., Shah, S.T., Lyons, J.A., Caffrey, M., Gellman, S.H., Steyaert, J., Skiniotis, G., Weis, W.I., Sunahara, R.K., and Kobilka, B.K. (2011) Crystal structure of the β_2 adrenergic receptor-Gs protein complex. *Nature* **477**, 549-555
7. Liang, Y.L., Khoshouei, M., Radjainia, M., Zhang, Y., Glukhova, A., Tarrasch, J., Thal, D.M., Furness, S.G., Christopoulos, G., Coudrat, T., Danev, R., Baumeister, W. Miller, L.J., Christopoulos, A., Kobilka, B.K., Wootten, D., Skiniotis, G., and Sexton, P.M. (2017) Phase-plate cryo-EM structure of a class B GPCR-G protein complex. *Nature* Epub ahead of print.

8. Stryer, L. (1991) Visual excitation and recovery. *J. Biol. Chem.* **266**, 10711-10714
9. Palczewski, K., Kumasaka, T., Hori, T., Behnke, C.A., Motoshima, H., Fox, B.A., Le Trong, I., Teller, D.C., Okada, T., Stenkamp, R.E., Yamamoto, M., and Miyano, M. (2000) Crystal structure of rhodopsin: A G protein-coupled receptor. *Science* **289**, 739-745
10. Li, J., Edwards, P.C., Burghammer, M., Villa, C., and Schertler, G.F. (2004) Structure of bovine rhodopsin in a trigonal crystal form. *J. Mol. Biol.* **343**, 1409-1436
11. Park, J.H., Scheerer, P., Hofmann, K.P., Choe, H.W., and Ernst, O.P. (2008) Crystal structure of the ligand-free G protein-coupled receptor opsin. *Nature* **454**, 183-187
12. Choe, H.W., Kim, Y.J., Park, J.H., Morizumi, T., Pai, E.F., Krauss, N., Hofmann, K.P., Scheerer, P., and Ernst, O.P. (2011) Crystal structure of metarhodopsin II. *Nature* **471**, 651-655
13. Scheerer, P., Park, J.H., Hildebrand, P.W., Kim, Y.J., Krauss, N., Choe, H.W., Hofmann, K.P., and Ernst, O.P. (2008) Crystal structure of opsin in its G protein-interacting conformation. *Nature* **455**, 497-502
14. Westfield, G.H., Rasmussen, S.G., Su, M., Dutta, S., DeVree, B.T., Chung, K.Y., Calinski, D., Velez-Ruiz, G., Oleskie, A.N., Pardon, E., Chae, P.S., Liu, T., Li, S., Woods, V.L. Jr., Steyaert, J., Kobilka, B.K., Sunahara, R.K., and Skiniotis, G. (2011) Structural flexibility of the Gαs α-helical domain in the β_2-adrenoceptor Gs complex. *Proc. Natl. Acad. Sci. U.S.A.* **108**, 16086-16091
15. Phillips, W.J., and Cerione, R.A. (1988) The intrinsic fluorescence of the α subunit of transducin. *J. Biol. Chem*. **263**, 15498-15505

16. Chae, P.S., Rasmussen, S.G., Rana, R.R., Gotfryd, K., Chandra, R., Goren, M.A., Kruse, A.C., Nurva, S. Loland, C.J., Pierre, Y., Drew, D., Popot, J.L., Picot, D., Fox, B.G., Guan, L., Gether, U., Byrne, B., Kobilka, B., and Gellman, S.H. (2010) Maltose-neopentyl glycol (MNG) amphiphiles for solubilization, stabilization and crystallization of membrane proteins. *Nat. Methods* **7**, 1003-1008
17. Fotiadis, D., Liang, Y., Filipek, S., Saperstein, D.A., Engel, A., and Palczewski, K. (2003) Atomic-force microscopy: rhodopsin dimers in native disc membranes. *Nature* **421**, 127-128
18. Majumdar, S., Ramachandran, S., and Cerione, R.A. (2006) Perturbing the linker regions of the α-subunit of transducin. *J. Biol. Chem*. **281**, 9219-9226
19. Lin, S.W., and Sakmar, T.P. (1996) Specific tryptophan UV-absorbance changes are probes of the transition of Rhodopsin to its active state. *Biochemistry* **35**, 11149-11159
20. Matthews, R.G., Hubbard, R., Brown, P.K., and Wald, G. (1963) Tautomeric forms of metarhodopsin. *J. Gen. Physiol.* **47**, 215-240
21. Svergun, D.I. (1992) Determination of the regularization parameter in indirect-transform methods using perceptual criteria. *J. Appl. Cryst.* **25**, 495-503
22. Rambo, R.P., and Tainer, J.A. (2013) Accurate assessment of mass, models and resolution by small-angle scattering. *Nature* **496**, 477-481
23. Fischer, H., de Oliveira Neto, M., Napolitano, H.B., Polikarpov, I., and Craievich, A.F. (2010) Determination of the molecular weight of proteins in solution from a single small-angle X-ray scattering measurement on a relative scale. *J. Appl. Cryst.* **43**, 101-109

24. Svergun, D.I. (1999) Restoring low resolution structure of biological macromolecules from solution scattering using simulated annealing. *Biophys. J.* **76**, 2879-2886

25. Svergun, D.I., Petoukhov, M.V. and Koch, M.H. (2001) Determination of domain structure of proteins from X-ray solution scattering. *Biophys. J.*, **80**, 2946-2953

26. Pérez, J., and Koutsioubas, A. (2015) Memprot: a program to model the detergent corona around a membrane protein based on SEC-SAXS data. *Acta Crystallogr. D Biol. Crystallogr.* **71**, 86-93

27. Petoukhov, M.V., Franke, D., Shkumatov, A.V., Tria, G., Kikhney, A.G., Gajda, M., Gorba, C., Mertens, H.D.T., Konarev, P.V. and Svergun, D.I. (2012) New developments in the ATSAS program package for small-angle scattering data analysis. *J. Appl. Cryst.* **45**, 342-350

28. Jastrzebska, B., Ringler, P., Lodowski, D.T., Moiseenkova-Bell, V., Golczak, M., Muller, S.A., Palczewski, K., and Engel, A. (2011) Rhodopsin-transducin heteropentamer: three-dimensional structure and biochemical characterization. *J. Struct. Biol.* **176**, 387-394

29. Jastrzebska, B., Ringler, P., Palczewski, K., and Engel, A. (2013) The rhodopsin-transducin complex houses two distinct rhodopsin molecules. *J. Struct. Biol*. **182**, 164-172

30. Xie, G., D'Antona, A.M., Edwards, P.C., Fransen, M., Standfuss, J., Schertler, G.F., and Oprian, D.D. (2011) Preparation of an activated rhodopsin/transducin complex using a constitutively active mutant of rhodopsin. *Biochemistry* **50**, 10399-10407

31. Maeda, S., Sun, D., Singhal, A., Foggetta, M., Schmid, G., Standfuss, J., Hennig, M., Dawson, R.J., Veprintsev, D.B., and Schertler, G.F. (2014) Crystallization scale

preparation of a stable GPCR signaling complex between constitutively active rhodopsin and G protein. *PLoS One* **9**, e98714

32. Kuhn, H., Bennett, N., Michel-Villaz, M., and Chabre, M. (1981) Interactions between photoexcited rhodopsin and GTP-binding protein: kinetic and stoichiometric analyses from light-scattering changes. *Proc. Natl. Acad. Sci. U.S.A*. **78**, 6873-6877
33. Bayburt, T.H., Leitz, A.J., Xie, G., Oprian, D.D., and Sligar, S.G. (2007) Transducin Activation by Nanoscale Lipid Bilayers Containing One and Two Rhodopsins. *J. Biol. Chem.* **282**, 14875-14881
34. Whorton, M.R., Jastrzebska, B., Park, P.S.H., Fotiadis, D., Engel, A., Palczewski, K., and Sunahara, R.K. (2008) Efficient Coupling of Transducin to Monomeric Rhodopsin in a Phospholipid Bilayer. *J. Biol. Chem.* **283**, 4387-4394
35. Bayburt, T.H., Vishnivetskiy, S.A., McLean, M.A., Morizumi, T., Huang, C.C., Tesmer, J.J., Ernst, O.P., Sligar, S.G., Gurevich, V.V. (2011) Monomeric rhodopsin is sufficient for normal rhodopsin kinase (GRK1) phosphorylation and arrestin-1 binding. *J. Biol. Chem.* **286**, 1420-1428
36. Vishnivetskiy, S.A., Ostermaier, M.K., Singhal, A., Panneels, V., Homan, K.T., Glukhova, A., Sligar, S.G., Tesmer, J.J., Schertler, G.F., Standfuss, J., Gurevich, V.V. (2013) Constitutively active rhodopsin mutants causing night blindness are effectively phosphorylated by GRKs but differ in arrestin-1 binding. *Cell. Signal.* **25**, 2155-2162
37. Kang, Y., Zhou, X.E., Gao, X., *et al*. (2015) Crystal structure of rhodopsin bound to arrestin by femtosecond X-ray laser. *Nature* **523**, 561-567

38. Whorton, M.R., Bokoch, M.P., Rasmussen, S.G., Huang, B., Zare, R.N., Kobilka, B., Sunahara, R.K. (2007) A monomeric G protein-coupled receptor isolated in a high-density lipoprotein particle efficiently activates its G protein. *Proc. Natl. Acad. Sci. U.S.A.* **104**, 7682-7687

39. Noel, J.P., Hamm, H.E., and Sigler, P.B. (1993) The 2.2 Å crystal structure of transducin-α complexed with GTPγS. *Nature* **366**, 654-663

40. Van Eps, N., Preininger, A.M., Alexander, N., Kaya, A.I., Meier, S., Meiler, J., Hamm, H.E., and Hubbell, W.L. (2011) Interaction of a G protein with an activated receptor opens the interdomain interface in the α subunit. *Proc. Natl. Acad. Sci. U.S.A.* **108**, 9420-9424

41. Min, K.C., Gravina, S.A., and Sakmar, T.P. (2000) Reconstitution of the vertebrate visual cascade using recombinant transducin purified from *Sf*9 cells. *Protein Expr. Purif.* **20**, 514-526

42. Ramachandran, S., and Cerione, R.A. (2011) A dominant-negative Gα mutant that traps a stable rhodopsin-Gα-GTP-βγ complex. *J. Biol. Chem.* **286**, 12702-12711

43. Skiba, N.P., Bae, H., and Hamm, H.E. (1996) Mapping of effector binding sites of transducin α-subunit using $G\alpha_t/G\alpha_{i1}$ chimeras. *J. Biol. Chem.* **271**, 413-424

44. Gasteiger, E., Hoogland, C., Gattiker, A., Duvaud, S., Wilkins, M.R., Appel, R.D., and Bairoch, A. (2005) Protein identification and analysis tools on the ExPASy server. In: John M. Walker (ed): *The Proteomics Protocols Handbook* (Humana Press) 571-607

45. Nielsen, S.S., Noergaard Toft, K., Snakenborg, D., Jeppesen, M.G., Jacobsen, J.K., Vestergaard, B., Kutter, J.P., and Arleth, L. (2009) BioXTAS RAW, a software

program for high-throughput automated small-angle X-ray scattering data reduction and preliminary analysis. *J. Appl. Cryst.* **42**, 959-964

46. Volkov, V.V., and Svergun, D.I. (2003) Uniqueness of *ab initio* shape determination in small-angle scattering. *J. Appl. Cryst.* **36**, 860-864
47. Kozin, M.B., and Svergun, D.I. (2001) Automated matching of high- and low-resolution structural models. *J. Appl. Cryst.* **34**, 33-41
48. Peisley, A., and Skiniotis, G. (2015) 2D projection analysis of GPCR complexes by negative statin electron microscopy. *Methods Mol. Biol.* **1335**, 29-38
49. Tang, G., Peng, L., Baldwin, P.R., Mann, D.S., Jiang, W., Rees, I., and Ludtke, S.J. (2007) EMAN2: an extensible image processing suite for electron microscopy. *J. Struct. Biol*. **157**, 38-46
50. Yang, Z., Fang, J., Chittuluru, J., Asturias, F.J., and Penczek, P.A. (2012) Iterative stable alignment and clustering of 2D transmission electron microscope images. *Structure* **20**, 237-247

Chapter 3

Cryo-EM Structure of the Rhodopsin-Transducin Complex

INTRODUCTION

Rhodopsin (Rho), the photoreceptor evolved for scotopic vision in vertebrates, is a prototypical member of the G protein-coupled receptor (GPCR) family, which is the largest family of membrane proteins in mammalian cells with over 800 members[1]. GPCRs share a common structural motif of seven transmembrane helices and are responsible for transmitting signals triggered by a wide variety of extracellular stimuli, including photons, odorants, hormones and neurotransmitters, across the cell membrane. These signals are transmitted through the activation of heterotrimeric G proteins (Gαβγ), with the active state being defined as the complex between agonist-bound receptor and nucleotide-free G protein[2]. In contrast to the vast diversity of GPCRs, there are only a relatively small number of G proteins, which are categorized based on the sequence similarity shared between their α subunits into four classes: G_S, G_i, G_q and G_{12}[3]. In the visual phototransduction pathway[4], the GPCR Rho is composed of the apoprotein opsin and a covalently bound ligand 11-*cis* retinal which acts as an inverse agonist for the receptor. The absorption of a photon induces the *cis-trans* isomerization of retinal, generating a 'full agonist' capable of activating the receptor. Activated Rho can then recruit transducin (G_T, its subunits are designated as $G\alpha_T$, $G\beta_1$, $G\gamma_1$), a member of the G_i family of heterotrimeric G proteins, and catalyze the exchange of GDP for GTP within

Cryo-EM data acquisition, image processing and 3D reconstructions were contributed by our collaborator Dr. Georgios Skiniotis and his lab member Dr. Hongli Hu at Stanford University.

the $G\alpha_T$ subunit. GTP-bound $G\alpha_T$ then binds and activates the effector enzyme, the cGMP phosphodiesterase (PDE6), which reduces the cytosolic concentration of the second messenger cGMP. The abundance of Rho in vertebrate retinae[5] and its relatively high stability make it an attractive model system for studying GPCR structural mechanisms. Crystallization efforts on Rho have yielded the first high-resolution structure of a GPCR in its inactive state[6], and subsequently, structures of the apoprotein opsin[7,8] and all-*trans* retinal-bound Rho[9]. In the past decade, with the development of techniques such as T4 lysozyme fusion[10,11], thermostabilizing mutagenesis[12,13] and *in meso* crystallization[14], the number of GPCR structures has increased dramatically, such that currently there are more than 200 high-resolution structures of GPCRs for over 40 different receptors[15]. However, only a small fraction of these structures are of activated receptors, and despite the *tour de force* achievement of the active-state β_2-adrenergic receptor-G_S protein complex (β_2AR-G_S) structure by Kobilka and colleagues in 2011[16], GPCR-G protein complexes have been generally unyielding to X-ray crystallography efforts.

Most recently, with the advent of direct electron detectors[17] and beam-induced motion correction softwares[18,19], single-particle cryo-electron microscopy (cryo-EM) has emerged as a powerful tool for high-resolution structural determination without the need for extensive protein engineering and crystallization. During the past year, cryo-EM has been used to obtain three structures of two different GPCRs, namely the calcitonin receptor[20] and the glucogon-like peptide-1 (GLP-1) receptor[21,22], coupled to the G_S protein. The available GPCR-G protein complex structures have yielded valuable structural information about the mechanisms of receptor activation and the interaction

between agonist-bound receptors and heterotrimeric G proteins. Moreover, they have illustrated how diverse GPCRs share topological similarities on their cytoplasmic regions and engage the same G_S protein. Despite this progress, the details underlying the observed specificity between GPCRs and their specific signaling partners from different G protein classes have for the most part remained elusive. The recent cryo-EM structures of μ-opioid receptor[23] and Rho[24] coupled to the inhibitory G_i protein have begun to address this question, revealing how G_i engages GPCRs in a different orientation than G_S. In order to further our understanding of GPCR-G protein coupling specificity, and to learn more about the mechanisms by which GPCRs activate their specific G protein partners, we have obtained a near-atomic resolution cryo-EM structure of the 126 kD complex between light-activated, native bovine Rho and its cognate G protein partner transducin. Analysis of this complex shows how a G_i-like G protein transducin engages an activated GPCR in a manner distinct from the interactions of GPCRs with the G_S protein, as well as reveals the diverse modes of coupling between GPCRs and different G proteins within the same inhibitory family. Moreover, this cryo-EM structure highlights the unique aspects regarding how light-activated Rho catalyzes GDP-GTP exchange on the $G\alpha_T$ subunit.

RESULTS

Isolation of a stable rhodopsin-transducin complex

The active-state Rho-G_T complex was formed with Rho and the G protein $\beta_1\gamma_1$ complex purified from bovine retinae, and a recombinant transducin α subunit in which 18 residues of bovine $G\alpha_T$ are replaced with corresponding residues from $G\alpha_{i1}$[25]; (from

here on referred to simply as $G\alpha_T$). The addition of $G\alpha_{i1}$ residues allowed $G\alpha_T$ to be expressed and purified in *E coli*, and a His_6-tag was introduced at its N-terminus to serve as a purification handle for subsequent extraction of the Rho-G_T complex from purified bovine rod outer segments (ROS)[26]. Recombinant $G\alpha_T$ can undergo Rho catalyzed GDP-GTP exchange and activate the downstream effector PDE6 as effectively as bovine $G\alpha_T$[27,28] and significantly better than G_i, which is poorly activated by Rho and is incapable of activating PDE6.

In order to form the Rho-$G\alpha_T$-$\beta 1\gamma 1$ (Rho-G_T) complex, purified bovine ROS membranes containing native dark-state Rho was initially mixed with $G\alpha_T$ and native bovine $\beta_1\gamma_1$ in the dark. The mixture was then illuminated with white light, resulting in the activation of Rho and the ensuing formation of the complex on the ROS membranes. The active-state complex was then extracted with the detergent lauryl maltose neopentyl glycol (LMNG)[29] and purified with Ni-immobilized-metal affinity and size exclusion chromatography. The Rho-G_T complex is stable at 4 °C in the dark for over a week and is fully active, as it readily dissociates upon the addition of GTPγS, a non-hydrolysable GTP analogue[26]. The monodispersity of the complex was confirmed with negative-stain EM and single-particle two-dimensional (2D) averaging[30].

Cryo-EM structure determination of the Rho-G_T complex

We utilized single-particle cryo EM to determine a high-resolution structure of the light-activated Rho-G_T complex without the addition of a nanobody or antibody fragment. Cryo-EM micrographs revealed monodispersed complex particles and 2D classification of the particles unveiled complex projections with clear secondary

structural features, including the transmembrane helix bundle of Rho embedded in a detergent micelle and all three subunits of G_T. Subsequent 3D reconstruction yielded a density map that accomodates a 1:1 complex consisting of monomeric Rho and G_T. Interestingly, there is a visible density for the helical domain of $G\alpha_T$ in the low resolution map (Fig. 3.1a), suggesting that this domain in nucleotide-free $G\alpha_T$ is more rigid compared to the helical domain in the β_2AR-G_S complex[31]. However, the helical domain within $G\alpha_T$ is still significantly more flexible compared to the other components making up the Rho-G_T complex. Therefore, in order to improve the resolution, densities for the helical domain and the detergent micelle were subtracted out. Refinement in 3D yielded a cryo-EM density map of the Rho-G_T complex with an indicated nominal global resolution of 4.5 Å (Fig. 3.1b). The quality of the cryo-EM map is highest in the receptor region and receptor-G protein interface. A near-atomic resolution structure of the Rho-G_T complex without the helical domain was built into the map (Fig. 3.1c) and allowed us for the first time to directly visualize how the photoreceptor specifically engages and activates its cognate signaling partner G_T.

Structure of the active-state rhodopsin

The first high-resolution GPCR structure solved by X-ray crystallography was obtained for Rho in its dark (inactive) state. Subsequently, a series of structures for Rho in its various signalling states were determined, namely, the apo protein opsin[7], the agonist-bound meta II state[9], meta II Rho bound to the $G\alpha_T$ C-terminal peptide ($G\alpha_T$CT)[9], and the Rho-arrestin complex[32].

Figure 3.1 Cryo-EM structure of the rhodopsin-transducin complex. a, low-resolution cryo-EM map showing the density of the α helical domain. **b,** orthogonal views of the refined cryo-EM density map. **c,** structure of the rhodopsin-transducin complex colored by subunit shown in the same views. Rho: red, $G\alpha_T$: green, $G\beta_1$: cyan, $G\gamma_1$: magenta.

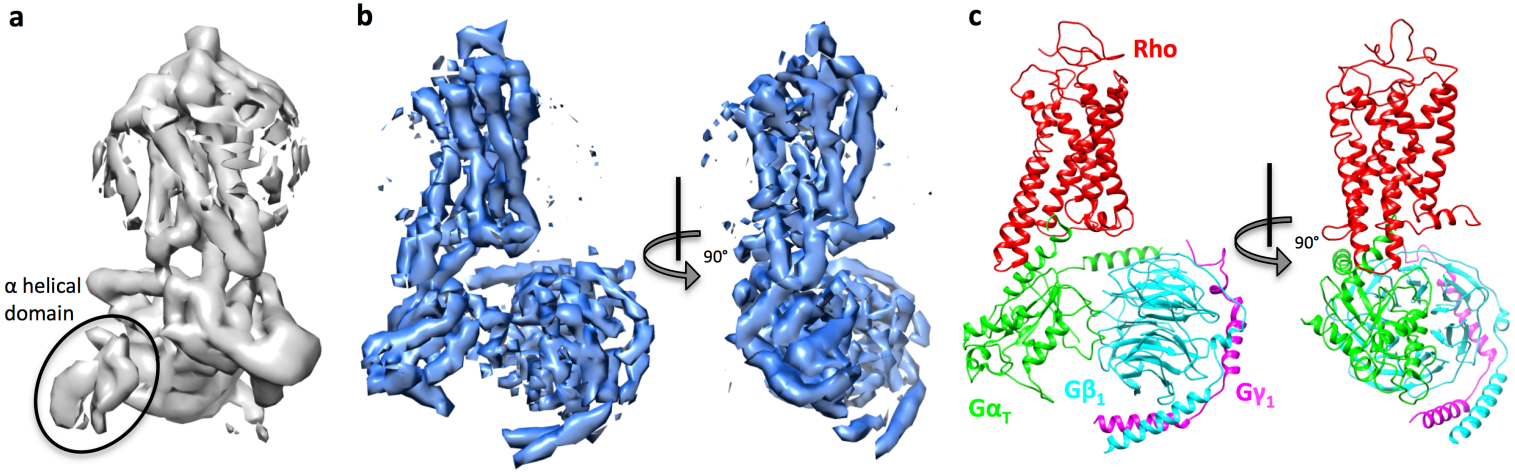
a
α helical
domain
b
90°
c
Rho
90°
Gα$_T$
Gβ$_1$
Gγ$_1$

In comparison to the inactive Rho structure, the most significant changes in the structure for G_T-bound light-activated Rho reported here are in the intracellular loop 3 (ICL3) region, which in dark-state Rho is a 15-residue-long extended loop. The N-terminal 10 residues of ICL3 fold into an α-helix forming a 15 Å downward extension of transmembrane helix 5 (TM5), with the shortening of ICL3 pulling TM6 outward by 7 Å. In addition, there are also subtle outward movements in ICL1 and ICL2, as well as in the cytoplasmic ends of TM1 and TM4, and a 13° horizontal rotation of helix 8 (H8). These concerted movements open up the cytoplasmic cavity of Rho and provide a binding interface to engage $G\alpha_T$ (Fig. 3.2a). The overall architecture of Rho in the Rho-G_T complex is similar to structures for $G\alpha_T$CT-bound Rho[9] (root mean squre deviation (RMSD) of 1.13 Å) (Fig. 3.2b) and the arrestin-bound Rho[30] complex (RMSD of 1.15 Å) (Fig. 3.2c). Residues in the highly conserved E(D)RY and NPxxY motifs of Rho, which are important for GPCR activation, adopt similar conformations in all three structures (Fig. 3.2d, e). There are subtle changes in the Rho-G_T structure compared to that for $G\alpha_T$CT-bound Rho, specifically, a 2.6 Å outward movement of ICL3 and a 1.7 Å downward movement of H8, allowing the receptor to better engage the full length G protein. Comparisons with the arrestin-bound Rho structure show a notable difference in ICL2, which moves 7.5 Å inward and forms an α helix while engaging arrestin. The ICL2 helix narrows the cytoplasmic cavity of the receptor preventing it from fully accommodating the larger signaling partner, the G protein, and could be a significant structural feature utilized by activated Rho to differentially interact with G_T versus arrestin.

Figure 3.2 Structural comparison between the transducin-bound rhodopsin and rhodopsin in various signaling states. a, orthogonal views of the superimposition between the G_T-bound (red) and inactive (magenta, PDB 1U19) rhodopsin. **b,** orthogonal views of the superimposition between the G_T-bound (red) and $G\alpha_T$CT-bound (green, PDB 3PQR) rhodopsin. **c,** orthogonal views of the superimposition between the G_T-bound (red) and arrestin-bound (yellow, PDB 5W0P) rhodopsin. **d,** comparison of residues from the conserved E(D)RY and NPxxY motifs in the G_T-bound and $G\alpha_T$CT-bound rhodopsin structures. **e,** comparison of residues from the conserved E(D)RY and NPxxY motifs in the G_T-bound and arrestin-bound rhodopsin structures.

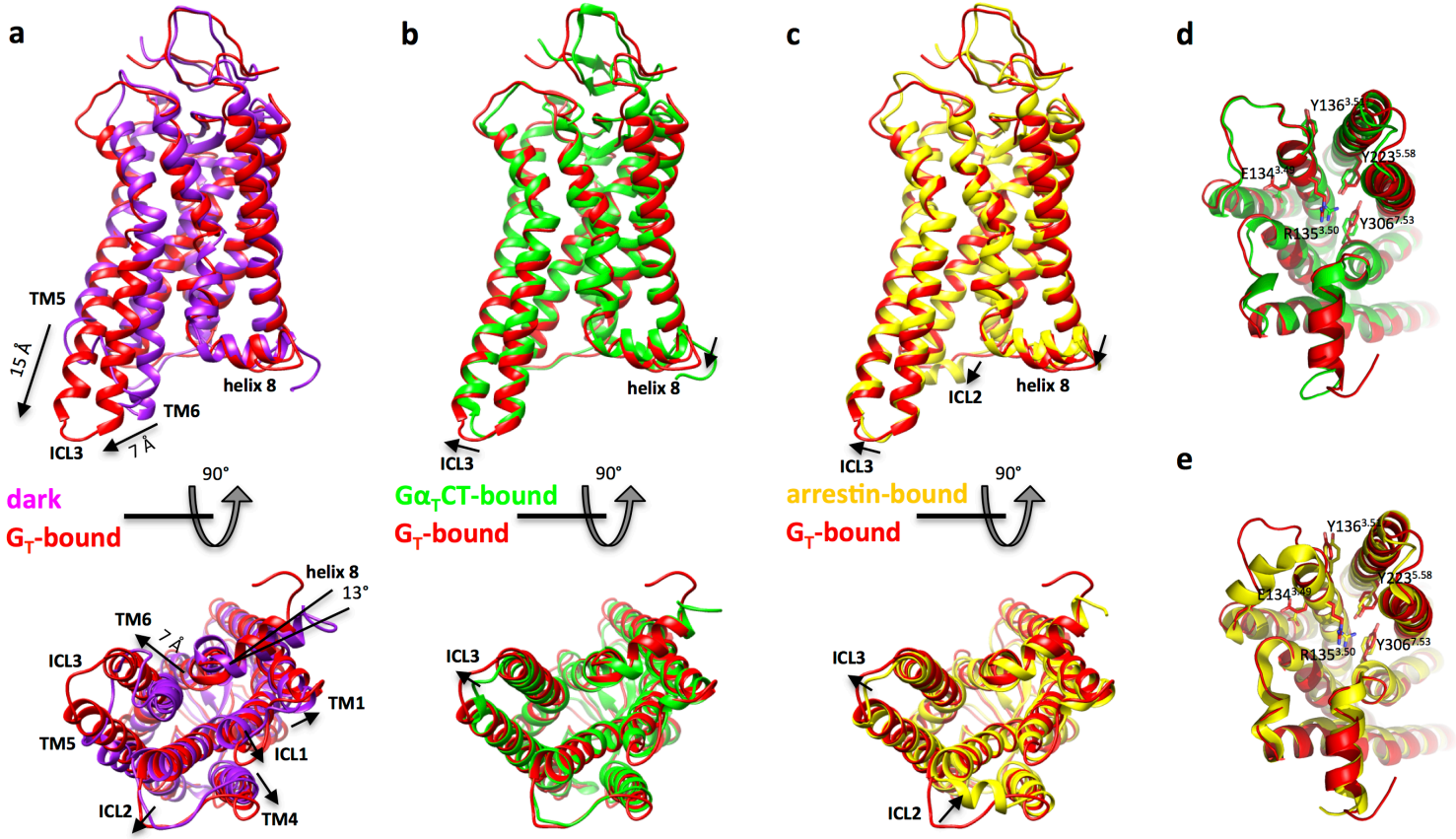
a
TM5
15 Å
helix 8
TM6
ICL3
7 Å
dark
G$_T$-bound
90°
helix 8
13°
TM6
7 Å
ICL3
TM1
TM5
ICL1
ICL2
TM4
b
helix 8
ICL3
Gα$_T$CT-bound
G$_T$-bound
90°
ICL3
c
ICL2
helix 8
ICL3
arrestin-bound
G$_T$-bound
90°
ICL3
ICL2
d
Y136$^{3.51}$
Y223$^{5.58}$
E134$^{3.49}$
R135$^{3.50}$
Y306$^{7.53}$
e
Y136$^{3.51}$
Y223$^{5.58}$
E134$^{3.49}$
R135$^{3.50}$
Y306$^{7.53}$

The Rho-G_T interface: insights into G protein-coupling specificity

In the Rho-G_T complex structure, Rho engages G_T through the $G\alpha_T$ subunit. This interaction is mainly mediated by extensive contacts between the cytoplasmic surface of Rho and the C-terminal α5 helix of $G\alpha_T$, together with an additional interaction between the ICL2 of Rho and the α_N-β_1 juncture of $G\alpha_T$. The overall architecture of the Rho-G_T complex shows significant differences when compared to the β_2AR-G_S complex.[16] The most notable difference in the receptor region is the orientation of TM6, which adopts a more closed conformation and moves inward by 10 Å in Rho (Fig. 3.3a). As a result of the distinct opening of TM6, $G\alpha_T$ engages Rho in a markedly different orientation compared to how $G\alpha_s$ binds to the β2-adrenergic receptor. The α5 helix in $G\alpha_T$ rotates away by 24° towards H8 in order to avoid clashing with the more inward-facing TM6 in Rho (Fig. 3.3a). This rotation propagates through the entire Ras-like domain of $G\alpha_T$ and results in a 21° rotation of the αN helix, leading to a 19 Å rigid body movement of the Gβγ subunits (Fig. 3.3b), giving rise to an orientation of the G protein that is similar to what has been observed in the recent Rho-G_i protein complex (Rho-G_i) structure[24], and as was reported in an electron paramagnetic resonance (EPR) study of the Rho-G_i complex[33]. The cytoplasmic positions of the receptor TM bundle in Rho-G_T are very similar to those in the recent μ-opioid receptor-G_i protein complex (μOR-G_i) structure[23] (Fig. 3.3c), suggesting that this smaller outward tilt of TM6 may be a common feature utilized by GPCRs activating the G_i-family G proteins. However, the ICL3 of μOR differs from that in Rho as it is extended at the N-terminal end through the unwinding of the last helical turn of TM5, resulting in an inward movement by about 10 Å (Fig. 3.3c).

Figure 3.3 Different G protein orientations in Rho-G_T complex, β_2AR-G_S complex and μOR-G_i complex. a, different Gα Ras domain α5 helix orientations in Rho-G_T complex and β_2AR-G_S complex (PDB 3SN6). Rho: red, $G\alpha_T$: green, β_2AR: orange, G_S: yellow. **b,** different G protein orientations in Rho-G_T complex and β_2AR-G_S complex. **c,** different Gα Ras domain α5 helix orientations in Rho-G_T complex and μOR-G_i complex (PDB 6DDF). Rho: red, $G\alpha_T$: green, μOR: cyan, G_i: magenta. **d,** different G protein orientations in Rho-G_T complex and μOR-G_i complex.

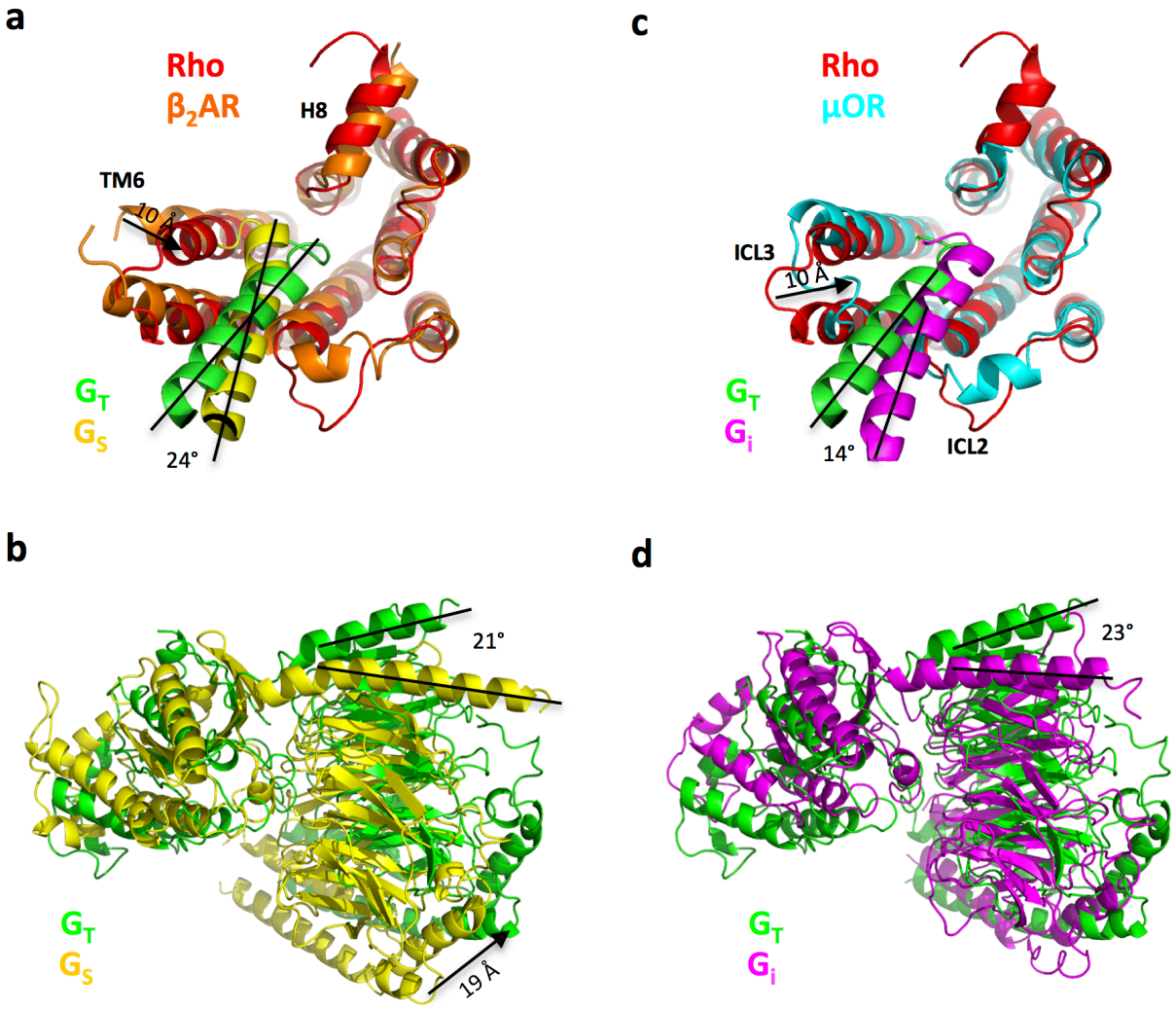
a
Rho
β2AR
H8
TM6
10 Å
GT
GS
24°
c
Rho
μOR
ICL3
10 Å
GT
Gi
14°
ICL2
b
21°
GT
GS
19 Å
d
23°
GT
Gi

Consequently, although the α5 helix in μOR-G_i terminates at nearly the same position as it does in the Rho-G_T complex, it tilts by 14° towards ICL2 as it exits the receptor, avoiding potential clashes with the more inward-facing ICL3 (Fig. 3.3c). As a result, the αN helix in G_i rotates by 23°, back to a similar receptor-coupling orientation adopted by G_S (Fig. 3.3d).

The α5 helix of $G\alpha_T$ inserts as a straight α helix into Rho, terminated by a 4-residue loop. The position of the C terminus (CT) of α5 agrees well with that of the $G\alpha_T$ peptide in the structure for the $G\alpha_T$CT-bound Rho and is in close proximity to H8 (Fig. 3.4a). However, this is different from the position of the α5 CT in the recent Rho-G_i structure, in which it shifts slightly downward out of the receptor (Fig. 3.4b). The closer proximity between the α5 CT of $G\alpha_T$ and Rho likely reflects the better coupling of Rho with G_T compared to its interaction with G_i. In the Rho-G_T complex, the α5 CT slightly kinks at the second helical turn and tilts by 5° toward to directly engaging H8 (Fig. 3.4a). The main-chain carbonyl groups of residues 346-DCGL-349 (H5.22-H5.25, common Gα numbering (CGN) system[34]) at the end of the α5 CT form a negatively charged surface that undergoes electrostatic interactions with the positive charges of the main-chain amino groups at the N terminus of H8 (Fig. 3.4c). This interaction is strengthened by extensive hydrogen bonding with Rho residues $R135^{3.50}$ (superscript indicating Ballesteros–Weinstein numbering for GPCRs[35]) from TM3, $E249^{6.32}$ from TM6, together with $K311^{8.48}$ and $Q312^{8.49}$ from H8 (Fig 4d). This network of charge interactions is also present, though to a lesser extent, in the μOR-G_i complex (Fig. 3.4e).

Figure 3.4 Comparison of the interactions between Gα C terminus and receptor in Rho complexes, μOR-G_i complex and β_2AR-G_S complex. a, comparison of $G\alpha_T$ C terminus orientation in Rho-G_T and Rho-$G\alpha_T$CT (PDB 3PQR) complexes. Rho: red, G_T: green, Rho-$G\alpha_T$CT: pink. **b,** comparison of $G\alpha_T$ C terminus orientation in Rho-G_T and Rho-G_i (PDB 3PQR) complexes. Rho: red, G_T: green, Rho-G_i: grey. **c,** electrostatic interaction between backbone carbonyl (red spheres) of $G\alpha_T$ C terminus and backbone amino groups (blue spheres) of helix 8 N terminus. **d,** interactions between $G\alpha_T$ C terminus and Rho. **e,** interactions between $G\alpha_i$ C terminus (magenta) and μOR (purple). **f,** interactions between $G\alpha_S$ C terminus (yellow) and β_2AR (orange).

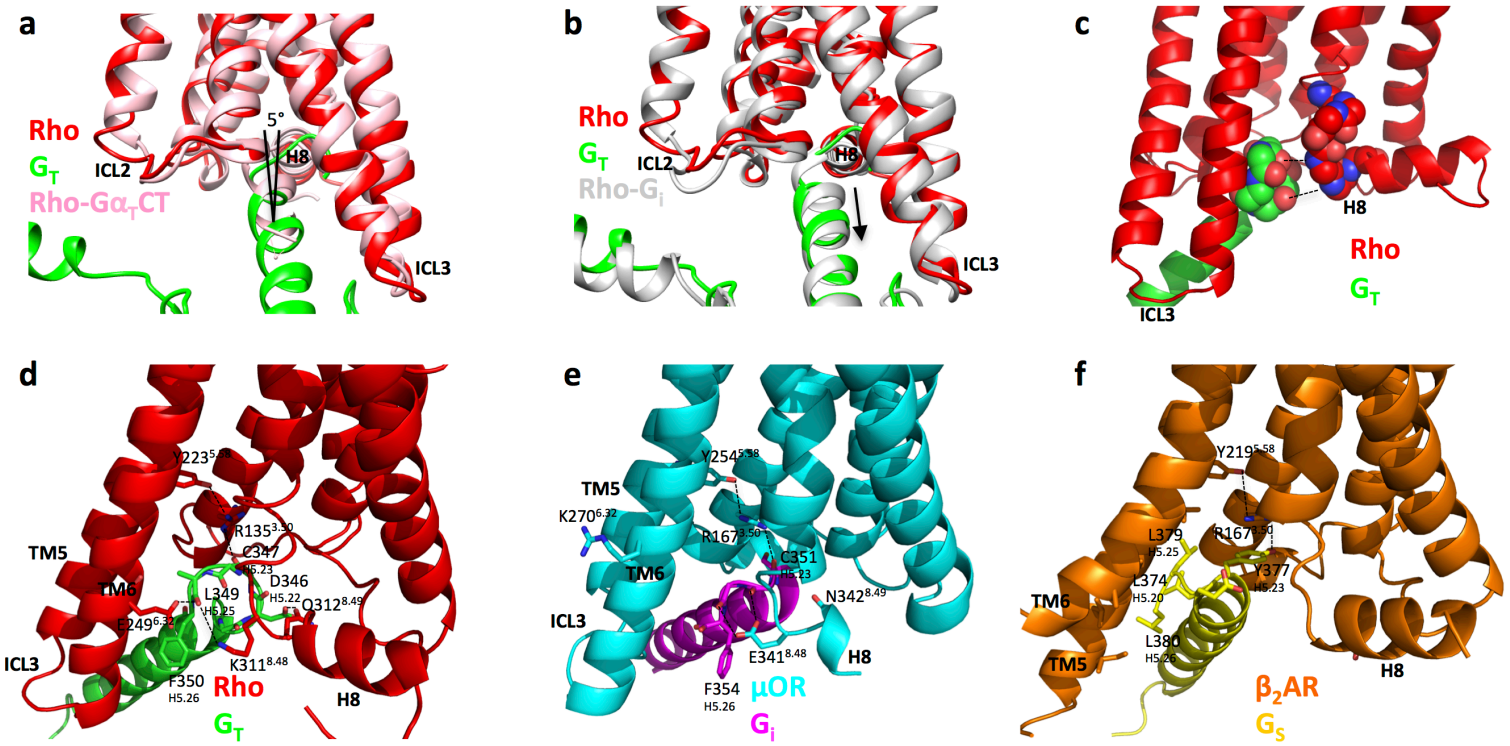
a
Rho
G_T
Rho-Gα_TCT
ICL2
5°
H8
ICL3
b
Rho
G_T
Rho-G_i
ICL2
H8
ICL3
c
H8
Rho
G_T
ICL3
d
$Y223^{5.58}$
$R135^{3.50}$
C347
H5.23
D346
H5.22
$Q312^{8.49}$
L349
H5.25
$F249^{6.33}$
$K311^{8.48}$
TM5
TM6
ICL3
F350
H5.26
Rho
G_T
H8
e
$Y254^{5.58}$
TM5
$K270^{6.32}$
$R167^{3.50}$
C351
H5.23
TM6
ICL3
$N342^{8.49}$
$E341^{8.48}$
H8
F354
H5.26
μOR
G_i
f
$Y219^{5.58}$
$R167^{3.50}$
L379
H5.25
L374
H5.20
Y377
H5.23
TM6
L380
H5.26
TM5
H8
β_2AR
G_S

Whereas in the β_2AR-G_S complex, it is replaced by hydrophobic interactions, as $G\alpha_S$ positions the H5.23-H5.26 tilt into the cavity formed by the more open TM6 and interacts with a large hydrophobic patch formed by TM5 (Fig. 3.4f). This significantly different mode of interaction provides a structural basis underscoring the importance of the α5 CT in determining G protein-coupling specificity[36]. Notably, despite the markedly different α5 CT positions, the backbone carbonyl of C347 (H5.22) in $G\alpha_T$ (C351 in $G\alpha_i$) adopts an almost identical position as the side-chain hydroxyl of Y391 (H5.22) and forms a hydrogen-bonding network with R135$^{3.50}$ from the conserved E(D)RY motif and Y223$^{5.58}$ in the Y(x)$_7$K(R) motif in TM5 (Fig. 3.4d,e,f), stablizing the receptor active-state conformation.

Following the C terminal polar interactions with Rho, the G_T α5 helix forms hydrophobic contacts through L344 (H5.20) and I340 (H5.16) with a hydrophobic patch at the interface between TM3 (V139$^{3.54}$) and TM5 (T229$^{5.64}$, V230$^{5.65}$, A233$^{5.68}$) (Fig. 3.5a). Similar hydrophobic interactions also exist in μOR-G_i, but are more extensive with further contribution from nonpolar residues in ICL3 (Fig. 3.5b). In β_2AR-G_S however, the corresponding residue at H5.16 position is Q384 and it forms polar interactions with β_2AR instead (Fig. 3.5c). As the α5 helix of $G\alpha_T$ exits Rho, it interacts with ICL3 through a network of polar interactions, involving T242$^{6.25}$ and Q237$^{5.72}$ from Rho, and K341 (H5.17), D337 (H5.13) from the α5 helix and Y316 (S6.2) from β6 strand of $G\alpha_T$ (Fig. 3.5a). Mutating any of the corresponding residues in $G\alpha_i$ to alanine would significantly impair complex formation with Rho[37], suggesting the importance of this polar network in stabilizing the nucleotide-free complex.

Figure 3.5 Comparison of receptor-G protein interfaces in Rho-G_T, μOR-G_i and β_2AR-G_S complexes. a, Interactions between G_T α5 helix and Rho. Rho: red, G_T: green. **b,** Interactions between G_i α5 helix and μOR. G_i: magenta, μOR: cyan. **c,** Interactions between G_S α5 helix and β_2AR. G_S: yellow, β_2AR: orange. **d,** Interactions between Rho ICL2 and G_T. **e,** Interactions between μOR ICL2 and G_i. **f,** Interactions between β_2AR ICL2 and G_S.

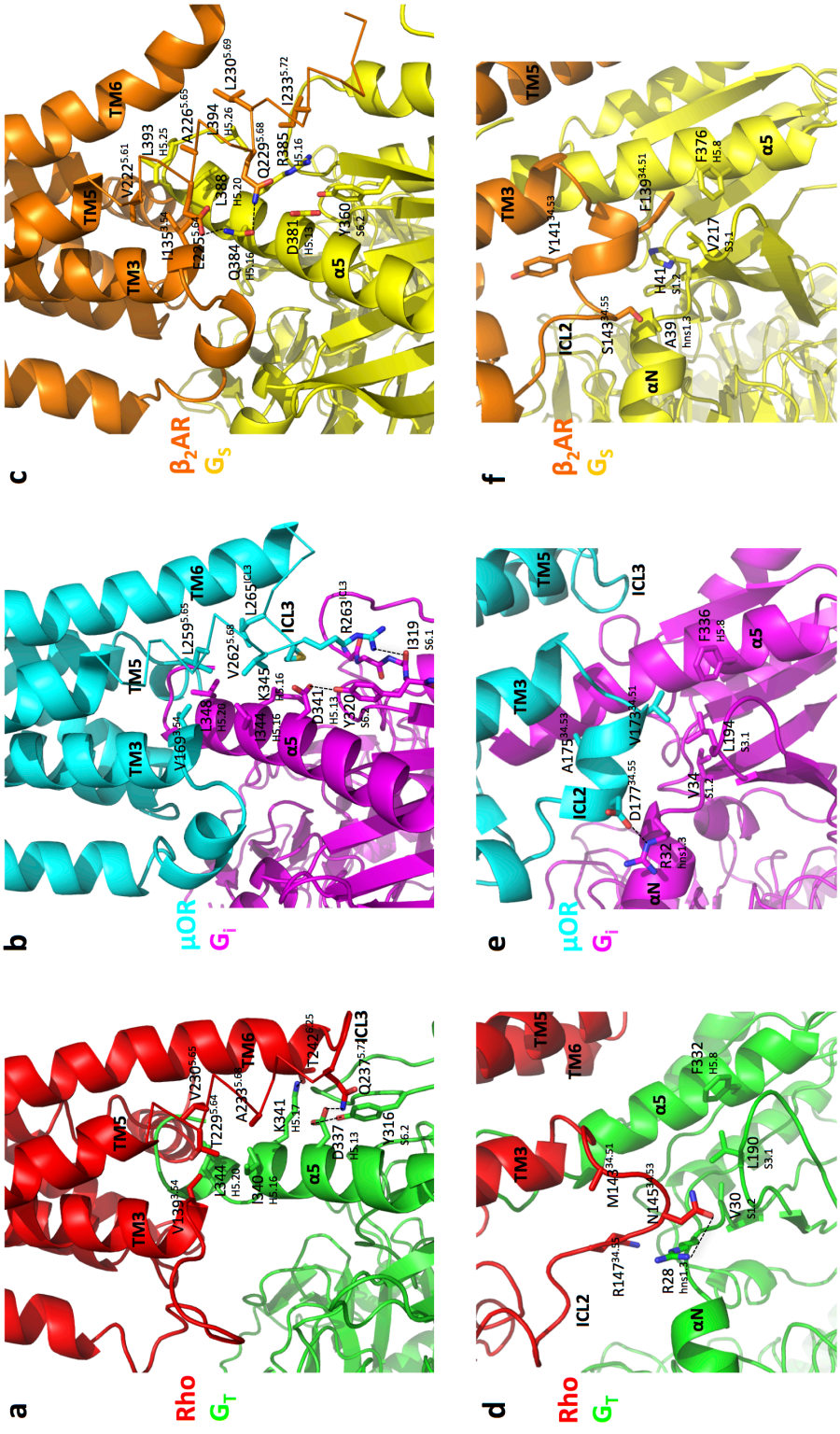
a
Rho
G_T
TM5
TM6
TM3
α5
ICL3
ICL2
αN
b
μOR
G_i
c
β_2AR
G_s
d
e
f

This interaction network is not observed in the β_2AR-G_S structure (Fig. 3.5c) and is different from the mixed polar and nonpolar interactions that occur between the ICL3 of μOR and $G\alpha_i$ (Fig. 3.5 b).

A second interaction site between Rho and G_T involves ICL2 (Fig. 3.5d). Unlike the cases for the μOR and the β_2AR (Fig. 3.5e,f), the ICL2 in Rho does not form a helix. Thus, as a result of the distinct orientation of G_T within the Rho- G_T complex, the ICL2 of Rho does not interact with the hydrophobic pocket formed by the α5 helix and the β2-β3 loop in $G\alpha_T$. Instead, there is only a small polar contact between N145 and the backbone carbonyl of S144 in ICL2, and R28 (hns1.3) from the αN-β1 juncture of $G\alpha_T$.

Structure of nucleotide-free G_T: Insights into G protein activation

Within the cryo-EM structure for the Rho-G_T complex, the most striking changes in the Ras-like domain of $G\alpha_T$, when compared to the X-ray structure for GDP-bound $G\alpha_T$ [38], involve the α5 helix, which rotates upwards by about 1.25 helical turns and inserts into the cytoplasmic crevice of the activated Rho (Fig. 3.6a). This rotational translation is accomplished through a loss in the helicity of the N-terminal 5 residues of the α5 helix, resulting in significant rearrangements of the interactions between the α5 helix and the remainder of the Ras-like domain. On the right side of the α5 helix (β5 and β6 strands) (Fig. 3.6b,c), D337 (H5.13) moves upward to contact the ICL3 of Rho and simultaneously interacts with Y316 (S6.2), pulling the β6 strand of $G\alpha_T$ toward the receptor. The β5 strand moves closer to the N terminal portion of the α5 helix stabilizing this region through π-π stacking between F263 (S5.5) and F330 (H5.6).

Figure 3.6 Changes in $G\alpha_T$ upon Rho binding. a, Overall structural comparison between G_T·GDP (PDB 1GOT) and nucleotide-free G_T. $G\alpha_T$·GDP: salmon, $G\beta_1\gamma_1$ in G_T·GDP: light blue, nucleotide-free $G\alpha_T$: green, $G\beta_1\gamma_1$ in nucleotide-free G_T: grey. **b,** Interactions between α5 helix and β5, β6 sheets in $G\alpha_T$·GDP. **c,** Interactions between α5 helix and β5, β6 sheets in nucleotide-free $G\alpha_T$. **d,** Interactions between α5 helix and β2, β3 sheets, α1 helix in $G\alpha_T$·GDP. **e,** Interactions between α5 helix and β2, β3 sheets, α1 helix in nucleotide-free $G\alpha_T$.

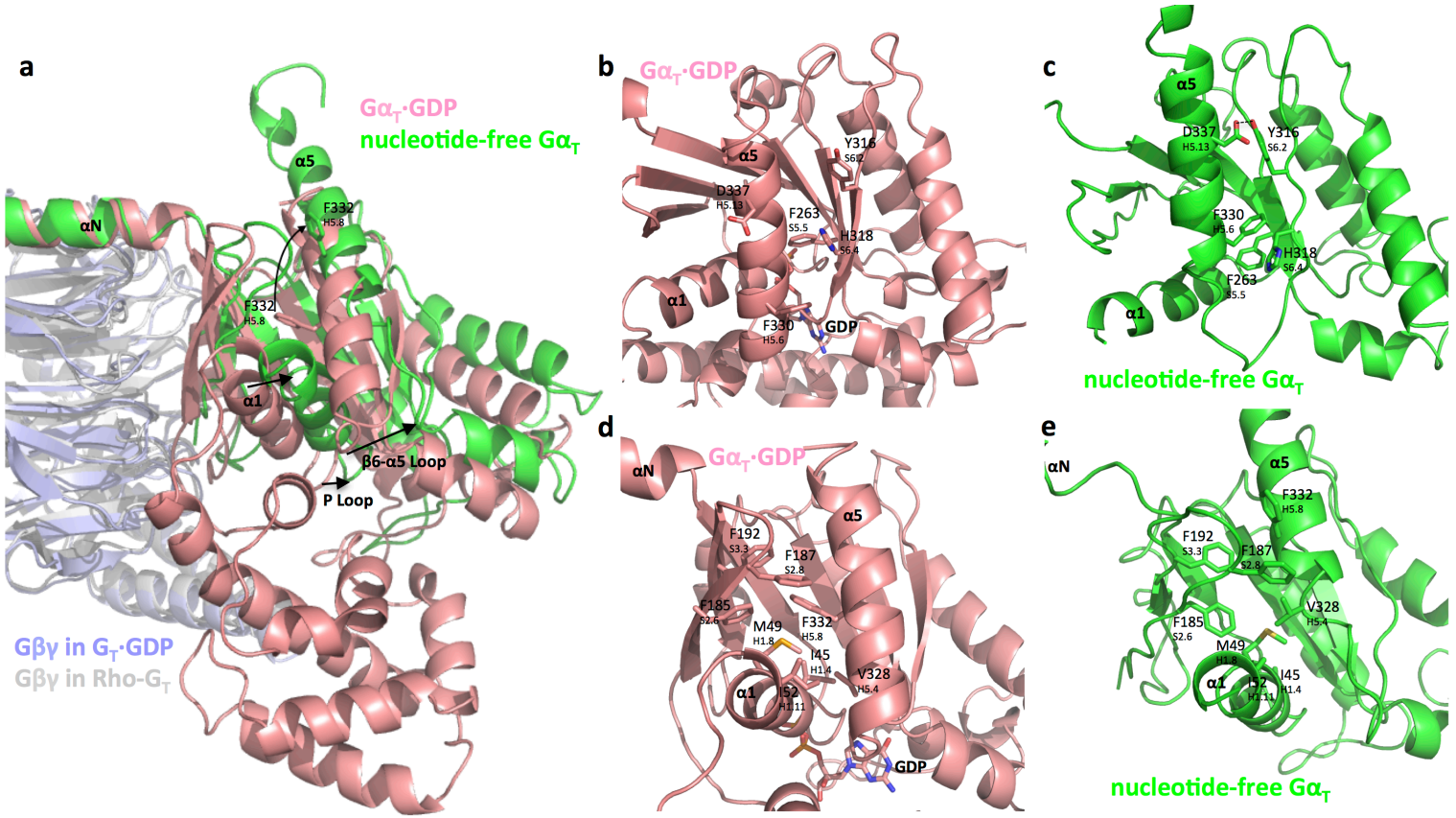
a
Gα$_T$·GDP
nucleotide-free Gα$_T$
αN
α5
F332
H5.8
F332
H5.8
α1
β6-α5 Loop
P Loop
Gβγ in G$_T$·GDP
Gβγ in Rho-G$_T$
b
Gα$_T$·GDP
α5
Y316
S6.2
D337
H5.13
F263
S5.5
H318
S6.4
α1
F330
H5.6
GDP
c
α5
D337
H5.13
Y316
S6.2
F330
H5.6
H318
S6.4
F263
S5.5
α1
nucleotide-free Gα$_T$
d
αN
Gα$_T$·GDP
α5
F192
S3.3
F187
S2.8
F185
S2.6
M49
H1.8
F332
H5.8
I45
H1.4
α1
I52
H1.11
V328
H5.4
GDP
e
αN
α5
F332
H5.8
F192
S3.3
F187
S2.8
V328
H5.4
F185
S2.6
M49
H1.8
α1
I52
H1.11
I45
H1.4
nucleotide-free Gα$_T$

The positions of these two Phe residues clash with H318 (S6.4), pushing the C-terminal portion of β6 strand outward. The concerted movements in the α5 helix and β6 strand pull the β6-α5 loop away from interacting with the guanine base of GDP through its conserved TCAT motif. On the left side of the α5 helix (β2, β3 strands and α1 helix) (Fig. 3.6d,e), its upward rotation removes the highly conserved F332 (H5.8) out of the hydrophobic pocket formed together with F185 (S2.6), F187 (S2.8) from β2, and F192 (S3.3) from β3. As a result, the β2-β3 loop moves closer to α5 helix to allow F187 (S2.8) and F192 (S3.3) to engage F332 (H5.8) at its new position, preserving the hydrophobic interaction. This motion brings F185 (S2.6) from β2 into the space freed up by F332 (H5.8), such that it contacts M49 (H1.8), pushing the α1 helix toward the N terminus of the α5 helix. In addition, the upward translation of the α5 helix destabilizes the position of the α1 helix by disrupting a hydrophobic network between V328 (H5.4) of the α5 helix, and I45 (H1.4) and I52 (H1.11) from the α1 helix. As the α1 helix directly connects to the P-loop, which binds to the β phosphate of GDP, changes in the conformation of the α1 helix perturb the P-loop, thus loosening its contact with GDP. Moreover, given that both the α1 helix and β2 strand are directly linked to the helical domain, their movements toward the α5 helix disrupt interdomain connections and promote the dissociation of helical domain from the Ras domain. The structure of the GTP-bound $G\alpha_T$ is very similar to that of the GDP-bound state, except for the inward movement of the Switch II region, which is resulted from ionic interactions formed between the N-terminal part of Switch II and the additional γ phosphate provided by GTP. As Switch II contributes to most of the contacts between $G\alpha_T$ and $G\beta_1$ subunits, the conformational changes in this region weakens the affinity of $G\alpha_T$ for the βγ subunits. In addition, the binding of GTP causes

structural changes in $G\alpha_T$, which are reverse to the changes that happen during receptor-promoted GDP dissociation described above. Therefore, the interactions on both the receptor-$G\alpha_T$ and the $G\beta_1$-$G\alpha_T$ interfaces are impaired, resulting in the dissociation of the complex.

In contrast to the marked changes occurring within the $G\alpha_T$ subunit, the conformation of the $G\beta_1\gamma_1$ subunits remain very similar in the Rho-G_T complex when compared the GDP-bound G_T heterotrimer (RMSD 1.16 Å), with the exception of the loop connecting the last two β strands (strands C and D) in the 2nd β propeller blade of the $G\beta_1$ subunit (i.e. 2nd CD loop, residues 127-KTREGNVR-134). This loop moves out of the β propeller by about 4 Å in the Rho-G_T complex (Fig. 3.7a). The density in this region is not well resolved in our cryo-EM map, suggesting that the 2nd CD loop may be flexible in the Rho-G_T complex. A previous hydrogen-deuterium exchange mass spectroscopy (HXMS) study on the β_2AR-G_S complex also showed that this is the only region in the G_S β_1 subunit that had an elevated level of flexibility upon complex formation[39]. Interestingly, when X-ray structures of the $G\alpha_T$ helical domain from the G_T·GDP heterotrimer were docked together with our cryo-EM Rho-G_T structure into the low-resolution cryo-EM map for the Rho- G_T complex, which has a density for the helical domain, the 2nd CD loop of $G\beta_1$ is in close proximity to the αB-αC loop in the helical domain, enabling possible polar contacts between E111 and E112 (H.hbhc.3, H.hbhc.4) from the helical domain, and R129 and R134 from the $G\beta_1$ subunit (Fig. 3.7b,c).

Figure 3.7 Interaction between $G\alpha_T$ helical domain and $G\beta_1$. a, Overall structural comparison between $G\beta_1\gamma_1$ in G_T·GDP (grey) and $G\beta_1\gamma_1$ in nucleotide-free G_T (green). **b,** $G\alpha_T$ helical domain orientation revealed by low-resolution cryo-EM map. **c,** Interaction between $G\alpha_T$ helical domain and $G\beta_1$. **d,** Trp fluorescence assay monitoring Rho-catalyzed nucleotide exchange in WT $G\alpha_T$ and helical domain mutants.

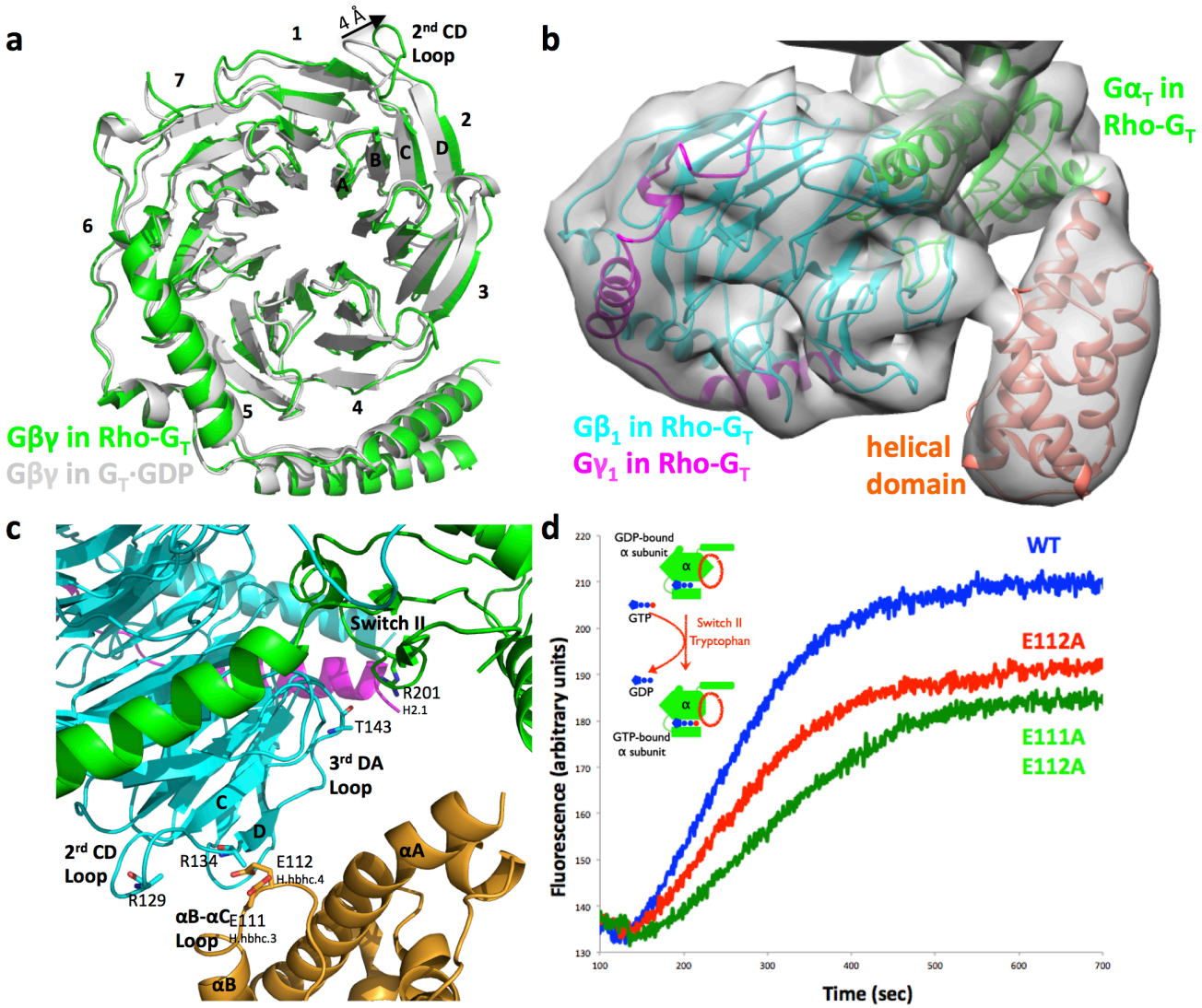
a
4 Å
1
2nd CD Loop
7
2
D
C
B
A
6
3
5
4
Gβγ in Rho-GT
Gβγ in GT·GDP
b
GαT in Rho-GT
Gβ1 in Rho-GT
Gγ1 in Rho-GT
helical domain
c
Switch II
R201
H2.1
T143
3rd DA Loop
C
D
2rd CD Loop
R134
E112
H.hbhc.4
αA
R129
αB-αC Loop
E111
H.hbhc.3
αB
d
GDP-bound α subunit
α
GTP
Switch II Tryptophan
GDP
GTP-bound α subunit
WT
E112A
E111A
E112A
Fluorescence (arbitrary units)
Time (sec)
220
210
200
190
180
170
160
150
140
130
100
200
300
400
500
600
700

Mutating the two Glu residues in the helical domain significantly slowed the rate of Rho-catalyzed nucleotide exchange (Fig. 3.7d), as read-out by changes in the intrinsic Trp fluorescence assay that occur as a result of the conformational changes in the Switch II (SW II) region of $G\alpha_T$[40]. The E111 and E112 residues lie within the solvent-exposed surface of G_T·GDP and are not involved in any intra- or inter-domain contacts; therefore, the slower rate of nucleotide exchange is likely due to the disruption of their interactions with $G\beta_1$ unpon complex formation. As the 2nd CD loop is directly linked through stand D to the 3rd DA loop (the loop connecting strand D of blade 2 to strand A of blade 3), which interacts with the N terminal portion of the Switch II region (SWII) in $G\alpha_T$ (Fig. 3.7c), the interaction with the helical domain may weaken the contact between $G\beta_1$ and SWII, facilitating the release of SWII from $G\beta_1$ upon GTP binding. The E111 and E112 (H.hbhc.3, H.hbhc.4) residues are conserved across G_T, G_i and G_S, and similar 2nd CD loop conformations have been observed for all three G proteins in their receptor-coupled state. Thus, the helical domain-Gβ interaction may be a common feature utilized to promote complex dissociation upon GTP binding.

DISCUSSION

In conclusion, we have reported here a high-resolution cryo-EM structure of a Rho-G_T complex formed on native retinae membrane with native Rho and G_T without the addition of either a nanobody or an antibody fragment. The Rho-G_T complex structure sheds new light upon the molecular basis of the G protein activation event. It shows how the upward insertion of the α5 helix of the Ras-like domain of a Gα subunit into the cytoplasmic crevice of the activated GPCR conveys signal to the nucleotide-binding

pocket, through the rearrangement of key hydrophobic interactions within the Ras-like domain, promoting the dissociation of GDP and the opening of the helical domain. Moreover, analysis of a low-resolution cryo-EM map of the Rho-G_T complex points to a potential role for the opened helical domain in facilitating the dissociation of the GPCR-G protein complex upon GTP binding, through the interactions of the helical domain with the Gβ subunit, and as further corroborated by biochemical studies.

The Rho-G_T complex structure also shows that G_T couples to Rho in an orientation that differs significantly from the G_S protein, as well as the G_i protein, in other GPCR-G protein structures that have thus far been reported, highlighting the diverse modes of coupling that exist between these important signaling proteins. Although the coupling specificity on the G protein part is largely determined by the residues at the C terminus of the α5 helix within the Ras-like domain of $G\alpha_T$, the specificity determinants on GPCRs is much more complex and are likely conferred by the cytoplasmic topology of the transmembrane bundle, especially the level of the TM6 outward tilt. Given the high degree of GPCR sequence heterogeneity, it remains difficult to predict, based on protein sequence, the G protein-coupling preference of a receptor[41]. This problem is further complicated by the dynamic nature of GPCR conformations[42] and the fact that some of these receptors are able to couple to more than one G protein[43]. Therefore, more GPCR-G protein structures will be needed in order to provide better correlations between receptor sequence and the 3D topology of its G protein-interacting surface.

METHODS

Purification of the Rho-G_T complex

The Rho-G_T complex was purified in essentially the same procedure as described in chapter 2, except in the final gel filtration step, LMNG detergent concentration was reduced to 0.005% (w/v) to reduce the amount of free micelles that may interfere with cryo-EM particle picking.

Cryo-EM data acquisition

A sample of 3.5 µl of purified Rho-G_T complex at a concentration of approximately 10 $mg \cdot ml^{-1}$ was applied to glow-discharged holey carbon grids (Quantifoil R2/2, 300 mesh), and subsequently vitrified using a Vitrobot Mark IV (FEI Company). The specimen was visualized with a Titan Krios electron microscope (FEI) operating at 300 kV accelerating voltage, at a nominal magnification of 29,000× using a K2 Summit direct electron detector (Gatan, Inc.) in counting mode, corresponding to a pixel size of 1.0 Å on the specimen level. In total, 12,616 images with defocus values in the range of −1.5 to −3.0 µm were recorded with a dose rate of about 9.0 electrons per $Å^2$ per second. The total exposure time was set to 10 s with intermediate frames recorded every 0.2 s, resulting in an accumulated dose of about 90 electrons per $Å^2$ and a total of 50 frames per movie stack.

Image processing and 3D reconstructions

Dose-fractionated image stacks were subjected to beam-induced motion correction using MotionCor2[19]. A sum of all frames, filtered according to exposure dose, in each image

stack was used for further processing. CTF parameters for each micrograph were determined by CTFFIND4[44]. Particle selection, two-dimensional classification and three-dimensional classification were performed on a binned dataset with a pixel size of 2 Å using RELION[45]. Particle projections were selected using semi-automated procedures and subjected to reference-free two-dimensional classification to discard false-positive particles or particles categorized in poorly defined classes. An *ab initio* map generated with VIPER[46] was used as initial reference model for maximum-likelihood-based 3D classification. Picked particles (1,656,447) were subjected to 3D classification with eight classes. Particles (422,637) from two best-looking classes were combined and subjected to another run of 3D classification with four classes. Three stable classes accounting for 250,451 particles showed detailed features for all subunits and were combined in subsequent 3D refinement and reconstruction after subtracting densities for the mobile α-helical domain and the detergent micelle from the raw micrographs. The final map has a global nominal resolution of 4.5 Å, based on the gold-standard Fourier shell correlation (FSC) using the 0.143 criterion.

Model building and refinement

The receptor structure from the Rho-Gα_TCT complex (PDB 3PQR) and the crystal structure of GDP-bound transducin heterotrimer (PDB 1GOT) were used as initial templates for the Rho-G_T complex model. All models were docked into the EM density map using Chimera[47], followed by iterative manual adjustment and real-space refinement using COOT[48]. The final model was subjected to global refinement and minimization in real space using the module phenix.real_space_refine in PHENIX[49].

Tryptophan fluorescence assay

Fluorescence measurements were carried out with a Varian eclipse spectrofluorimeter. UROS was light activated (Rho) by incubation on ice under ambient light for 5 min. Rho-catalyzed nucleotide exchange on the α_T subunit in detergents was monitored by premixing 5 nM Rho and 300 nM $\beta_1\gamma_1$ in HMN buffer (20 mM HEPES, pH 7.5, 2 mM $MgCl_2$, 100 mM NaCl, 1 mM DTT) with 50 μM GTPγS and 0.01% (w/v) LMNG detergent, monitoring tryptophan fluorescence (excitation: 300 nm; emission: 345 nm) in real-time upon the addition of 300 nM α_T.

REFERENCES

1. Fredriksson, R., Lagerström, M. C., Lundin, L.-G. & Schiöth, H. B. The G-Protein-Coupled Receptors in the Human Genome Form Five Main Families. Phylogenetic Analysis, Paralogon Groups, and Fingerprints. *Mol. Pharmacol.* **63,** 1256–1272 (2003).
2. Lean, A. D., Stadel, J. M. & Lefkowitz, R. J. A ternary complex model explains the agonist-specific binding properties of the adenylate cyclase-coupled beta-adrenergic receptor. *J. Biol. Chem.* **255,** 7108–7117 (1980).
3. Simon, M. I., Strathmann, M. P. & Gautam, N. Diversity of G proteins in signal transduction. *Science* **252,** 802–808 (1991).
4. Stryer, L. Visual excitation and recovery. *J. Biol. Chem.* **266,** 10711–10714 (1991).
5. Nickell, S., Park, P. S.-H., Baumeister, W. & Palczewski, K. Three-dimensional architecture of murine rod outer segments determined by cryoelectron tomography. *J. Cell Biol.* **177,** 917–925 (2007).
6. Palczewski, K. *et al.* Crystal structure of rhodopsin: A G protein-coupled receptor. *Science* **289,** 739–745 (2000).
7. Park, J. H., Scheerer, P., Hofmann, K. P., Choe, H.-W. & Ernst, O. P. Crystal structure of the ligand-free G-protein-coupled receptor opsin. *Nature* **454,** 183–187 (2008).
8. Scheerer, P. *et al.* Crystal structure of opsin in its G-protein-interacting conformation. *Nature* **455,** 497–502 (2008).
9. Choe, H.-W. *et al.* Crystal structure of metarhodopsin II. *Nature* **471,** 651–655 (2011).

10. Rosenbaum, D. M. *et al.* GPCR engineering yields high-resolution structural insights into beta2-adrenergic receptor function. *Science* **318,** 1266–1273 (2007).
11. Chun, E. *et al.* Fusion Partner Toolchest for the Stabilization and Crystallization of G Protein-Coupled Receptors. *Struct. England1993* **20,** 967–976 (2012).
12. Serrano-Vega, M. J., Magnani, F., Shibata, Y. & Tate, C. G. Conformational thermostabilization of the β1-adrenergic receptor in a detergent-resistant form. *Proc. Natl. Acad. Sci.* **105,** 877–882 (2008).
13. Vaidehi, N., Grisshammer, R. & Tate, C. G. How do mutations thermostabilize G protein-coupled receptors? *Trends Pharmacol. Sci.* **37,** 37–46 (2016).
14. Caffrey, M. & Cherezov, V. Crystallizing Membrane Proteins Using Lipidic Mesophases. *Nat. Protoc.* **4,** 706–731 (2009).
15. Isberg, V. *et al.* GPCRdb: an information system for G protein-coupled receptors. *Nucleic Acids Res.* **44,** D356–D364 (2016).
16. Rasmussen, S. G. F. *et al.* Crystal structure of the β2 adrenergic receptor–Gs protein complex. *Nature* **477,** 549–555 (2011).
17. Bammes, B. E., Rochat, R. H., Jakana, J., Chen, D.-H. & Chiu, W. Direct electron detection yields cryo-EM reconstructions at resolutions beyond 3/4 Nyquist frequency. *J. Struct. Biol.* **177,** 589–601 (2012).
18. Li, X. *et al.* Electron counting and beam-induced motion correction enable near-atomic-resolution single-particle cryo-EM. *Nat. Methods* **10,** 584–590 (2013).
19. Zheng, S. Q. *et al.* MotionCor2: anisotropic correction of beam-induced motion for improved cryo-electron microscopy. *Nat. Methods* **14,** 331–332 (2017).

20. Liang, Y.-L. *et al.* Phase-plate cryo-EM structure of a class B GPCR–G-protein complex. *Nature* **546,** 118–123 (2017).
21. Zhang, Y. *et al.* Cryo-EM structure of the activated GLP-1 receptor in complex with a G protein. *Nature* **546,** 248–253 (2017).
22. Liang, Y.-L. *et al.* Phase-plate cryo-EM structure of a biased agonist-bound human GLP-1 receptor–Gs complex. *Nature* **555,** 121–125 (2018).
23. Koehl, A. *et al.* Structure of the μ-opioid receptor–G i protein complex. *Nature* 1 (2018). doi:10.1038/s41586-018-0219-7
24. Kang, Y. *et al.* Cryo-EM structure of human rhodopsin bound to an inhibitory G protein. *Nature* 1 (2018). doi:10.1038/s41586-018-0215-y
25. Skiba, N. P., Bae, H. & Hamm, H. E. Mapping of Effector Binding Sites of Transducin α-Subunit Using Gαt/Gαil Chimeras. *J. Biol. Chem.* **271,** 413–424 (1996).
26. Gao, Y. *et al.* Isolation and structure–function characterization of a signaling-active rhodopsin–G protein complex. *J. Biol. Chem.* **292,** 14280–14289 (2017).
27. Majumdar, S., Ramachandran, S. & Cerione, R. A. Perturbing the Linker Regions of the α-Subunit of Transducin A NEW CLASS OF CONSTITUTIVELY ACTIVE GTP-BINDING PROTEINS. *J. Biol. Chem.* **279,** 40137–40145 (2004).
28. Ramachandran, S. & Cerione, R. A. A Dominant-negative Gα Mutant That Traps a Stable Rhodopsin-Gα-GTP-βγ Complex. *J. Biol. Chem.* **286,** 12702–12711 (2011).
29. Chae, P. S. *et al.* Maltose-neopentyl glycol (MNG) amphiphiles for solubilization, stabilization and crystallization of membrane proteins. *Nat. Methods* **7,** 1003–1008 (2010).

30. Peisley, A. & Skiniotis, G. 2D Projection Analysis of GPCR Complexes by Negative Stain Electron Microscopy. *Methods Mol. Biol. Clifton NJ* **1335,** 29–38 (2015).

31. Westfield, G. H. *et al.* Structural flexibility of the Gαs α-helical domain in the β2-adrenoceptor Gs complex. *Proc. Natl. Acad. Sci.* **108,** 16086–16091 (2011).

32. Zhou, X. E. *et al.* Identification of Phosphorylation Codes for Arrestin Recruitment by G Protein-Coupled Receptors. *Cell* **170,** 457-469.e13 (2017).

33. Van Eps, N. *et al.* G_i - and G_s -coupled GPCRs show different modes of G-protein binding. *Proc. Natl. Acad. Sci.* **115,** 2383–2388 (2018).

34. Flock, T. *et al.* Universal allosteric mechanism for Gα activation by GPCRs. *Nature* **524,** 173–179 (2015).

35. Ballesteros, J. A. & Weinstein, H. [19] Integrated methods for the construction of three-dimensional models and computational probing of structure-function relations in G protein-coupled receptors. in *Methods in Neurosciences* (ed. Sealfon, S. C.) **25,** 366–428 (Academic Press, 1995).

36. Conklin, B. R., Farfel, Z., Lustig, K. D., Julius, D. & Bourne, H. R. Substitution of three amino acids switches receptor specificity of Gqα to that of Giα. *Nature* **363,** 274–276 (1993).

37. Sun, D. *et al.* Probing Gαi1 Protein Activation at Single Amino Acid Resolution. *Nat. Struct. Mol. Biol.* **22,** 686–694 (2015).

38. Lambright, D. G. *et al.* The 2.0 Å crystal structure of a heterotrimeric G protein. *Nature* **379,** 311–319 (1996).

39. Chung, K. Y. *et al.* Conformational changes in the G protein Gs induced by the β_2 adrenergic receptor. *Nature* **477,** 611–615 (2011).

40. Phillips, W. J. & Cerione, R. A. The intrinsic fluorescence of the alpha subunit of transducin. Measurement of receptor-dependent guanine nucleotide exchange. *J. Biol. Chem.* **263,** 15498–15505 (1988).
41. Flock, T. *et al.* Selectivity determinants of GPCR-G protein binding. *Nature* **545,** 317–322 (2017).
42. Nygaard, R. *et al.* The Dynamic Process of β2-Adrenergic Receptor Activation. *Cell* **152,** 532–542 (2013).
43. Kilts, J. D. *et al.* β2-Adrenergic and Several Other G Protein–Coupled Receptors in Human Atrial Membranes Activate Both Gs and Gi. *Circ. Res.* **87,** 705–709 (2000).
44. Rohou, A. & Grigorieff, N. CTFFIND4: Fast and accurate defocus estimation from electron micrographs. *J. Struct. Biol.* **192,** 216–221 (2015).
45. Scheres, S. H. W. Chapter Six - Processing of Structurally Heterogeneous Cryo-EM Data in RELION. in *Methods in Enzymology* (ed. Crowther, R. A.) **579,** 125–157 (Academic Press, 2016).
46. Penczek, P. A., Grassucci, R. A. & Frank, J. The ribosome at improved resolution: new techniques for merging and orientation refinement in 3D cryo-electron microscopy of biological particles. *Ultramicroscopy* **53,** 251–270 (1994).
47. Pettersen, E. F. *et al.* UCSF Chimera--a visualization system for exploratory research and analysis. *J. Comput. Chem.* **25,** 1605–1612 (2004).
48. Emsley, P. & Cowtan, K. Coot: model-building tools for molecular graphics. *Acta Crystallogr. D Biol. Crystallogr.* **60,** 2126–2132 (2004).

49. Adams, P. D. *et al.* PHENIX: a comprehensive Python-based system for macromolecular structure solution. *Acta Crystallogr. D Biol. Crystallogr.* **66,** 213–221 (2010).

Chapter 4

Conclusion

G protein-coupled receptors (GPCRs) comprise the largest known family of integral membrane proteins and are encoded by over 1% of the genome in vertebrates[1]. They are responsible for sensing a vast range of extracellular signals and control cellular responses through activation of heterotrimeric G proteins. As a result of the diverse roles played by GPCRs in human physiology, these membrane receptors represent the most exploited type of drug targets with over 30% of small molecule drugs used today targeting this membrane protein family[2]. Therefore, structural information of GPCRs, especially GPCRs in their G protein-interacting active state, is of great importance. However, due to the intrinsic structural plasticity of GPCRs and their biochemical instability, structural determinations of GPCRs have proven to be extremely challenging.

In my thesis research, I have utilized the vertebrate visual phototransduction cascade as a model system for studying GPCR-G protein interactions. In this system, the photoreceptor molecule rhodopsin is a prototypical GPCR and is the founding member of the largest GPCR subfamily, the rhodopsin-like family. Rhodopsin has a covalently bound ligand, *11-cis* retinal, which functions as an inverse agonist that stabilizes rhodopsin in its inactive state in the dark. The absorption of photons induces the isomerization of *11-cis* retinal to *all-trans* retinal, which becomes an agonist for the receptor, causing structural changes at its intracellular surface. Activated rhodopsin catalyzes the nucleotide exchange within its cognate heterotrimeric G protein-signaling

partner transducin, which is a member of the inhibitory G_i protein family. The GTP-bound transducin then interacts with the downstream effector enzyme, cGMP phosphodiesterse (PDE6), and results in the reduction of cytosolic levels of the second messenger molecule, cGMP. The phototransduction system is highly advantageous for structural studies, as all of its component proteins can be purified from native tissue, bovine retinae, in milligram amounts.

In chapter 2, I utilized the purified retinal rod outer segment membranes, which is naturally enriched in rhodopsin (about 50% of the membrane area is occupied by rhodopsin[3]), and was able to form a nucleotide-free rhodopsin-transducin complex on the native membrane upon light exposure. The resulting membranes were then pelleted down by centrifugation to remove dissociated GDP and free transducin molecules. The rhodopsin-transducin complex was extracted through solubilization with the detergent lauryl maltose neopentyl glycol (LMNG)[4], which has been identified as being able to maintain complex stability over a wide concentration range, as monitored by using the changes in the intrinsic tryptophan fluorescence that occur within α_T during rhodopsin-catalyzed nucleotide exchange[5]. The solubilized complex was then purified with a combination of immobilized metal affinity chromatography (IMAC) and gel filtration steps. The resulting complex is composed of one rhodopsin molecule and one transducin molecule based on both UV-Vis spectroscopy and radioactive nucleotide-binding assays. The purified complex was then further characterized with negative-stain electron microscopy (EM) and small-angle X-ray scattering (SAXS), which revealed that the complex is monodisperse and has a similar overall architecture to the previously characterized β_2 adrenergic receptor-G_S protein complex. Similar to what has been

observed for the β_2 adrenergic receptor-G_S protein complex[6], the helical domain of the transducin α subunit adopts an open conformation in the rhodopsin-transducin complex and has a certain degree of flexibility.

In chapter 3, I and my collaborators utilized cryo electron microscopy (cryo-EM) to obtain a 4.5Å structure of the detergent-solubilized rhodopsin-transducin complex without the addition of any stabilizing nanobody or antibody fragments. The local resolution is highest at the receptor core and the receptor-G protein interface, allowing me to model most of the amino acid side chains in these regions. Our structural model revealed that transducin engages rhodopsin mostly through the C terminal helix of its α subunit and interacts mainly with transmembrane helix (TM) 5, TM6 and the loop that links them, intracellular loop 3 (ICL3). This mode of interaction is significantly different than what has been observed in both recent receptor-G_S protein complex structures[7–10] and other GPCR-G_i complex structures[11–13], in which the G protein α subunit binds the receptor at both ICL2 and the TM5-ICL3-TM6 region. As a result of the strikingly different interaction preferences, the overall orientation of the G protein transducin in the complex is distinct from those observed in other GPCR-G protein complexes. In addition, our cryo-EM map, before refinement, revealed a density for the helical domain of the α_T subunit that is located next to the density of the β subunit, suggesting a possible interaction between them. Mutations of polar residues on the helical domain that have been predicted to contact the β subunit based on the cryo-EM map significantly reduced the rate of rhodopsin-catalyzed nucleotide exchange as monitored by the tryptophan fluorescence assay. These results point to an active role played by the helical domain and the β subunit in promoting receptor-mediated G protein activation.

Included in appendix chapters 1 and 2 are detailed protocols for purifying the rhodopsin-transducin complex and reconstitution of the detergent-solubilized complex into lipid nanodisc particles.

The G protein transducin shares the same β_1 subunit with the G_S protein. As the nanobody Nb35, which was raised against the β_2 adrenergic receptor-G_S protein complex, binds at the interface between α and β subunits[7], we hypothesized that it should be possible to generate a similar nanobody for the rhodopsin-transducin complex by only mutating residues on the interface between the α subunit and Nb35. Based on a homology model generated with the structure of the nucleotide-free G_S α subunit[14], we introduced 12 mutations within the α_T subunit and 3 additional mutations on Nb35 (Fig. 4.1a). The mutations introduced on the α subunit did not impair its ability to undergo rhodopsin-catalyzed nucleotide exchange and the nanobody mutant was able to bind the rhodopsin-transducin complex formed with the mutated α_T subunit in high affinity, as demonstrated by the 1:1 ratio co-elution of the complex and nanobody in size exclusion chromatography (Fig. 4.1b). We have applied the rhodopsin-transducin-nanobody complex to cryo-EM structural determination and were able to obtain a 3.4Å-resolution map for the complex. I am currently in the process of refining the cryo-EM map and building a structural model based on the data. The higher-resolution nanobody complex will make it possible to visualize the rhodopsin-transducin complex in much finer detail and through comparison with the previous structure of the rhodopsin-transducin complex without nanobody, shed light on the possible perturbations caused by nanobody-binding on receptor-G protein complexes.

Figure 4.1 Engineering of nanobody that binds to the rhodopsin-transducin complex. a, A homology model of transducin α subunit overlaid with the nucleotid-free G_S α subunit (PDB 3SN6) illustrating the interface between Nb35 and the α subunit. The transducin α subunit is in red, G_S α subunit is in green and Nb35 is in yellow. **b,** Gel filtration profiles and SDS-PAGE gel showing the nanobody binding to rhodopsin-transducin complex.

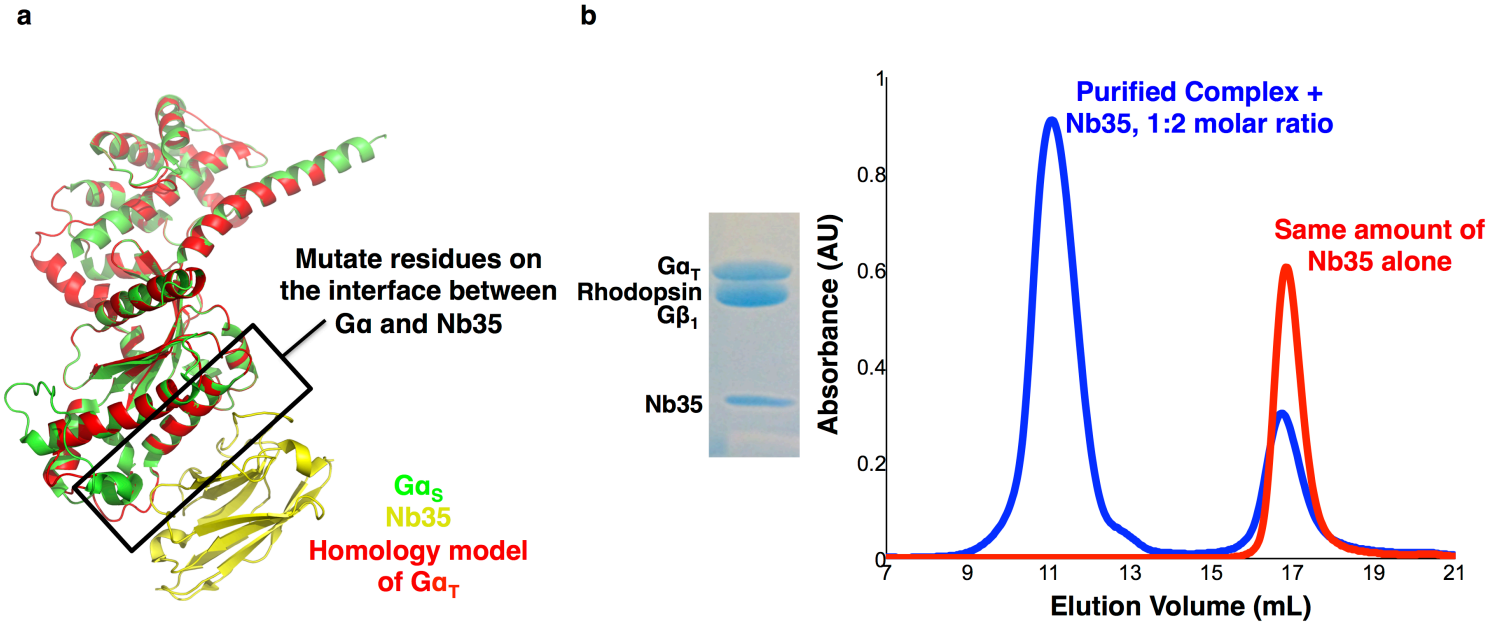
a
Mutate residues on
the interface between
Gα and Nb35
$G\alpha_S$
Nb35
Homology model
of $G\alpha_T$
b
$G\alpha_T$
Rhodopsin
$G\beta_1$
Nb35
Absorbance (AU)
Purified Complex +
Nb35, 1:2 molar ratio
Same amount of
Nb35 alone
Elution Volume (mL)

We are also planning on utilizing interesting transducin α subunit mutants previously developed in our lab, such as the S43N mutant[15], which remains associated with rhodopsin even in the presence of GTP. Structures of complexes formed with transducin mutants would allow us to capture the GPCR-G protein signaling complex in various states along the G protein activation process and would provide invaluable mechanistic details for understanding this important signaling pathway.

In addition to providing a source for milligram quantities of rhodopsin and transducin molecules, the vertebrate visual phototransduction system also allows for extraction of the native effector enzyme PDE6. PDE6 is a prototypical member of the cyclic nucleotide PDE enzyme family, which contains 11 related gene families coding about 100 protein isoforms[16]. PDEs regulate the level of cyclic nucleotide second messenger molecules, cAMP and cGMP, in cells by catalyzing their hydrolysis. As PDEs play a critical role in almost every regulatory system in the body, they are highly valued pharmaceutical targets. PDE6 is composed of four subunits, two non-identical catalytic subunits α and β (each about 100 kD) and two identical inhibitory γ subunits (about 10 kD). Each catalytical subunit (α and β) contains two tandem GAF domains and a C-terminal catalytic domain, which is isoprenylated for membrane association. A major question in the field is how GTP-bound Gα activates PDE6. The consensus nowadays is that Gα·GTP binds PDEγ and displaces, but does not dissociate, PDEγ from the catalytic subunits. As PDE6 has two binding sites (two PDEγ) for Gα·GTP, it is not clear whether it needs two or one Gα·GTP to become fully active and whether the two catalytic subunits α and β behave equally in catalyzing cGMP hydrolysis. Previous strudies in our lab utilizing a transducin C-terminal peptide specific antibody AS/7 have shown that

complexation between this antibody and the GTP-bound transducin α subunit in a 1:2 ratio resulted in a 2-5 fold potentiation of PDE6 activity, suggesting the possible existence of a 2:1 transducin:PDE6 complex[17]. Additionally, we have also previously identified a PDE γ subunit mutant that only binds to one of the two binding sites on the catalytic PDE α and β subunits and is incapable of inhibiting the activity of the enzyme[18]. This finding points to the conclusion that the binding sites on the PDE α and β subunits are different. We are currently in the process of utilizing cryo-EM to determine a high-resolution structure of the PDE6 holoenzyme in its inactive form and are also working on purifying a stable complex between GTP-bound transducin α subunit and activated PDE6 enzyme.

In summary, we have utilized the vertebrate visual phototransduction system to characterize GPCR-G protein interactions, and have been able to obtain a 4.5 Å structure of a nucleotide-free GPCR-G protein complex, the rhodopsin-transducin complex, which has furthered our understanding of the receptor-mediated G protein activation process. This model system also provides the potential for future structural studies of G protein-effector interactions and has proven to be an invaluable system for studying the GPCR-G protein signaling cascade.

REFERENCES

1. Bockaert, J. & Pin, J. P. Molecular tinkering of G protein-coupled receptors: an evolutionary success. *EMBO J.* **18,** 1723–1729 (1999).
2. Santos, R. *et al.* A comprehensive map of molecular drug targets. *Nat. Rev. Drug Discov.* **16,** 19–34 (2017).
3. Palczewski, K. G Protein–Coupled Receptor Rhodopsin. *Annu. Rev. Biochem.* **75,** 743–767 (2006).
4. Chae, P. S. *et al.* Maltose-neopentyl glycol (MNG) amphiphiles for solubilization, stabilization and crystallization of membrane proteins. *Nat. Methods* **7,** 1003–1008 (2010).
5. Phillips, W. J. & Cerione, R. A. The intrinsic fluorescence of the alpha subunit of transducin. Measurement of receptor-dependent guanine nucleotide exchange. *J. Biol. Chem.* **263,** 15498–15505 (1988).
6. Westfield, G. H. *et al.* Structural flexibility of the Gαs α-helical domain in the β2-adrenoceptor Gs complex. *Proc. Natl. Acad. Sci.* **108,** 16086–16091 (2011).
7. Rasmussen, S. G. F. *et al.* Crystal structure of the β2 adrenergic receptor–Gs protein complex. *Nature* **477,** 549–555 (2011).
8. Liang, Y.-L. *et al.* Phase-plate cryo-EM structure of a class B GPCR–G-protein complex. *Nature* **546,** 118–123 (2017).
9. Zhang, Y. *et al.* Cryo-EM structure of the activated GLP-1 receptor in complex with a G protein. *Nature* **546,** 248–253 (2017).
10. Liang, Y.-L. *et al.* Phase-plate cryo-EM structure of a biased agonist-bound human GLP-1 receptor–Gs complex. *Nature* **555,** 121–125 (2018).

11. Koehl, A. *et al.* Structure of the μ-opioid receptor–G i protein complex. *Nature* 1 (2018). doi:10.1038/s41586-018-0219-7

12. Draper-Joyce, C. J. *et al.* Structure of the adenosine-bound human adenosine A 1 receptor–G i complex. *Nature* 1 (2018). doi:10.1038/s41586-018-0236-6

13. García-Nafría, J., Nehmé, R., Edwards, P. C. & Tate, C. G. Cryo-EM structure of the serotonin 5-HT 1B receptor coupled to heterotrimeric G o. *Nature* **558,** 620–623 (2018).

14. Waterhouse, A. *et al.* SWISS-MODEL: homology modelling of protein structures and complexes. *Nucleic Acids Res.* **46,** W296–W303 (2018).

15. Ramachandran, S. & Cerione, R. A. A Dominant-negative Gα Mutant That Traps a Stable Rhodopsin-Gα-GTP-βγ Complex. *J. Biol. Chem.* **286,** 12702–12711 (2011).

16. Conti, M. & Beavo, J. Biochemistry and Physiology of Cyclic Nucleotide Phosphodiesterases: Essential Components in Cyclic Nucleotide Signaling. *Annu. Rev. Biochem.* **76,** 481–511 (2007).

17. Phillips, W. J., Trukawinski, S. & Cerione, R. A. An antibody-induced enhancement of the transducin-stimulated cyclic GMP phosphodiesterase activity. *J. Biol. Chem.* **264,** 16679–16688 (1989).

18. Berger, A. L., Cerione, R. A. & Erickson, J. W. Delineation of two functionally distinct gammaPDE binding sites on the bovine retinal cGMP phosphodiesterase by a mutant gammaPDE subunit. *Biochemistry (Mosc.)* **38,** 1293–1299 (1999).

Appendix Chapter 1

Protocol for Purification of the Rhodopsin-Transducin Complex

INTRODUCTION

G protein-coupled receptors (GPCRs) comprise the largest family of transmembrane proteins in humans with about 800 members[1] and are targets for over 30% of all drugs on the market[2]. They share a signature structural motif of seven transmembrane helixes and transmit signals from a vast array of extracellular stimuli, including hormones, neurotransmitters, odorant and photons, across the plasma membrane[3] and thus modulate a wide range of cellular responses. This process is achieved mostly through the activation of their canonical signaling partners, heterotrimeric G proteins, which are composed of three subunits, the nucleotide-binding α subunit and two constitutively associated subunits β and γ. And they can be classified into four different types based on the amino acid sequence similarity of the α subunits: G_S, G_i, G_q and G_{12}[4].

Despite the striking diversity of the GPCR family, in humans there are only 16 genes encoding 21 different α subunits[5]. And thus each G protein must be able to interact with a large number of different GPCRs. Furthermore there have been evidence showing that some GPCRs, for example the β_2 adrenergic receptor[6], can couple to more than one G proteins. Therefore proper regulation of the specificity between GPCRs and G proteins is vital for signal transduction inside cells. However, due to the intrinsic flexibility and instability of GPCRs and the GPCR-G protein complexes, it has been very challenging to

extract and purify these proteins and elucidate the structural mechanism underlying this specificity.

In recent years, with the development of a wide range of techniques, including novel protein engineering[7], *in meso* crystallization[8], micro-focus beamlines[9] at synchrotron facilities, and cryo-electron microscopy[10], the number of GPCR structures have been growing almost exponentially, among which three are high-resolution structures of GPCR-G protein complexes, namely the β_2 adrenergic receptor-G_S protein complex (solved by X-ray crystallography)[11] and the calcitonin receptor-G_S protein complex[12] and the glucagon-like peptide 1 receptor- G_S protein complex[13] (both solved with cryo-electron microscopy). As all these complex structures are of the same G protein G_S, structural information of complexes formed with different classes of G proteins would be crucial for understanding the specificity between GPCRs and G proteins. And to this end, the visual photo-transduction cascade would be an ideal system, as its G protein transducin belongs to the G_i family.

The visual photo-transduction system is a prototypical GPCR-signaling system. Rhodopsin, the GPCR, has a covalently bound inverse agonist 11-cis retinal which photo-isomerizes into all-trans retinal and becomes an agonist for rhodopsin upon light-activation. Light-activated rhodopsin then binds and catalyzes the exchange of GDP for GTP in the heterotrimeric G protein transducin (G_T, subunits designated as α_T, β_1 and γ_1). The GTP-bound α_T can then turn on cGMP phosphodiesterase (PDE) which hydrolyzes cGMP to GMP, eventually leading to visual neuron signals[14]. This system offers certain advantages for obtaining structural insights into GPCR-signaling, as each of the principle components can be purified from native tissue in large quantities. As a result, rhodopsin

represents the first and only GPCR for which X-ray crystal structures[15-19] have been solved in the native form.

Here we present a method for extracting and purifying the complex between light-activated rhodopsin and nucleotide-free transducin directly from the native retinal membranes[20] (as shown in Fig. 5.1) using proteins components purified from bovine retinae and an α_T/α_{i1} chimera (α_T) which can be expressed in *E coli* and undergo rhodopsin catalyzed nucleotide exchange and activate PDE in a similar manner as native α_T[21]. Forming the complex on membrane allows for easy seperation of the proteins from the GDP dessociated from G_T upon activation by centrifugation, which is destabilizing for the complex. Moreover, as both rhodopsin and G_T are lipid-modified (rhodopsin is palmitolated at its C-terminus[22], α_T has N-terminal myristoylation[23] and γ_1 is farnesylated at the C-terminus[24]), formation of the complex on membrane prior to detergent-extraction would allow for proper engagement among these lipid modifications. The resulting complex can then be solibilized with a mild detergent lauryl maltose neopentyl glycol (LMNG), extracted by utilizing a His_6-tag on α_T and further purified with size-exclusion chromatography (SEC). The purified complex has a 1:1 ratio of rhodopsin to transducin, which can be verified with UV-Vis spectroscopy, as the ligand all-trans retinal has a distinct absorbtion as 380 nm. The complex is very stable and can be stored at 4 °C in the dark for over a week without suffering from much dissociation. This method can also potentially be applied to other recombinantly expressed receptors from insect cells or mamalian cells by forming complexes directly on purified cell membranes.

Figure 5.1 Rhodopsin-transducin complex purification scheme

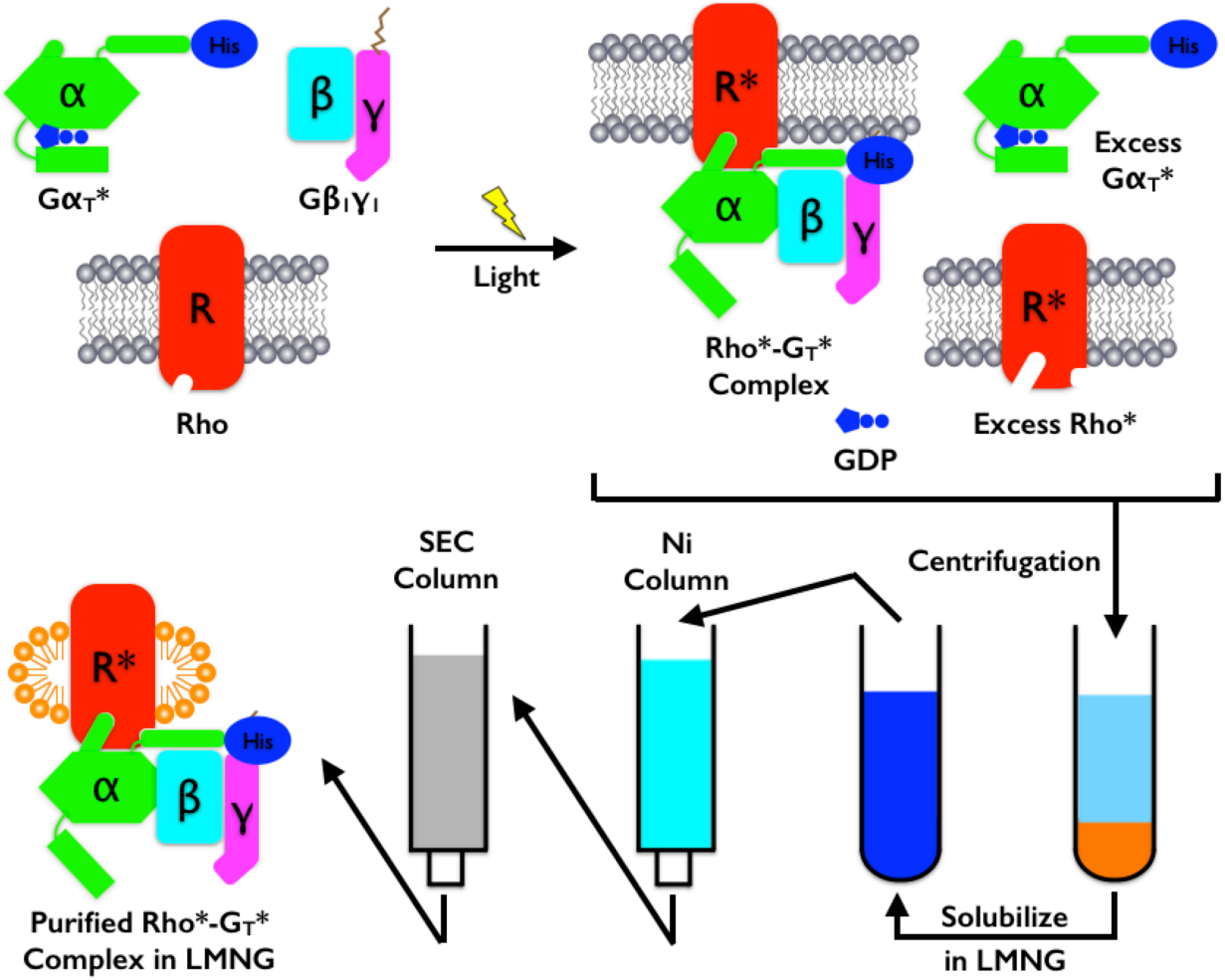
His
α
β
γ
Gαt*
Gβ1γ1
R
Rho
Light
R*
His
α
β
γ
Rho*-Gt*
Complex
GDP
His
α
Excess
Gαt*
R*
Excess Rho*
SEC
Column
Ni
Column
Centrifugation
R*
His
α
β
γ
Purified Rho*-Gt*
Complex in LMNG
Solubilize
in LMNG

MATERIALS

Formation and extraction of the rhodopsin-transducin complex

1. Bovine retinae can be obtained from W L Lawson Company (Omaha, NE).

2. HMN buffer: 20 mM HEPES pH 7.5, 2 mM $MgCl_2$, 100 mM NaCl, 100 μM TCEP.

3. The detergent lauryl maltose neopentyl glycol (LMNG) can be obtained from Anatrace and all other chemicals can be purchased from either Sigma or VWR.

4. Aluminum foil.

5. A tabletop microcentrifuge and an end-to-end rocker kept in a cold room at 4 °C.

6. 1.7 mL microcentrifuge tubes and 15 mL conical tubes.

7. A desk lamp with standard UV filter.

8. Floor lamps covered with 3M 616 lithographer's tape.

Chromatographic purification of the rhodopsin-transducin complex

1. A 1 mL HisTrap HP column (GE Life Sciences)

2. An FPLC equipped with a UV absorbance monitor set at 280 nm and a fraction collector and kept in a cold box at 4 °C. A desk lamp covered with 3M 616 lithographer's tape.

3. HisTrap buffer A: 20 mM HEPES pH 7.5, 2 mM $MgCl_2$, 100 mM NaCl, 100 μM TCEP, 0.02% LMNG.

4. HisTrap buffer B: HisTrap buffer A + 500 mM imidazole pH 7.5.

5. A Superdex 200 10/300 GL column (GE Life Sciences)

6. SEC buffer: 20 mM HEPES pH 7.5, 2 mM $MgCl_2$, 100 mM NaCl, 100 μM TCEP, 0.003% LMNG.

7. Amicon Ultra-0.5 mL centrifugal filters with 100 kD molecular weight cutoff (EMD Millipore).

Characterization of the purified complex with UV-Vis spectroscopy and analytical SEC

1. A UV-Vis spectrophotometer.

2. A Superdex 200 10/300 GL column (GE Life Sciences)

3. An FPLC equipped with a UV absorbance monitor set at 280 nm and a fraction collector and kept in a cold box at 4 °C. A desk lamp covered with 3M 616 lithographer's tape.

4. SEC buffer: 20 mM HEPES pH 7.5, 2 mM $MgCl_2$, 100 mM NaCl, 100 μM TCEP, 0.003% LMNG.

METHODS

Formation and extraction of the rhodopsin-transducin complex

1. Both dark-state rhodopsin (in the form of urea-washed rod outer segment membrane) and transducin $\beta_1\gamma_1$ subunits can be purified from bovine retinae as described previously[25-26] and are stored in HMN buffer with 10% glycerol at -80 °C. Typical concentrations of rhodopsin and $\beta_1\gamma_1$ are 280 μM and 40 μM respectively. (see Note 1)

2. The N-terminally His_6-tagged α_T/α_{i1} chimera (α_T), in which residues from 215 to 295 in α_T, except for residues 244 and 247, are replaced with corresponding residues from α_{i1}, can be expressed and purified from *E coli* BL21(DE3) as described previously[21] and stored in HMN buffer with 10% glycerol at 44 μM concentration at -80 °C. (see Note 2)

3. Thaw one 500 µL aliquot each of rhodopsin, α_T and $\beta_1\gamma_1$ on ice and mix them in a 1.7 mL microcentrifuge tube, resulting in 7:1.1:1 molar ratio of rhodopsin:α_T:$\beta_1\gamma_1$. Incubate mixture on ice in the dark for 5 min. (see Note 3 and 4)

4. In a cold room, lay the tube containing the mixture on to a end-to-end rocker and place a desktop lamp about 10 cm above the tube. Turn on both the rocker and the lamp and expose to mixture to light for about 20 min. (see Note 5)

5. All following steps should be carried out in the dark with red lights. Spin the tube at 16,000 g in a tabletop microcentrifuge for 30 min in the cold room.

6. Carefully asperate out and discard the supernatant. The rhodopsin-transducin complex and excess rhodopsin will be in the membrane pellet at the bottom of the tube.

7. Resuspend the pellet with 2 mL cold HMN buffer with 1% LMNG and transfer the suspension into a 15 mL conical tube. Wrap the tube in foil and gently rock it in the cold room for 30 min. (see Note 6)

8. Add 8 mL cold HMN buffer to the tube and wrap the tube in foil again and gently rock it in the cold room for an additional 60 min.

Chromatographic purification of the rhodopsin-transducin complex

1. Equilibrate a 1 mL HisTrap HP column with 10 mL HisTrap buffer A at 1 mL/min on an FPLC equipped with a UV absorbance monitor set at 280 nm. (see Note 7)

2. Add 0.2 mL HisTrap buffer B to the solubilized complex and load the mixture onto the column at 1 mL/min. (see Note 8)

3. Wash the column with 20 mL 4% B at 1 mL/min. (see Note 9)

4. Elude with a 10 mL 4-40% B gradient and an additional 10 mL 40% B step gradient at 1 ml/min. Collect 1 mL fractions. (see Note 10)

5. Concentrate the fractions containing the complex with two 0.5 mL 100 kD molecular weight cutoff Amicon concentrators at 14,000 g for 3 min each time in a tabletop microcentrifuge kept in a dark cold room with red lights. And wash three times with HisTrap buffer A on the concentrators to remove imidazole. Final volume of the complex is about 200 μL. At this stage the complex can be either stored wrapped in foil on ice overnight or used directly for the next step. (see Note 11)

6. Equilibrate a Superdex 200 10/300 GL column with 60 mL SEC buffer at 0.4 mL/min.

7. Inject the complex from step 5 onto the column run at 0.4 mL/min with SEC buffer. Collect 0.4 mL fractions. (a typical SEC profile is shown in Fig. 5.2)

8. Pool fractions containing the complex from step 7 and concentrate with a 0.5 mL 100 kD molecular weight cutoff Amicon concentrator to about 100 μL. This is the final purified complex and the concentration should be about 10 mg/mL. (see Note 12)

Characterization of the purified complex with UV-Vis spectroscopy and analytical SEC

1. The concentration of the complex can be measured with a UV-Vis spectrophotometer at 280 nm (A_{280nm}) using the extinction coefficient ε_{280nm}=155070 $M^{-1}cm^{-1}$, and molecular weight Mw=126040 Da. (see Note 13)

2. The purity of the complex can be assessed with UV-Vis spectroscopy by measuring the absorbance at 280 nm (A_{280nm}, the absorbance of the protein moieties) and 380 nm (A_{380nm}, the absorbance of all-trans retinal) (a typical spectrum is shown in Fig. 5.3A). The A_{280nm}/ A_{380nm} ratio should be 3.69, indicating a 1:1 rhodopsin:transducin complex. If the complex is contaminated with excess G_T of excess rhodopsin, the ratio will be either higher or lower than 3.69. (see Note 14)

Figure 5.2 SEC profile of rhodopsin-transducin complex purification and SDS-PAGE gel of concentrated peak fractions

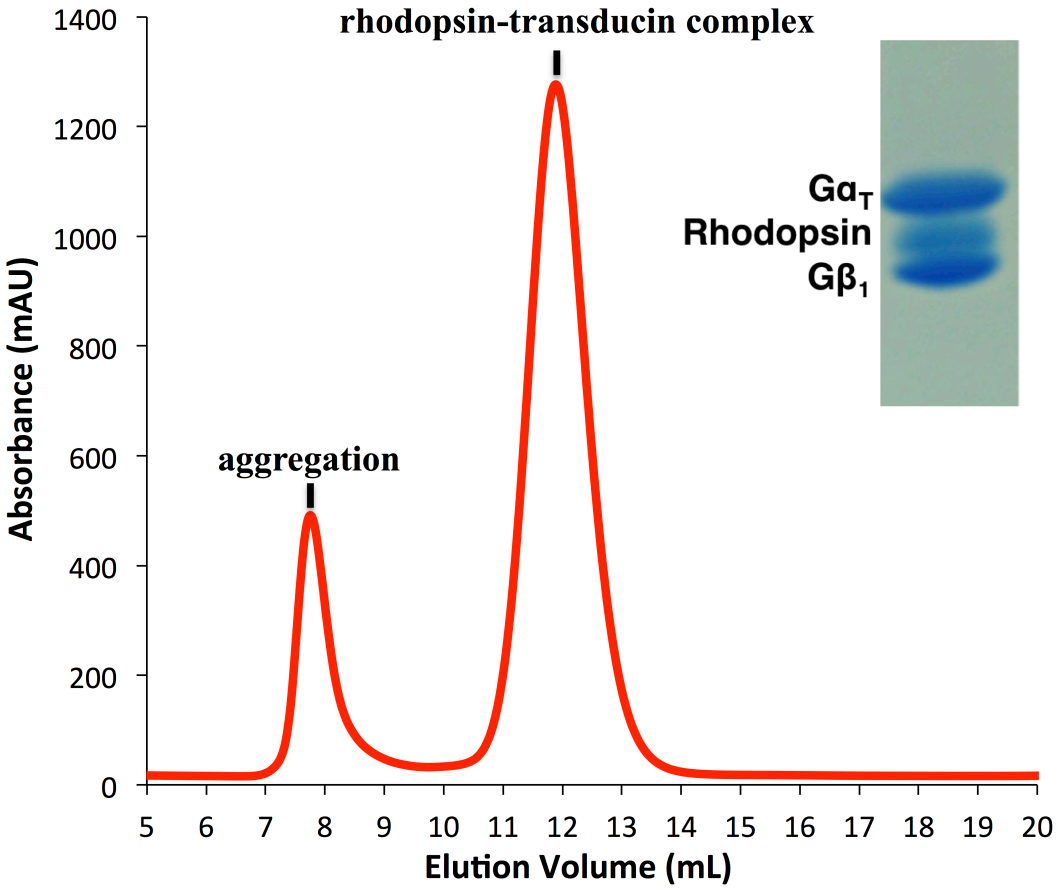
rhodopsin-transducin complex
aggregation
Gα$_T$
Rhodopsin
Gβ$_1$
Absorbance (mAU)
1400
1200
1000
800
600
400
200
0
5
6
7
8
9
10
11
12
13
14
15
16
17
18
19
20
Elution Volume (mL)

Figure 3. UV-Vis spectrum and analytical SEC profiles of the purified rhodopsin-transducin complex A, UV-Vis spectrum of purified complex. B, Analytical SEC profiles of Day 1 (blue) and Day 7 (orange) complexes.

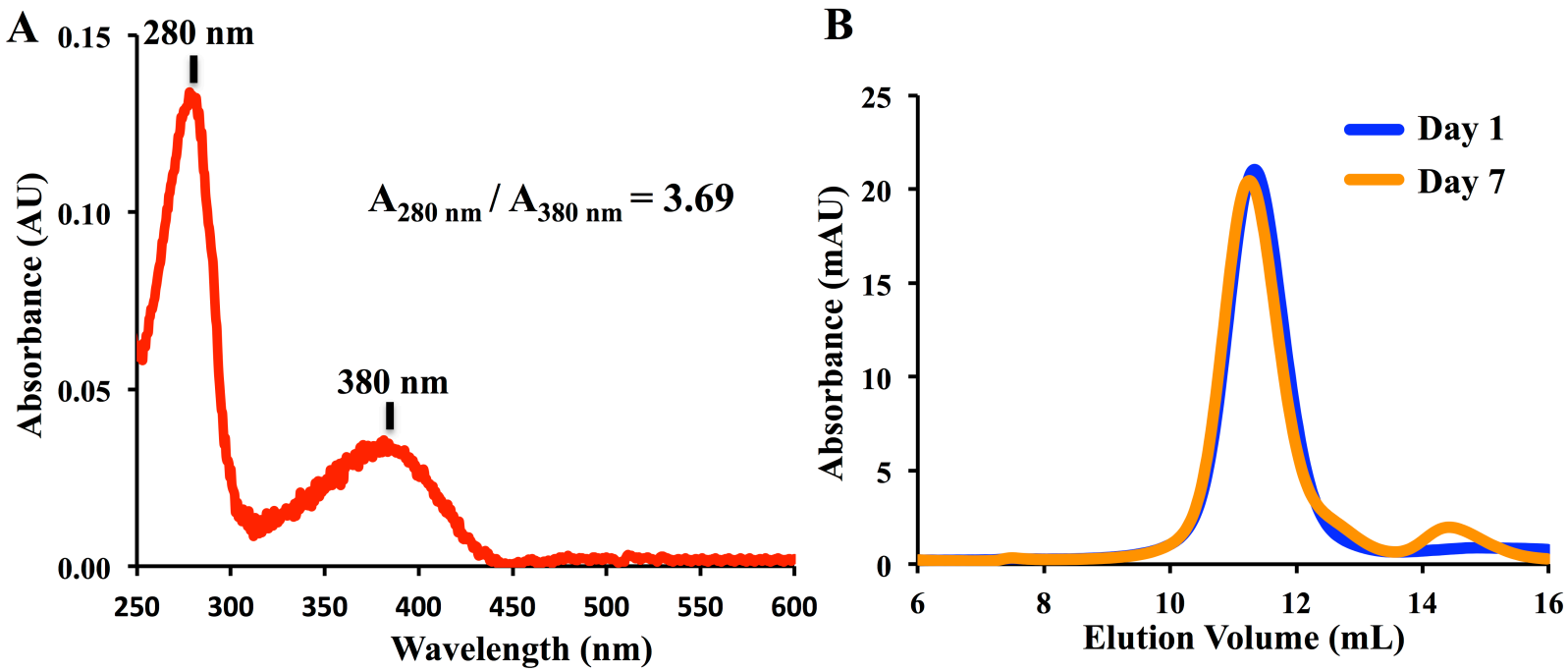
A
280 nm
380 nm
$A_{280\ nm} / A_{380\ nm} = 3.69$
Absorbance (AU)
0.15
0.10
0.05
0.00
250
300
350
400
450
500
550
600
Wavelength (nm)
B
Day 1
Day 7
Absorbance (mAU)
25
20
15
10
5
0
6
8
10
12
14
16
Elution Volume (mL)

3. The integrity of the complex can be routinely assessed with analytical SEC by injecting 5 μL of 10 mg/mL complex diluted with SEC buffer to 100 μL onto a Superdex 200 10/300 GL column pre-equilibrated with SEC buffer run at 0.4 mL/min. The complex will elute as a sharp symmetrical peak if it is intact (typical analytical SEC profiles shown in Fig. 5.3B). The purified complex is generally stable for over a week when kept at 4 °C wrapped in foil.

NOTES

1. Typically about 300 mg of rhodopsin and 15 mg of $\beta_1\gamma_1$ can be purified from 300 bovine retinae. All proteins can be aliquoted into 500 μL aliquots in 1.7 mL microcentrifuge tubes, resulting in 140 nM rhodopsin, 20 nM $\beta_1\gamma_1$ and 22 nM α_T in each tube. Rhodopsin aliquots should be wrapped in foil individually to avoid exposure to light.

2. The 10% molar excess of α_T ensures that all $\beta_1\gamma_1$ is utilized as $\beta_1\gamma_1$ is harder to purify and more valuble than α_T.

3. The large molar excess of rhodopsin is necessary because rhodopsin is very densely packed on retinal membrane and as a result a large portion of it is not easily accessible to transducin. This is not necessary if using membranes from insect cells or mammalian cells.

4. Extra care must be taken to ensure that rhodopsin is not exposed to light prior to the following light activation step.

5. To provide a controlled light exposure, all other lights in the cold room should be turned off. All following steps should be conducted in the dark with red lights.

6. Prolonged incubation in 1% LMNG will cause the complex dissociation.

7. The FPLC should be kept in a cold box set at 4 °C with the glass doors covered with foil to prevent light exposure inside and a red light can be kept inside the cold box to facilitate visuallization.

8. The addition of 0.2 mL buffer B results in a imidazole concentration of 10 mM which prevents the binding of excess rhodopsin to the column.

9. This step further removes contamination from excess rhodopsin and also lowers the detergent concentration from 0.2% to 0.02%.

10. The complex will start to come off the column at around 10% B and peak at 40% B.

11. Prolonged incubation with imidazole can destabilize the complex. Therefore, it is necessary to remove imidazole if complex were to be stored overnight. It is recommeded to concentrate the fractions starting from those with high imidazole concentrations, and as a result the final imidazole concentration before washing will be much lower. During concentrating and washing, it is recommended to invert the concentrators several times to alleviate protein aggregation during centrifugation.

12. The complex peak will be contained in four 0.4 mL fractions. During concentrating and washing, it is recommended to invert the concentrators several times to alleviate protein aggregation during centrifugation.

13. Concentration (in mg/mL) = $A_{280nm} \times Mw/\varepsilon_{280nm}$.

14. The extinction coefficients used are as follows: rhodopsin (ε_{280nm} = 61,800 $M^{-1}cm^{-1}$, ε_{380nm} = 42,000 $M^{-1}cm^{-1}$), α_T (ε_{280nm} = 35,870 $M^{-1}cm^{-1}$), and $\beta_1\gamma_1$ (ε_{280nm} = 57,400 $M^{-1}cm^{-1}$).

REFERENCES

1. Bjarnadóttir, T. K. et al. (2006) Comprehensive repertoire and phylogenetic analysis of the G protein-coupled receptors in human and mouse. Genomics 88, 263–273

2. Ma, P., and Zemmel, R. (2002) Value of novelty? Nat. Rev. Drug Discov. 1, 571-572

3. Fredriksson, R., Lagerstrom, M. C., Lundin, L. G. & 8. Schiöth, H. B. (2003) The G-protein-coupled receptors in the human genome form five main families. Phylogenetic analysis, paralogon groups, and fingerprints. Mol. Pharmacol. 63, 1256–1272

4. Simon, M. I., Strathmann, M. P. & Gautam, N. (1991) Diversity of G proteins in signal transduction. Science 252, 802–808

5. Downes, G. B. & Gautam, N. (1999) The G protein subunit gene families. Genomics 62, 544–552

6. Li, F., De Godoy, M. & Rattan, S. (2004) Role of adenylate and guanylate cyclases in β1-, β2-, and β3-adrenoceptor-mediated relaxation of internal anal sphincter smooth muscle. J. Pharmacol. Exp. Ther. 308, 1111–1120

7. Rosenbaum, D.M., Cherezov, V., Hanson, M.A., Rasmussen, S.G., Thian, F.S., Kobilka, T.S., Choi, H.J., Yao, X.J., Weis, W.I., Stevens, R.C., and Kobilka, B.K. (2007) GPCR engineering yields high-resolution structural insights into b2-adrenergic receptor function. Science. 318, 1266-1273

8. Caffrey, M., and Cherezov, V. (2009) Crystallizing membrane proteins using lipidic mesophases. Nat. Protoc. 4, 706-731

9. Xu, S.; Fischetti R.F. (2007) Proc. SPIE. 6665, 66650X1-66650X8

10. Bai, X. C., McMullan, G. & Scheres, S. H. (2015) How cryo-EM is revolutionizing structural biology. Trends Biochem. Sci. 40, 49–57

11. Rasmussen, S.G., DeVree, B.T., Zou, Y., Kruse, A.C., Chung, K.Y., Kobilka, T.S., Thian, F.S., Chae, P.S., Pardon, E., Calinski, D., Mathiesen, J.M., Shah, S.T., Lyons, J.A., Caffrey, M., Gellman, S.H., Steyaert, J., Skiniotis, G., Weis, W.I., Sunahara, R.K., and Kobilka, B.K. (2011) Crystal structure of the b2 adrenergic receptor-Gs protein complex. Nature 477, 549-555

12. Liang, Y-L., Khoshouei, M., Radjainia, M., Zhang, Y., et al. (2017) Phase-plate cryo-EM structure of a class B GPCR–G-protein complex. Nature 22327

13. Y. Zhang, et al. (2017) Cryo-EM structure of the activated GLP-1 receptor in complex with a G protein Nature, 546, 248-253

14. Stryer, L. (1991) Visual excitation and recovery. J. Biol. Chem. 266, 10711-10714

15. Palczewski, K., Kumasaka, T., Hori, T., Behnke, C.A., Motoshima, H., Fox, B.A., Le Trong, I., Teller, D.C., Okada, T., Stenkamp, R.E., Yamamoto, M., and Miyano, M. (2000) Crystal structure of rhodopsin: A G protein-coupled receptor. Science 289, 739-745

16. Li, J., Edwards, P.C., Burghammer, M., Villa, C., and Schertler, G.F.X. (2004) Structure of bovine rhodopsin in a trigonal crystal form. J. Mol. Biol. 343, 1409-1436

17. Park, J.H., Scheerer, P., Hofmann, K.P., Choe, H.W., and Ernst, O.P. (2008) Crystal structure of the ligand-free G-protein-coupled receptor opsin. Nature 454, 183-187

18. Choe, H.W., Kim, Y.J., Park, J.H., Morizumi, T., Pai, E.F., Krauss, N., Hofmann, K.P., Scheerer, P., and Ernst, O.P. (2011) Crystal structure of metarhodopsin II. Nature 471, 651-655

19. Scheerer, P., Park, J.H., Hildebrand, P.W., Kim, Y.J., Krauss, N., Choe, H.W., Hofmann, K.P., and Ernst, O.P. (2008) Crystal structure of opsin in its G-protein-interacting conformation. Nature 455, 497-502

20. Gao, Y. et al. (2017) Isolation and structure-function characterization of a signaling-active rhodopsin-G protein complex. J. Biol. Chem. 292, 14280–14289

21. Skiba, N. P., Bae, H., and Hamm, H. E. (1996) Mapping of effector binding sites of transducin alpha-subunit using G alpha t/G alpha i1 chimeras. J. Biol. Chem. 271, 413–424

22. Ballesteros, J. A., Shi, L. & Javitch, J. A. (2001) Structural mimicry in G protein-coupled receptors: implications of the high-resolution structure of rhodopsin for structure–function analysis of rhodopsin-like receptors. Mol. Pharmacol. 60, 1–19

23. Chen, C. A. & Manning, D. R. (2001) Regulation of G proteins by covalent modification. Oncogene 20, 1643–1652

24. Zhang, F. L. & Casey, P. J. Protein prenylation: molecular mechanisms and functional consequences. Annu. Rev. Biochem. 65, 241–269 (1996).

25. Min, K.C., Gravina, S.A., and Sakmar, T.P. (2000) Reconstitution of the Vertebrate Visual Cascade Using Recombinant Transducin Purified from Sf9 Cells. Protein Expr. Purif. 20, 514-526

26. Ramachandran, S. and Cerione, R.A. (2011) A dominant-negative Gα Mutant That Traps a Stable Rhodopsin-Gα-GTP-βγ Complex. J. Biol. Chem. 286, 12702-12711

Appendix Chapter 2

Reconstitution of Rhodopsin-Transducin Complex into Lipid Nanodiscs

INTRODUCTION

Transmembrane proteins, such as G protein-coupled receptors (GPCRs), are not soluble in aqueous solutions due to the presence of large hydrophobic surfaces, which are necessary for their insertion into lipid bilayers. Therefore, in order to maintain proper folding, detergents are required during the extraction of these proteins from the membrane. And in the case of GPCRs, as they adopt a high level of structural flexibility[1], most conventional detergents, for example octyl glucoside (OG) and dodecyl maltoside (DDM) are not sufficient for maintaining their stability and signaling activities. Recently, a series of novel detergents, such as maltose neopentyl glycol (MNG) [2] and glyco-diosgenin (GDN) [3], have been developed featuring a more rigid architecture, which is intended to place subtle restraints on protein conformational flexibility. And they have proven to be very successful at sustaining the structural integrity and activity of GPCRs and have helped usher in the recent rapid growth in the number of high-resolution GPCR and GPCR-G protein complex structures. However, despite the high stability of GPCRs in MNG and GDN, the hydrophobic environment provided by the detergent micelles is still very different from the native membrane environment, as these detergents tend to have very large micelles that are much thicker than lipid membranes and may distort the conformation of hydrophilic residues close to the hydrophobic belt. In addition, GPCRs have been known to interact with lipids in the membrane. For example, the

photochemical properties[4] of the GPCR rhodopsin in the visual phototransduction pathway and its coupling efficiency to the heterotrimeric G protein transducin[5] are sensitive to its lipid environment composition and tightly bound phospholipids molecules have been seen in a high-resolution rhodopsin crystal structure[6]. Moreover, GPCRs are often palmitoylated on one or more cysteines at the intracellular side[7], and a lipid bilayer environment would allow for proper orientation of these lipid modifications. Therefore, it is clear that a reconstituted lipid bilayer environment would be the best conduit for studying the biophysical properties of GPCRs and nanodiscs provide a perfect solution to address this challenge.

Nanodiscs are comprised of a circular lipid bilayer center, into which a transmembrane protein can be incorporated, and two molecules of membrane scaffold protein (MSP), which is a modified form of human high-density lipoprotein apoA-1[8]. MSP contains a series of amphipathic α helixes that can wrap around the lipids and thus stabilize the bilayer disc in aqueous solutions. The size of the nanodiscs is very monodisperse and can be easily adjusted by varying the number of amphipathic helixes in MSP[9-10]. In the case of rhodopsin, the GPCR in the visual phototransduction pathway, nanodiscs have been used to study the stoichiometry of its interaction with the G protein transducin[11-12], rhodopsin kinase and arrestin[13]. And more recently double electron-electron resonance (DEER) has been used to characterize rhodopsin incorporated into nanodiscs and revealed that the activated receptor is in equilibrium among multiple conformations which is very different from the single conformation observed in DDM micelles[14]. Moreover, with the recent development in cryo-electron microscopy technology[15], nanodiscs have proven to be a great environment for obtaining high-

resolution structures of transmembrane proteins, as it helps maintain them in a native-like environment and can allow for interactions between annular phospholipids and proteins[16].

Here we present a method for reconstituting the purified detergent-solubilized rhodopsin-transducin complex[17], the GPCR-G protein complex in visual phototransduction, (as described in a previous chapter) into nanodiscs. A truncated version of MSP (MSP1D1ΔH5)[18] was chosen as the size of the resulting nanodiscs is only big enough to accommodate one receptor complex, thus ensuring a homogeneous preparation. The process starts with mixing purified complex with MSP and lipids solubilized in detergents in a specific ratio and then the detergent can be slowing removed by incubation with Bio-Beads. During detergent removal, the nanodiscs self-assemble and incorporate the receptor complex. The resulting complex-embedded nanodiscs can then be further purified with size exclusion chromatography (SEC). As the receptor rhodopsin has a covalently bound agonist all-trans retinal, which has a distinct UV absorption at 380 nm, the 1:1 ratio between nanodisc and complex can be verified by UV-Vis spectroscopy. The purified complex-embedded nanodiscs can be used in further biophysical characterizations, such as small-angle X-ray scattering (SAXS) and negative-stain electron microscopy, and potentially be applied to cryo-electron microscopy for obtaining high-resolution structures of the rhodopsin-transducin complex. In addition, as the composition of the lipids used in nanodisc formation can be varied, the resulting nanodiscs can also be used for studying the effects of different lipids on this GPCR-G protein complex.

MATERIALS

Incorporation of rhodopsin-transducin complex into nanodiscs

1. The lipid 1-palmitoyl-2-oleoyl-sn-glycero-3-phosphocholine (POPC) can be obtained from Avanti Polar Lipids and all other chemicals can be purchased from either Sigma or VWR.

2. HMN buffer: 20 mM HEPES pH 7.5, 2 mM $MgCl_2$, 100 mM NaCl, 100 μM TCEP.

3. 10% (w/v) sodium cholate in HMN buffer.

4. Methanol

5. Purified rhodopsin-transducin complex in HMN buffer plus 0.003% lauryl maltose neopentyl glycol as described in previous chapter.

6. Bio-Beads SM-2 resin can be obtained from Bio-Rad.

7. A sonic dismemrator.

8. A scale accurate to 0.1 mg.

9. A tabletop microcentrifuge and an end-to-end rocker kept in a cold room at 4 °C.

10. 0.7 mL and 1.7 mL microcentrifuge tubes.

11. 1 mL disposable syringes with Luer-Lok tips.

12. 0.22 μm PVDF syringe filters

13. Aluminum foil.

14. Floor lamps covered with 3M 616 lithographer's tape.

SEC purification of rhodopsin-transducin complex embedded nanodiscs

1. An FPLC equipped with a UV absorbance monitor set at 280 nm and a fraction collector and kept in a cold box at 4 °C. A desk lamp covered with 3M 616 lithographer's tape.

2. A Superdex 200 10/300 GL column (GE Life Sciences)

3. HMN buffer: 20 mM HEPES pH 7.5, 2 mM $MgCl_2$, 100 mM NaCl, 100 μM TCEP.

4. Amicon Ultra-0.5 mL centrifugal filters with 100 kD molecular weight cutoff (EMD Millipore).

5. A tabletop microcentrifuge kept in a cold room at 4 °C.

6. Aluminum foil.

7. Floor lamps covered with 3M 616 lithographer's tape.

Characterization of the complex-embedded nanodiscs with UV-Vis spectroscopy

1. A UV-Vis spectrophotometer.

METHODS

Incorporation of rhodopsin-transducin complex into nanodiscs

1. The membrane scaffolding protein MSP1D1ΔH5 can be expressed and purified from *E coli* BL21(DE3) as described previously[9] using a pET28a vector harboring an N-terminal His_6-tag DNA sequence followed by the MSP1D1 gene with DNA sequence corresponding to residues 121-142 deleted and stored in HMN buffer with 10% glycerol at 300 μM concentration at -80 °C. (see Note 1)

2. Weigh out 5 mg POPC in a 0.7 mL microcentrifuge tube. Add 75 μL HMN buffer to the lipid and vortex for 1 min to achieve a uniform suspension. Sonicate the tube at maximum intensity in water bath for 1 min. Add 56.6 μL 10% (w/v) sodium cholate to the suspension and vortex the mixture for 1 min. Sonicate the tube at maximum intensity in water bath for 1 min. This result in 50 mM POPC solubilized in HMN buffer containing100 mM sodium cholate. (see Note 2)

3. Weigh out 200 mg Bio-Beads in a 1.7 mL microcentrifuge tube. Incubate with 1.5 mL methanol for 1 min. Spin the tube in a tabletop microcentrifuge for 0.5 min at maximum speed. Gently aspirate out and discard the supernatant. Repeat this process with 1.5 mL HMN buffer instead for three times and store the equilibrated Bio-Beads on ice.

4. The ratio between MSP, lipids and the rhodopsin-transducin complex is critical for obtaining homogeneous complex-embedded nanodiscs. The optimal molar ratio is 1:3:50 complex:MSP1D1ΔH5:POPC. (see Note 3)

5. Mix 50 μL 300 μM MSP1D1ΔH5 with 5 μL 50 mM POPC from step 2, resulting in 3:50 ratio of MSP1D1ΔH5:POPC. Incubate on ice for 20 min.

6. All following steps should be carried out in the dark with red lights. Add 5.3 μL 10% sodium cholate (232.6 mM) and 63.1 μL 10 mg/mL (79.3 μM) purified rhodopsin-transducin complex to the mixture and incubate on ice for another 20 min. (see Note 4)

7. Weigh out 123 mg wet Bio-Beads in a 0.7 mL microcentrifuge tube. Add the mixture from step 6 to the tube, wrap the tube with foil and incubate it on an end-to-end rocker in a cold room set at 4 °C overnight. (see Note 5)

8. Spin the tube from step 7 in a tabletop microcentrifuge kept in a dark cold room with red lights for 0.5 min at maximum speed. Gently aspirate out the supernatant and filter it with a 0.22 μm PVDF syringe filter.

SEC purification of rhodopsin-transducin complex embedded nanodiscs

1. Equilibrate a Superdex 200 10/300 GL column with 60 mL HMN buffer at 0.4 mL/min on an FPLC equipped with a UV absorbance monitor set at 280 nm and a fraction collector. (see Note 6)

2. Inject the complex-embedded nanodiscs from the previous section onto the column run at 0.4 mL/min with HMN buffer. Collect 0.4 mL fractions (a typical SEC profile is shown in Fig. 6.1).

3. Pool fractions containing the complex-embedded nanodiscs from step 2 and concentrate the fractions with one 0.5 mL 100 kD molecular weight cutoff Amicon concentrator to about 100 μL at 14,000 g for 3 min each time in a tabletop microcentrifuge kept in a dark cold room with red lights. This is the final purified complex-embedded nanodiscs and the concentration is typically about 3 mg/mL. The nanodiscs can be stored wrapped in foil at 4 °C for over a week. (see Note 7)

Characterization of the complex-embedded nanodiscs with UV-Vis spectroscopy

1. The concentration of the complex-embedded nanodiscs can be measured with a UV-Vis spectrophotometer at 280 nm (A_{280nm}) using the extinction coefficient ε_{280nm}=197,930 $M^{-1}cm^{-1}$, and molecular weight Mw=170,240 Da. (see Note 8)

2. The number of rhodopsin-transducin complexes in each nanodisc can be assessed with UV-Vis spectroscopy by measuring the absorbance at 280 nm (A_{280nm}, the absorbance of the protein moieties) and 380 nm (A_{380nm}, the absorbance of all-trans retinal) (a typical spectrum is shown in Fig. 6.2). The A_{280nm}/ A_{380nm} ratio should be 4.70, indicating a 1:1 molar ratio of complex:nanodisc. (see Note 9)

Figure 6.1 SEC profile of complex-embedded nanodiscs and SDS-PAGE gel of concentrated peak fractions.

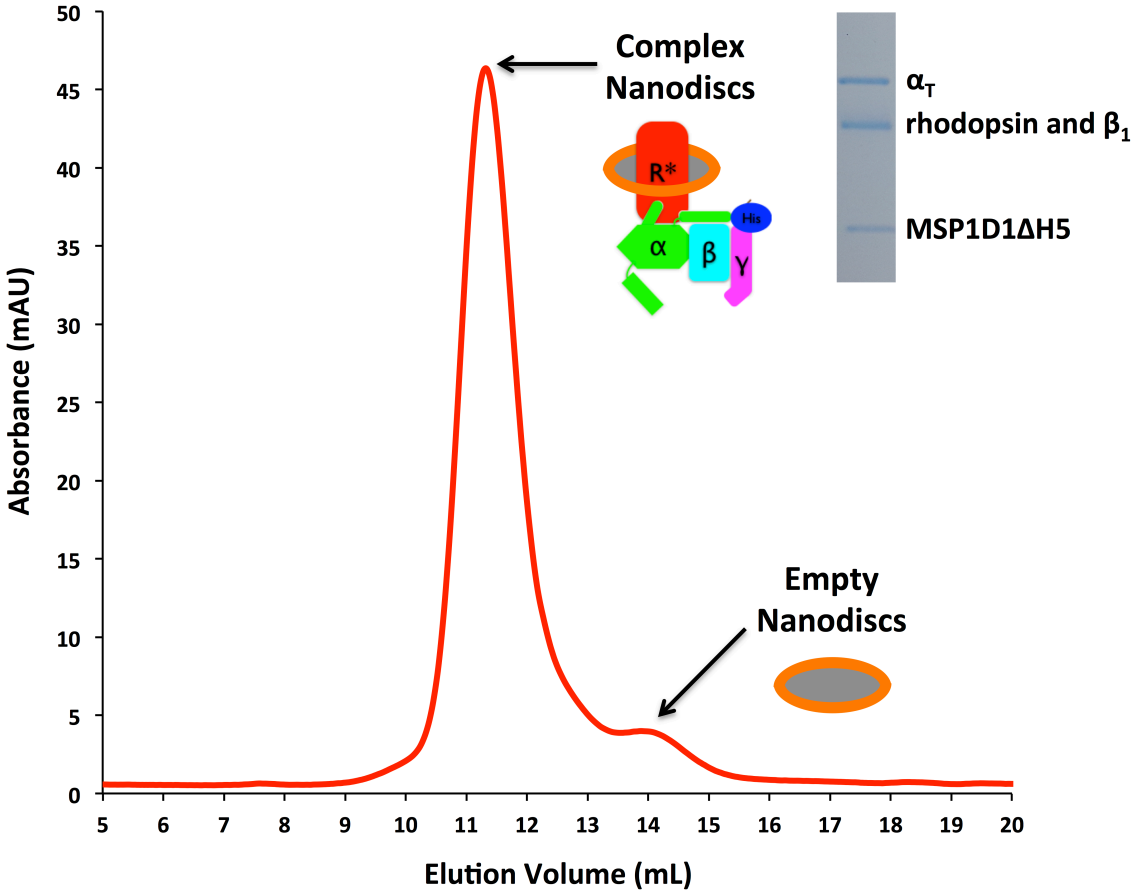
Absorbance (mAU)
Elution Volume (mL)
Complex Nanodiscs
Empty Nanodiscs
R*
α
β
γ
His
α_T
rhodopsin and β_1
MSP1D1ΔH5

Figure 6.2 UV-Vis spectrum of the purified complex-embedded nanodiscs

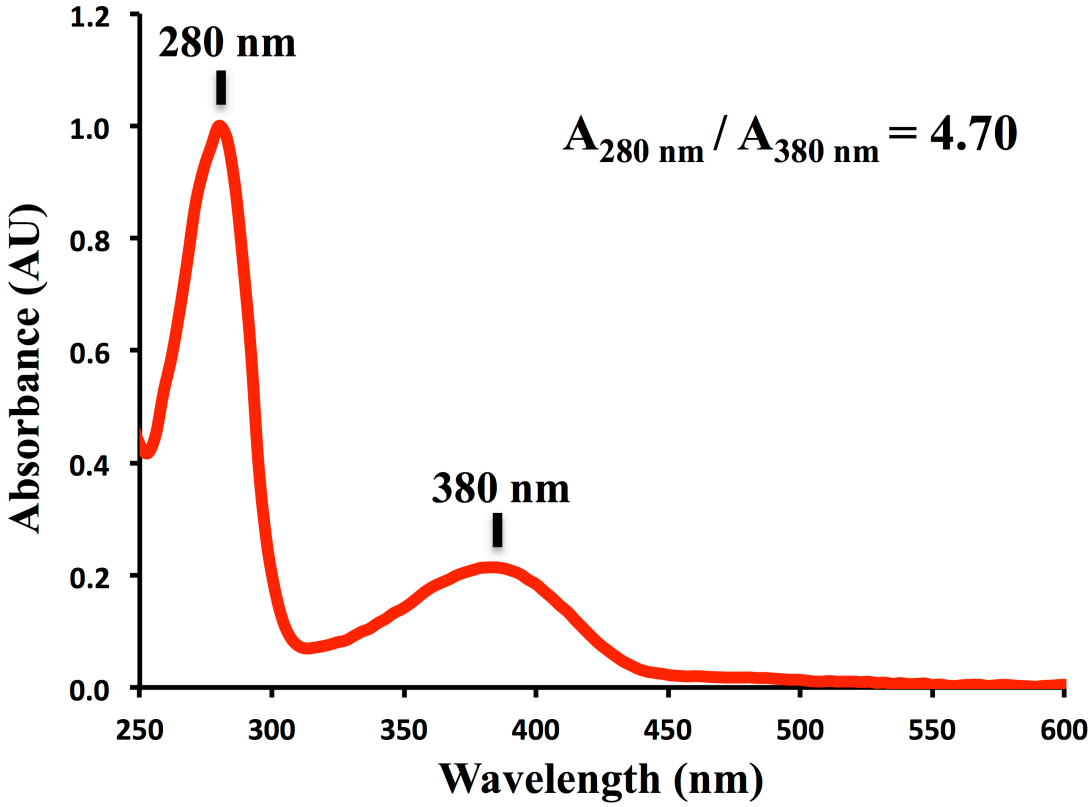
280 nm
380 nm
$A_{280\ nm} / A_{380\ nm} = 4.70$
Absorbance (AU)
Wavelength (nm)
1.2
1.0
0.8
0.6
0.4
0.2
0.0
250
300
350
400
450
500
550
600

NOTES

1. The protein sequence of MSP1D1ΔH5 is as follows:

MGHHHHHHDYDIPTTENLYFQGSTFSKLREQLGPVTQEFWDNLEKETEGLRQEM
SKDLEEVKAKVQPYLDDFQKKWQEEMELYRQKVEPLGEEMRDRARAHVDALR
THLAPYSDELRQRLAARLEALKENGGARLAEYHAKATEHLSTLSEKAKPALEDL
RQG LLPVLESFKVSFLSALEEYTKKLNTQ

2. The lipids (stored at -20 °C) are hygroscopic and should be allowed to come to room temperature before opening the vial. The detergent-solubilized lipids can be stored at -80 °C for up to 6 months.

3. The excess MSP and lipids ensures only one complex is incorporated into each nanodisc. If MSP1D1 is used, the ratio should be 1:3:145 complex:MSP1D1:POPC.

4. The addition of 10% sodium cholate maintains the cholate concentration at 14 mM, above its cmc of 9.5 mM. As the rhodopsin-transducin complex is light sensitive, all steps onward should be conducted in the dark with red lights.

5. The ratio of Bio-Beads to nanodisc mixture is 1 mg wet Bio-Beads to 1 μL solution.

6. The FPLC should be kept in a cold box set at 4 °C with the glass doors covered with foil to prevent light exposure inside and a red light can be kept inside the cold box to facilitate visuallization.

7. The complex-embedded nanodiscs peak will be contained in four 0.4 mL fractions. During concentrating, it is recommended to invert the concentrators several times to alleviate protein aggregation during centrifugation.

8. Concentration (in μM) = $A_{280nm} \times 10^6 / \varepsilon_{280nm}$. Concentration (in mg/mL) = $A_{280nm} \times Mw / \varepsilon_{280nm}$.

9. The extinction coefficients used are as follows: rhodopsin (ε_{280nm} = 61,800 $M^{-1}cm^{-1}$, ε_{380nm} = 42,000 $M^{-1}cm^{-1}$), transducin (ε_{280nm} = 93,270 $M^{-1}cm^{-1}$) and MSP1D1ΔH5 (ε_{280nm} = 21,430 $M^{-1}cm^{-1}$).

REFERENCES

1. Preininger, A. M., Meiler, J., & Hamm, H. (2013). Conformational flexibility and structural dynamics in GPCR-mediated G protein activation: a perspective. Journal of Molecular Biology, 425(13), 2288–2298

2. Chae, P. S., Rasmussen, S. G. F., et al. (2010). Maltose-neopentyl glycol (MNG) amphiphiles for solubilization, stabilization and crystallization of membrane proteins. Nature Methods, 7(12), 1003–1008

3. Chae, P. S., Rasmussen, S. G. F., et al. (2012). A New Class of Amphiphiles Bearing Rigid Hydrophobic Groups for Solubilization and Stabilization of Membrane Proteins. Chemistry (Weinheim an Der Bergstrasse, Germany), 18(31), 9485–9490

4. Brown, M.F. (1994) Modulation of rhodopsin function by properties of the membrane bilayer Chem. Phys. Lipids, 73, 159-180

5. Kaya, A. I., Thaker, T. M., Preininger, A. M., Iverson, T. M., & Hamm, H. E. (2011). Coupling Efficiency of Rhodopsin and Transducin in Bicelles. Biochemistry, 50(15), 3193–3203

6. Li, J., Edwards, P.C. et al. (2004) Structure of bovine rhodopsin in a trigonal crystal form. J. Mol. Biol., 343, 1409-1438

7. Goddard, A. D., & Watts, A. (2012). Regulation of G protein-coupled receptors by palmitoylation and cholesterol. BMC Biology, 10, 27

8. Bayburt T.H., Grinkova Y.V., Sligar S.G. Self-assembly of discoidal phospholipid bilayer nanoparticles with membrane scaffold proteins. Nano Lett. 2002;2:853–856

9. Ritchie, T.K., Grinkova, Y.V., et al. (2009) Reconstitution of membrane proteins in phospholipid bilayer nanodiscs. Methods in Enzymology, 464, 211-231

10. Bayburt, T.H., Sligar, S.G. (2010) Membrane protein assembly into nanodiscs. FEBS Lett., 584, 1721-1727

11. Bayburt, T.H., Leitz, A.J., et al. (2007) Transducin activation by nanoscale lipid bilayers containing one and two rhodopsins. J Biol Chem. 282(20), 14875-81

12. Whorton, M. R., Jastrzebska, B., Park, P. S.-H., Fotiadis, D., Engel, A., Palczewski, K., & Sunahara, R. K. (2008). Efficient Coupling of Transducin to Monomeric Rhodopsin in a Phospholipid Bilayer. The Journal of Biological Chemistry, 283(7), 4387–4394

13. Bayburt, T. H., Vishnivetskiy, S. A., et al. (2011). Monomeric Rhodopsin Is Sufficient for Normal Rhodopsin Kinase (GRK1) Phosphorylation and Arrestin-1 Binding. The Journal of Biological Chemistry, 286(2), 1420–1428.

14. Van Eps, N., Caro, L. N., Morizumi, T., Kusnetzow, A. K., Szczepek, M., Hofmann, K. P., … Hubbell, W. L. (2017). Conformational equilibria of light-activated rhodopsin in nanodiscs. Proceedings of the National Academy of Sciences of the United States of America, 114(16), E3268–E3275.

15. Bai, X. C., McMullan, G. & Scheres, S. H. (2015) How cryo-EM is revolutionizing structural biology. Trends Biochem. Sci. 40, 49–57

16. Gao, Y., Cao, E., Julius, D., & Cheng, Y. (2016). TRPV1 structures in nanodiscs reveal mechanisms of ligand and lipid action. Nature, 534(7607), 347–351

17. Gao, Y. et al. (2017) Isolation and structure-function characterization of a signaling-active rhodopsin-G protein complex. J. Biol. Chem. 292, 14280–14289

18. Hagn, F., Etzkorn, M., Raschle, T., & Wagner, G. (2013). Optimized Phospholipid Bilayer Nanodiscs Facilitate High-Resolution Structure Determination of Membrane Proteins. Journal of the American Chemical Society, 135(5), 1919–1925